Yaxin Liang

Flux decline and concentration polarization during ceramic nanofiltration for polyethylene glycols, silica, and phosphate retention

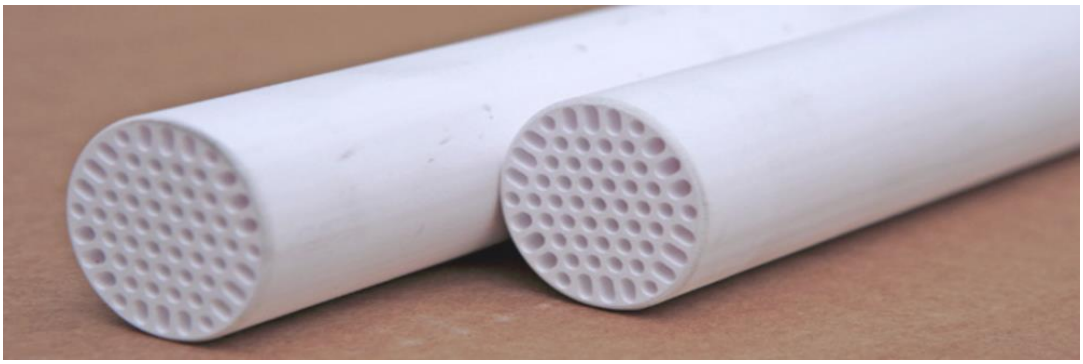

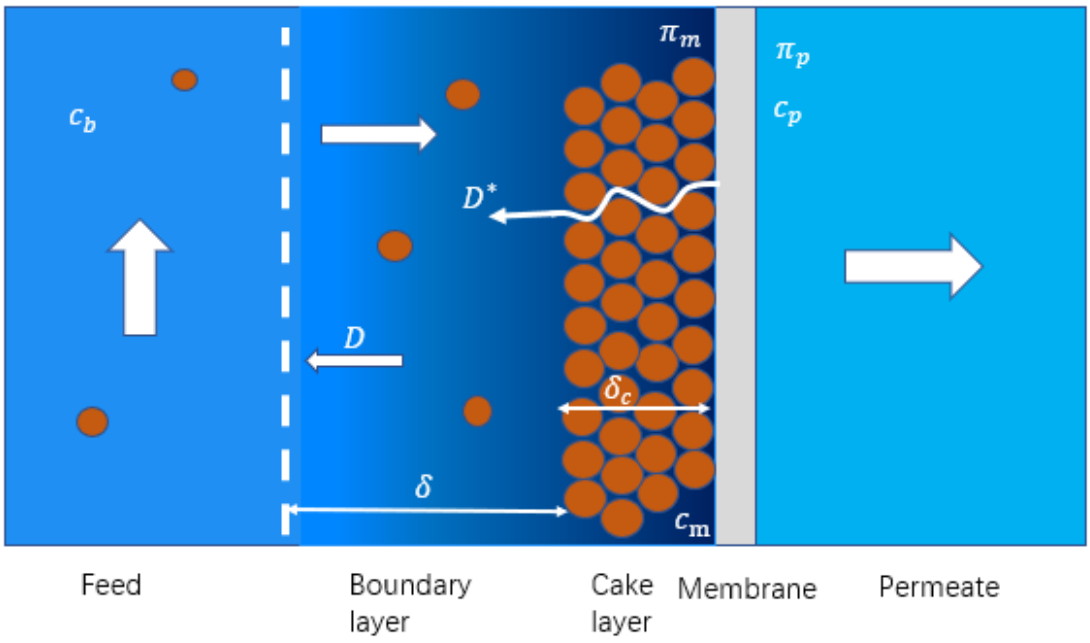

Flux decline and concentration polarization during ceramic nanofiltration for polyethylene glycols, silica, and phosphate retention

Yaxin Liang

for the degree of:
Master of Science in Civil Engineering

Date of submission: 06/15/2019
Date of defence: 06/21/2019

Graduation Committee:

Prof. dr. ir. Luuk Rietveld	TU Delft
Dr. ir. Bas Heijman	TU Delft
Prof. dr. Ernst J.R. Sudhölter	TU Delft

Sanitary Engineering Section, Department of Water Management
Faculty of Civil Engineering and Geosciences
Delft University of Technology, Delft

TU Delft

Preface

This master thesis is the outcome of my master programme of Sanitary Engineering in Water Management department in Civil Engineering and Geosciences Faculty of TU Delft University, The Netherlands. I spent two tough but wonderful years in this beauty campus, and I would like to give my deepest gratitude to all the people who guided me, supported me, and encouraged me.

Firstly, I would like to thank my promotor, Professor Luuk Rietveld, for all the feedback about my research, especially the help in improving the structure and readability of my thesis. I particularly grateful to Bas, my daily supervisor, for the professional guidance and the unconditional support during my whole graduation work. When I struggled with the undesirable results and had no progress, it is him that gave me lots of advice and supported me to change the plan. I would like to thank Prof. Ernst Sudhölter for the feedback and suggestions during my research.

Then, I would like to thank the researchers and staff in the water lab: Ran Shang, Irene Caltran, and Franca Kramer, who gave me the lots of support in experiments. I also would like to thank Sander, Frank and Armand who spent a lot of time on helping me fixed my pump. Also, thanks to Shuo, Bin and Mingliang, I spent a delightful time in the lab regardless of the tough experiments.

Finally, I would like to thank my family for the continuous encouragement along my life, and also thanks to my friends, Jiaxin, Chang, Yingfei, Floriana, Sarah and Mengya, we encouraged each other and had some colourful memories together.

Yaxin Liang
June 2019, Delft

Abstract

For all pressure driven membranes, one of the main problems which hinders the membrane practical application is the permeate flux reduction due to the solute accumulation on the membrane surface. The most popular explanation for the flux decline supported by Bhattachajee &Bhattacharya (1993), contains two mechanisms: concentration polarization(CP) and fouling.

The influence of CP is noteworthy in ceramic nanofiltration system. On the one hand, CP can influence the performance of membrane separation by decreasing the retention of the molecules. On the other hand, CP could have a desirable effect which can be used for membrane surface modification. In the past three or four decades, several different models have been used to verify the existence of CP or cake-enhanced CP(CECP) effect and try to quantify it. However, all these methods or models have their own limitations. Therefore, it is essential to build a new model or adjust the constants in the empirical model according to the practical situation.

The flux decline behaviour of a ceramic nanofiltration membrane in the presence of polyethylene glycols (PEGs) and silica was investigated to examine the control factor in flux decline and calculate the CP factor in the filtration. The control factor in flux decline for PEGs is CP, while for silica, both CP and fouling are important. Based on the reversibility of CP and fouling, the Gel-polarization model together with the corresponded filtration method generated the modified Gel-polarization model which is suitable for calculating the fouling resistance and the osmotic pressure on the membrane. Sherwood formula is appropriate for calculating CP factor with calibrated constants.

The flux decline behaviour, as well as the CECP model developed in this work, was used to investigate the possible CP&CECP during ceramic nanofiltration for phosphate retention. CECP model based on Sherwood relation can be used to investigate the influence of the fouling layer on CP with measured permeate flux, fouling mass, and an assumed/measured porosity of the fouling layer. Based on the CECP model analysis, lower crossflow velocity and cake layer porosity, larger permeate flux and fouling mass can produce a higher CECP factor. The change of permeability in phosphate retention can be used to calculate CP factors, however, the adsorption and electroviscous effect had influence on the accuracy of the results. CECP factor is not able to be measured by the change of permeability since the unstable fouling layer can influence the discovery of permeability decrease. The presence of calcium has a serious negative impact on phosphate retention probably due to the lower electrostatic repulsion of phosphate.

Contents

List of figure and form

List of Acronyms

CECP	Cake-enhanced Concentration Polarization
CP	Concentration Polarization
EfOM	Effluent Organic Matter
EPS	Extracellular Polymeric Substances
HPLC	High-Performance Liquid Chromatography
IC	Ion Chromatography
MF	Microfiltration
MW	Molecular Weight
MWCO	Molecular Weight Cut-off
NF	Nanofiltration
NOM	Natural Organic Matter
PEGs	Polyethylene Glycols
PSD	Particle Size Distribution
RO	Reverse Osmosis
SI	Saturation Index
TMP	Transmembrane Pressure
UF	Ultrafiltration

List of symbols

Nomenclature

A	membrane section area [m^2]
A_m	effective membrane area [m^2]
$A_1\ A_2\ A_3$	constants of *Formula from Nikolova & Islam (1998)*
a_p	particle radius [m]
c	solute concentration
c_b	solute concentration in the bulk
c_f	solute concentration in the feed stream
c_p	solute concentration in the permeate stream.
c_m	solute concentration on the membrane
D	diffusion coefficient of the solute in the solvent [m^2/s]
D^*	diffusion coefficient of the solute in the fouling layer [m^2/s]
d_h	(tubular) hydraulic diameter of the membrane channel [m]
d_h^*	hydraulic diameter of the membrane under fouling condition [m]
d_p	mean diameter of the particle [m]
f	friction number
f_{os}	osmotic coefficient that converts salt concentration to osmotic pressure
J	permeate flux $[L/(m^2 \cdot \mathrm{h})]$
J_w	permeate flux of demi water $[L/(m^2 \cdot \mathrm{h})]$
J_t	permeate flux of target solution $[L/(m^2 \cdot \mathrm{h})]$
J_r	recovered permeate flux $[L/(m^2 \cdot \mathrm{h})]$
k	Boltzmann constant ($1.38 \times 10^{-23}\ J/K$)
K / K_s	mass transfer coefficient [m/s]
K^*	mass transfer coefficient in the fouling layer [m/s]
K_{eff}	effective mass transfer coefficient [m/s]
$L_{20℃}$	temperature-corrected permeability at 20℃ $[L/m^2 \cdot \mathrm{h} \cdot \mathrm{bar}]$
M	molecular weight of PEG [g/mol]
M_d	mass of deposit layer [kg]
P_w	permeability of the membrane with demi water $[L/(m^2 \cdot \mathrm{h} \cdot \mathrm{bar})]$
P_t	permeability of the target solution $[L/(m^2 \cdot \mathrm{h} \cdot \mathrm{bar})]$
ΔP	transmembrane pressure [bar]
P'	wetted perimeter [m]
R	universal gas constant [L·bar/(mol·K)]
R_m	hydraulic membrane resistance [m^{-1}]
R_{cp}	concentration polarization resistance [m^{-1}]
R_f	fouling resistance [m^{-1}]
R_o	retention rate [-]
r	radius of the channel [m]
Re	Reynolds number [-]

Sc	Schmidt number [-]
Sh	Sherwood number [-]
S_{MW}	a standard deviation of molecular weight [Da]
T	temperature [℃]/[K]
u	cross-flow velocity [m/s]
v	kinematic viscosity [m^2/s]
Δx	membrane thickness [m]
y	distance from the membrane surface [m]

Greek letters

α	specific resistance of the deposit layer
β	concentration polarization coefficient [-]
β_c	cake enhanced concentration polarization coefficient [-]
δ	thickness of the boundary layer [m]
δ_c	deposit layer thickness [m]
π_m	osmotic pressure on the membrane [bar]
π_p	osmotic pressure on the permeate [bar]
$\Delta\pi$	transmembrane osmotic pressure [bar]
$\Delta\pi^*$	osmotic pressure difference under fouling condition [bar]
μ	dynamic viscosity [kg/(m·s)]
μ_w	dynamic viscosity of demi water [kg/(m·s)]
μ_t	dynamic viscosity of target solution [kg/(m·s)]
ρ	density of the solution [$\mathrm{kg/m}^3$]
ρ_p	density of the particle [$\mathrm{kg/m}^3$]
ε	membrane porosity [-]
$\sigma(\mathrm{MW}_s)$	reflection coefficient for different molecular weight (MW_s)of PEGs [-]
φ_s	osmotic potential [bar]

1 Introduction

1.1. Background information

The high demand for drinking water of high quality and the need for complex wastewater treatment have increased the application of separation technologies, such as ultrafiltration (UF), microfiltration (MF), nanofiltration (NF) and reverse osmosis (RO)(Raman et al.,1994). The characteristics of NF make it suitable for multivalent ions removal, water softening and disinfection by-product precursors removal (Labban et al., 2017). In addition, since the interest in sewer mining has increased the potential for wastewater reclamation (Metcalf et al., 2010) and resource recovery, nanofiltration has become a good alternative for concentrating nutrients, such as phosphate.

With the development of material and technology, ceramic nanofiltration membranes, compared with the polymeric membranes, obtained a high mechanical strength and chemical stability, which makes it suitable for water reclamation (Kramer et al., 2015). The properties of ceramic membrane can decrease the cleaning times to once in 2-4 days instead of once an hour with polymeric membranes, which is more environmentally friendly due to the highly saved water, chemicals, and energy consumption. Even though the initial investment costs can be 3-10 times higher than with the installation of traditional polymeric membranes (Samaei et al., 2018), it still has a promising future in wastewater separation.

For all pressure-driven membrane filtration systems, the flux decline which could be caused by concentration polarization (CP) and fouling, hinders the practical application of membranes. CP refers to an emerging solute gradient on the membrane interface which leads to an increasing concentration on the membrane surface (Verberk, 2015). The larger concentration difference between the membrane surface and the permeate is, the larger the driving force for solutes passing through the membrane. In the end, this could lead, e.g., to a lower phosphate retention rate. In addition, it is known from literature (Heijman et al., 2007; Nghiem et al., 2007; Shang et al., 2014), that the presence of organic matter in the feed stream can enhance the CP effect, which is called Cake-enhanced concentration polarization (CECP).

On the one hand, CP can thus influence the performance of membrane separation by decreasing the retention of molecules. On the other hand, the effect of CP could have a positive effect and be used for membrane surface modification. When non-uniformity of the membrane surface or defects are found in commercial ceramic membrane products, especially for those with small MWCO, nanoparticles can be filtered and, the CP effect can then increase the solute concentration on the membrane surface and help these nanoparticles coating the defects or nonuniform area (Bernstein et al., 2011). Because of the high thermal and chemical stabilities and the suitable particle size, especially zeolite crystal layer coating is gradually attracting the attention of the membrane separation industry (Yang et al.,2016). As the precursors of zeolite crystals, silica could have an essential influence on the performance of the coating.

1.2. Problem statement

Even though the most popular explanation for flux decline contains CP and fouling, the contributions of these two factors to flux decline vary from different solutes and operational conditions. If the control factor in flux decline is clear, a more targeted approach can be used to control the decreasing flux. It is essential to investigate the control factor and quantify CP and fouling in flux decline. Since CP has more potential to be controlled than fouling, in the past three or four decades, several different methods have been used to quantify CP or CECP effect. If CP can be described by the model which contains the related influencing factors, it will be much convenient to control the flux decline and the solute concentration near the membrane surface. A higher retention of the solute and a better membrane coating could be achieved based on the information from the model.

For the molecules smaller than the membrane pore size, such as PEG with a specific molecular weight (MW) and multivalent ions, the changing retention under different operational conditions could be a sign related to CP and studied with methods such as thermodynamic approaches created by Kedem and Spiegler (1996). For the molecules larger than the membrane pore size, such as silica or macro organic matter, the decline of the permeate flux could be used to describe the CP, such as Sherwood correlation or filtration model (Sablani et al., 2001). In addition, several new technologies have occurred these years, such as using holographic interferometry to visualize the polarization layer (Fernández-Sempere et al., 2009), or the method by analysing the post steady state transient data to identify the flux-controlled factor (Zaidi et al.,2004). However, all these methods or models have their own limitations. One of the most important reasons is that the empirical model or equation may sometimes not be suitable for several experiments and extra constant calibration should be done before executing the experiments. Even though Gel-polarization model is one of the most popular models, the difficulty in separating CP and fouling hinders its application in practice. Therefore, it is essential to modify a model or adjust the constant in the empirical model according to the practical situation.

1.3. Research questions

The main objective of this research is to investigate the flux decline and CP during ceramic nanofiltration for polyethylene glycols (PEGs), silica, and phosphate retention. Silica was investigated since it is an important precursor of the well-known modifier, zeolite. However, silica could produce a thick cake layer near the membrane surface which can influence the model calibration. PEGs which have a low potential for forming a cake layer were chosen to calibrate the model instead. Since phosphate is one of the main objectives in sewer mining concept, it could be interesting to investigate the influence of CP and CECP on phosphate retention.

The whole research is divided into two parts, one part is focusing on the flux decline and CP factor of PEGs and silica, which have larger molecule size than the membrane pore size. Another part is investigating the influence of CP and CECP on phosphate (whose molecule size is smaller than the membrane pore size) retention. From the research objectives, detailed research questions

were formulated:

For the flux decline and CP effect of PEGs and silica

1. What is the control factor (CP or fouling) in flux decline under different operational conditions?

2. How to modify the Gel-polarization model to make it suitable for investigating CP and fouling with measured data? And what are the advantages and disadvantages of the modified Gel-polarization model?

3. How to calibrate the constants in the Sherwood model and what is the calibrated equation? And what are the advantages and disadvantages of the Sherwood model?

For the flux decline and CP&CECP effect of phosphate:

1. What are the influencing factors for CECP in phosphate retention by building a CECP model and making theoretical analysis?

2. Can the CP&CECP factor be calculated by the change of permeability/flux and is it the same with the theoretical model?

1.4. Outline of the thesis

In this study, the flux decline and CP during ceramic nanofiltration for PEGs, silica, and phosphate retention were investigated.

Chapter 2 describes the flux decline theory in the membrane filtration system for macromolecules whose sizes are larger than the membrane. Several flux decline models and relative mechanisms of CP and fouling are also presenting in this chapter. In addition, retention mechanisms of phosphate, as well as the influencing factors which containing CECP, were discussed in chapter3.

In chapter 4, a modified Gel-polarization model for PEGs and silica based on the flux decline and recovery is presented. A CECP model for phosphate was built based on the Sherwood relation and the characteristics of the fouling layer.

Chapter 5 describes the research approach, experiment materials and the methods for PEGs, silica, and phosphate retention.

Chapter 6 shows the results and discussions for PEGs and silica, including the flux decline, fouling formation, CP factor calculation and Sherwood constant calibration. Results of phosphate retention and the CP&CECP factors are presented in chapter 7.

Conclusions were drawn based on the results for PEGs, silica and phosphate in chapter 8. Relative recommendations for further investigation are also presented.

2 Literature review on PEGs & silica filtration

2.1. Macromolecules

Macromolecules, containing proteins, silica, PEGs, refer to large molecules usually created by the polymerization of smaller monomers. In practice, ultrafiltration membranes with a MWCO of 1-300 kDa are suitable for filtrating macromolecules (Bacchin et al., 2002).

2.1.1 PEGs

In order to investigate the retention of macromolecules in the ultrafiltration process, PEGs have often been chosen as standard macromolecules (Ganguly & Bhattacharya, 1994). As it is reported by Ghose et al. (2000), PEGs do not form a thick precipitate or gel on the membrane and can be used in commercial applications. Moreover, PEGs are organic without ion charge which can exclude the rejection caused by electrostatic adsorption or repulsion, happening between the solute and the membrane (Blanc et al., 1998; Sarrade et al.,1994). Additionally, the molecular weight (MW) of the PEGs is able to be controlled, which provides more possibility for investigating the filtration behaviour with the MW of the solute.

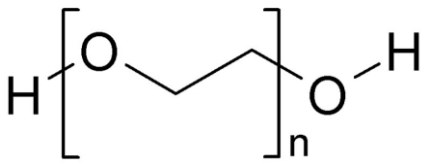

Figure 2. 1 *PEGs general structural formula*

Physical properties of PEGs vary from different molecular weights due to the chain length effects. The status at room temperature is different, liquid (PEG 200–600), semisolids (PEG 1470), semi crystalline solids (PEG 3000–20000 and above) and resinous solids for higher molecular weights (>100 000) (Majumdar et al., 2010). PEG is known for its high-water solubility which can achieve 50 mg/mL H_2O (Sigma-Aldrich). PEGs are widely applied as adhesives, thickeners, contactlens fluids, stabilizers, friction reduction agents, plasticizers, solubilizing agents for drugs and matrices for fast-release dosage forms (Craig et al., 1995).It is reported by Brikov et al. (2016), a gel layer is formed by the interaction of a water–glycol solution of poly(ethylene glycol) (PEG) with calcium chloride dihydrate. The state of the PEGs' solution could be different with the presence of other ions or material.

2.1.2 Silica

Silica dioxide, also known as silica, is an oxide of silicon which has different structures and uses. Fumed silica also known as pyrogenic silica, is a kind of powder with an extremely low bulk density and high surface area which is widely used as a thickening agent and anticaking agent (Flörke, et al., 2000). Fumed silica is made from flame pyrolysis of silicon tetrachloride ($SiCl_4$) or from quartz sand vaporized in a 3000 °C electric arc furnace (Garrett, 1992). A colloidal silica suspension is stable because of the electrostatic repulsion between the nanometer-sized silica particles (Gauthier et al., 2007). As it is reported by Qomariyah et al. (2018), stable colloidal silica can be prepared by removing the sodium ion of sodium silicate via ion-exchange to obtain active silicic acid which is then titrated with a potassium hydroxide (KOH) solution to form the colloidal silica.

The solubility of silica dioxide in water strongly depends on its crystalline form (Vivero-Escoto, 2011). For colloidal silica, the suspension is unstable under a low pH and high ion strength. The suspension concentrating process is usually achieved by adjusting pH and by evaporation. The maximum concentration in suspension depends on the particle size. For example, the suspension can be concentrated to more than 50% with a particle diameter larger than 50nm, while it is only able to achieve 30% with a diameter of 10nm (Manufacturer indiamart).

2.2. Fouling mechanisms

In the last three or four decades, several researchers have been focused on the fundamental theories of solute accumulation. The most popular explanation for the flux decline with time which was supported by Bhattachajee &Bhattacharya (1993), contains two mechanisms. The first one is CP, refers to the retained liquid-solute and the increased osmotic pressure on the membrane. The second one is fouling, and most of which contains adsorption, pore-blocking, deposition and formation of a gel layer which are generally considered to be irreversible. As a result, the flux decreases by the increasing filtration resistance.

Earlier studies attributed fouling mainly to pore blocking and cake layer formation (Hermia,1982; Davis,1992). Pore blocking can increase the membrane resistance while the cake layer formation can add an additional resistance layer on top of the membrane. Vela et al. (2008) divided the pore blocking effect into three basic types according to their behaviours: complete blocking, intermediate blocking and standard blocking (Figure 2.2). Their research showed that the fouling mechanism depends on the operational conditions and all these three mechanisms and the cake layer formation could happen at the same time during the ultrafiltration of the PEG molecules.

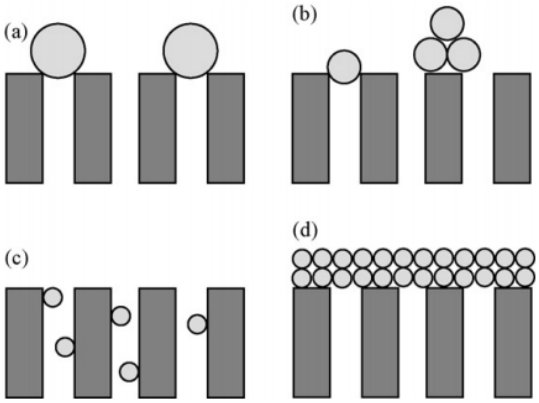

Figure 2. 2 *Illustration of the fouling mechanisms considered by the models: (a) complete blocking; (b) intermediate blocking; (c) standard blocking and (d) cake layer formation. (Vela et al.,2008)*

According to Song (1998), based on the fouling mechanisms, the whole flux decline process can be divided into three stages: a) starting by a rapid permeate flux drop from the initial permeate flux, b) following by a continuously slow flux decline in long-term process, c) ending with steady-state flux (Figure 2.3). They mentioned that in the first stage, the dominant process is pore blocking since less than one layer of the particle is enough to achieve the obvious flux decline. The growth of cake layer thickness is a slow process which should be the main reason for the gradual decline in the second stage. Experiments carried out by Fernández-Sempere et al. (2009), who were using PEG-10000 as the feed solution in dead-end ultrafiltration, showed similar results. The flux decline was much faster during the first few minutes and became slow with time. Further they mentioned that in the dead-end system to achieve the final stationary state takes far more than 1 hour.

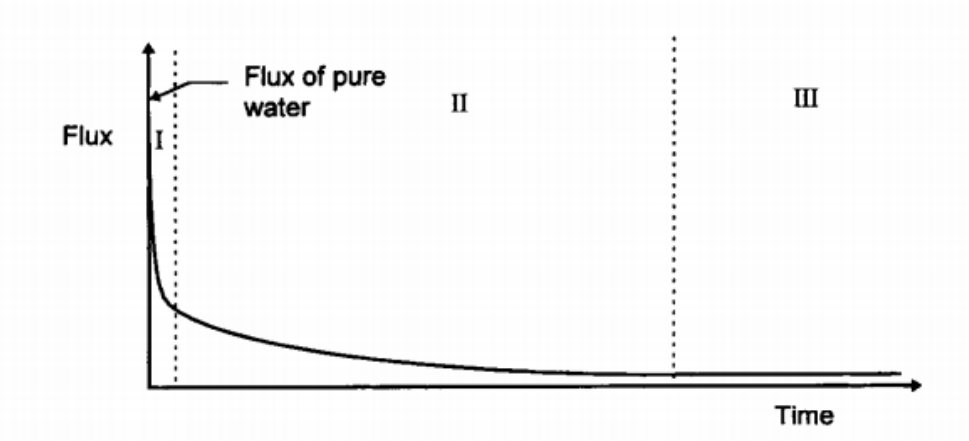

Figure 2. 3 a*) starting by a rapid permeate flux drop from the initial permeate flux, b) following by a continuously slow flux decline in a long-term process, c) ending with steady-state flux. (Song,1998)*

Based on the theory of Song (1998), Bacchin et al. (2002) proposed a model to describe the flux decline during a cross-flow filtration of colloids and divided the fouling layer, or irreversible layer, into two mechanisms, the gelation mechanism and the deposition mechanism. A loose layer with a low fractal dimension was formed by gelation, while a compact ordered deposit layer was formed by deposition. In addition, experiment carried out by Shang et al. (2015) demonstrated

that humic substances and biopolymers in surface water can cause the irreversible fouling. During the filtration of proteins, such as bovine serum albumin (BSA), a deposited layer, which is irreversible, can be formed (Opong & Zydney, 1991).

During ultrafiltration of PEGs (molecules larger than the membrane pore size), the deposition mechanism can be described by the formation of a compact deposit layer which is also called a gel layer. However, Bhattacharjee &Datta (2003) suggested that the gel layer was not formed during their experiments, using PEG-6000 as the feed solution, being ultrafiltrated by a membrane with MWCO of 5000 Da. The formation condition of a gel layer is that the membrane surface concentration should exceed the solubility of the PEG. The data showed in their experiments never exceeded its solubility. The same conclusion can be drawn during the Dextran experimental data conducted by Karode (2001). Instead of the gel layer, the group of Bhattacharjee proposed a ‘gel type’ layer to describe the irreversible layer, which is consistent with the theory of gelation.

Based on the adsorption theory, Churaev et al. (2005) created a model to describe the relationship between adsorption of PEG molecules inside the pores of an ultrafiltration membrane and the flux decline during the filtration. However, the major limitation of this model is that it focuses on the adsorption inside pores and introduces a reflection coefficient, which means that the model is only suitable for the particle smaller than the membrane pore size. In addition, the mass transfer coefficient is based on an empirical formula and could probably not be suitable for different other practical conditions. These limitations could highly influence the application of the model in complex and unstable systems. However, an interesting point of view is that he described the adsorption as reversible fouling which means after backwashing or water flushing, the permeability of the membrane could be recovered. Nikolova and Islam (1998), in their experiments of ultrafiltration with dextran, also found that flux decline is governed by the effect of both CP and adsorption, both of which are reversible. Due to the fact that the osmotic pressure is quite small resulted from the large MW of dextran, the adsorption effect was found to have a decisive role in the filtration. These results are only able to be obtained under no-fouling or no gel layer formation conditions. For different molecules, such as PEG with a relatively small diameter, the influence of osmotic pressure could be obvious, and the explanation is not suitable.

Fernández-Sempere et al. (2009) used real-time holographic interferometry to visualize the polarization layer during dead-end ultrafiltration of PEG-10000. The results from their experiments showed the existence of an reversible adsorption process on the membrane surface. However, as reported by Cherkasov et al. (1995), the recovery of membrane permeability, as well as the reversibility of the adsorption layer, is determined by the relative thickness of the adsorbed polymer layer.

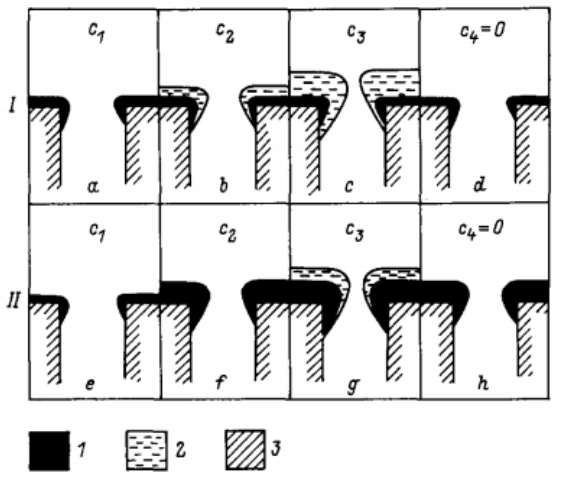

Figure 2. 4 *Gel layer formation on the surface of an ultrafiltration membrane from (I) hydrophilic and (II) hydrophobic material [C is solute concentration, C1 < C2 < C3], (1) adsorption layer, (2) Gel-polarization layer, (3) membrane material. (Cherkasov et al.,1995)*

In Figure 2.4, it is shown that a thicker irreversible adsorption layer is more attracted by hydrophobic membrane than by hydrophilic membranes. Moreover, the membrane hydrophilicity does not influence the membrane selective properties, while the intensity of CP does. Also, the reversibility of the fouling layer could result from the membrane material. In general, organic membranes, such as cellulose acetate membranes, used by Fernández-Sempere, have more chances for adsorption than inorganic membranes due to the larger contact angle (more hydrophobic) of the polymeric membrane (Xu, 2008)

2.3. CP during flux decline

In addition to the fouling during flux decline, CP is also of importance. CP refers to a solute gradient on the membrane interface which leads to an increasing concentration on the membrane surface (Verberk,2015). Osmotic pressure difference ($\Delta\pi$) is a parameter to describe the difference in concentration of solutes in feed and permeate due to the retention of solutes by the membrane.

$$\Delta\pi = \pi_m - \pi_p \tag{2.1}$$

Where π_m is the osmotic pressure on the membrane and π_p is the osmotic pressure in the permeate. A higher osmotic pressure difference across the membrane can produce a stronger driving force for the solute passing through the membrane which leads to a lower retention.

Even though the CP is inevitable, it can be reduced by adjusting the operating conditions and a proper design of the filtration system (Bhattacharjee & Datta,2001). One of the most influencing operational factors is the transmembrane pressure (TMP or ΔP). From the results of several researchers (Zaidi et al., 2004; Song,1998), within a certain range, CP is increasing with an increasing operational pressure. As it is described by Bacchin (2002), the flux increases under increasing TMP, resulting from the increased driving force. But after a first stage, the flux remains stationary with further increased pressure, and this stationary flux is called limiting flux.

Bhattacharjee (2001) suggested that a gel layer is often formed under the limiting flux circumstances. The critical flux which is a criterion for the transition between CP and fouling is therefore used to describe the point where the irreversible fouling layer is formed. Therefore, in order to control the fouling mechanisms or decrease the CP factor, transmembrane pressure could be a crucial parameter. There are also other parameters which can influence the CP models, such as hydrodynamic condition (cross-flow velocity) and the solute characteristic (particle size, viscosity) (Schulz & Ripperger,1989).

2.4. Basic flux decline model

Several basic models have been developed to describe the flux decline in membrane filtration systems in the last century. The three most famous models, based on different theories, are 1) resistance in series; 2) osmotic pressure;3) Gel-polarization model (Makardij et al.,2002).

2.4.1 Resistance in series model

In the resistance in series model, the decline in flux is because of various, additional resistances, such as membrane resistance, fouling resistance, adsorption resistance, and CP resistance. One possible resistance in series model is shown in equation 2.2.

$$\mathrm{J} = \frac{\Delta P}{\mu(R_m + R_{cp} + R_f)} \tag{2.2}$$

where, J is the permeate flux, ΔP is the transmembrane pressure, μ is the dynamic viscosity, and R_m ,R_{cp} and R_f are the hydraulic membrane resistance, CP resistance and fouling resistance, respectively. Even though the model can describe several resistances occurring during the filtration, the model is not easy to apply in practice (Song,1998). The biggest obstacle is that there is no well-known method to describe or measure the factor R_{cp} directly. The CP resistance is based on the concentration of solute accumulated near the membrane, which is a function of the permeate flux. Since the fouling factor is also a function of the permeate flux, it is not possible to separate these two factors.

2.4.2 Osmotic pressure model

Unlike the hard-measurable factor R_{cp}, a constant pressure drop in the CP layer, developed by Song and Elimelech (1995), is able to be defined by the thermodynamic properties. Later on, the osmotic pressure has been used to describe the pressure drop across the membrane due to concentration difference (Denisov,1994). The permeate flux based the on the filtration model is given by equation 2.3.

$$\mathrm{J} = \frac{\Delta P - \Delta\pi}{\mu R_m} \tag{2.3}$$

Where, $\Delta\pi$ is the osmotic pressure difference across the membrane. However, one limitation of the model is that the only variable which can influence the flux is the osmotic pressure. This

means that the model is only suitable for those studies using high soluble macromolecule as feed solution, without fouling occurring during the filtration process (Choe et al., 1986). Therefore, relative models based on the same theory are also called osmotic-pressure- controlled (OPC) model.

It is reported by Stanley and Strey (2003), that the influencing factor of PEG's osmotic pressure is not only the concentration of the solute, but also the temperature and molecular weight. The results showed that the osmotic pressure of PEG decreases as the temperature increases, which is because of the release of structured water molecules from the polymer chain. The osmotic pressure of the solution with the same weight percent of PEG400 and PEG8000 showed a huge difference (PEG400 has a much higher osmotic pressure). That is because the weight percent is not able to represent the molecule concentration. All these factors need to be taken into account when designing a proper experiment to demonstrate the CP phenomenon.

2.4.3 Sherwood film theory model

The model developed by Sherwood shows another method to value the CP effect which also reflects the theory of osmotic pressure control. A concentration profile of the membrane is established within a boundary layer generated by the hydrodynamic conditions (Figure 2.5). The convection transport is caused by the pressure gradient across the membrane, while the diffusion transport is caused by the higher concentration at the membrane surface than in the bulk. At 他 the steady state condition, a mass balance on the membrane surface can be achieved.

$$\mathrm{Jc} = \mathrm{D}\frac{dc}{dy} + Jc_p \tag{2.4}$$

where c and c_p are the solute concentration in the boundary layer and in the permeate, D is the diffusion coefficient of the solute in the solvent and y is the distance from the membrane surface. Integration of this equation with the boundary conditions. $\mathrm{x} = 0$, $\mathrm{c} = c_m \ and \ X = \delta$, $c = c_b$ resulted in the film model theory,

$$\frac{c_m - c_p}{c_b - c_p} = \exp\left(\frac{J\delta}{D}\right) = \beta \tag{2.5}$$

where δ is the thickness of the boundary layer and β is the CP coefficient. The ratio between D and δ is called mass transfer coefficient (K).

$$\mathrm{K} = \frac{D}{\delta} \tag{2.6}$$

The flux due to diffusion only depends on the diffusion coefficient, which is given by Fick's first law. It can be understood as the magnitude of the molar flux through a surface per unit concentration gradient out-of-plane (COMSOL). Therefore, in a specific dilute solution under the same condition, the diffusion coefficient is the same. It makes it possible to calculate the CP factor by directly measuring the film layer thickness with optical or microelectrode equipment. However, the direct thickness measurement usually needs to be conducted with a running filtration system and has a high requirement of the related equipment (Bader & Veenstra,1996). Thus, an indirect, estimative method for the mass transfer coefficient is needed.

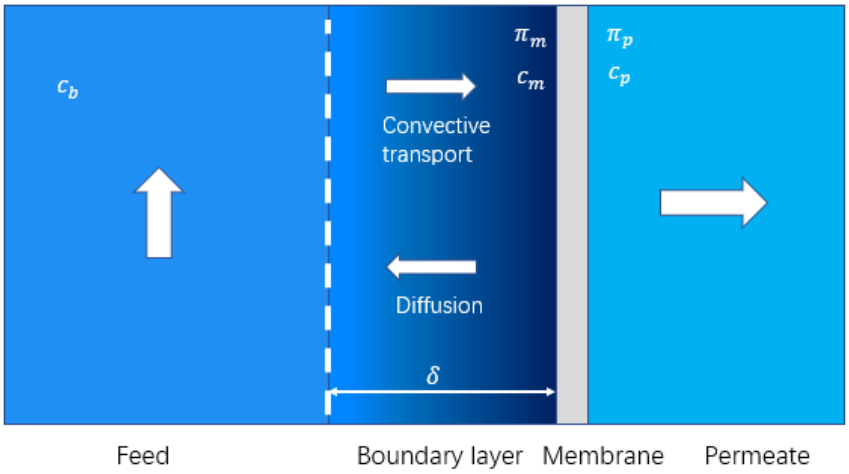

Figure 2. 5 *Virgin membrane filtration profile with CP parameters and the main transport mechanisms.*

The mass transfer coefficient can be described by the Sherwood relationship which contains Sherwood number (Sh), Reynolds number (Re) and Schmidt number (Sc). This correlation has the empirical form which is similar to Chilton-Colburn analogy (Bader and Veenstra,1996)

$$\mathrm{Sh} = \frac{K d_h}{D} = a\,\mathrm{Re}^b Sc^c \tag{2.7}$$

where d_h is the (tubular) hydraulic diameter of the membrane channel, a, b and c are empirical constants. The above mass transfer coefficient is derived from the nonporous smooth flow. The dimensionless Reynolds number is an important parameter to predict the flow pattern in different flow conditions. The definition of the Reynolds number is shown in equation 2.8.

$$\mathrm{Re} = \frac{u d_h}{v} \tag{2.8}$$

where v is the kinematic viscosity of the fluid, d_h is the (tubular) hydraulic diameter of the membrane channel. From the formula, we can derive that the Reynolds number strongly depends on the membrane dimension, hydrodynamic conditions and physical properties of the flow. In general, the Reynolds number below 2100 is defined as laminar flow, while larger than 4000 is turbulent flow. In laminar flow, the motion of the particles in the fluid is moving in straight lines parallel to the membrane surface (Noakes & Sleigh,2019) which is responsible for a stagnant layer near the membrane interface. As it is described by Déon et al. (2009), the thickness of the stagnant layer decreases as the cross-flow velocity increases in the filtration of the salt solution. It could be a good method to decrease the CP effect by increasing the cross-flow velocity, which is increasing the Reynolds number and transiting the flow pattern to turbulent flow.

The dimensionless Schmidt number is defined as the ratio of kinematic viscosity (v) and diffusion coefficient (D), see equation 2.9.

$$\mathrm{Sc} = \frac{v}{D} \tag{2.9}$$

The Schmidt number is used to describe the connection of both hydrodynamic layer and mass-transfer layer. The diffusion coefficient is a crucial constant for a solute in a specific dilute solution. For PEG molecules the diffusion coefficient is related to the MW. Usually, molecules with a higher

molecular weight have a smaller diffusion coefficient which means less diffusivity, leading to a relatively large CP under similar conditions (Sherwood et al.,1975).

Even though the mass transfer formula is widely used in pipe flow, the limitation of the formula was criticized by several researchers (Jonsson,1984; Belfort and Nagata,1985), since the roughness of the membrane and the change of flow properties by the CP are not considered. Therefore, a new friction factor f was introduced to the Sherwood formula, $\mathrm{Sh}{\sim}a\,\mathrm{Re}^{b}Sc^{c}\,f^{m}$. Especially in the turbulent flow (Re>10000), several experiments showed the constant m to be equal to 1 or 1/2. Several researchers suggested that there is no simple form of Sherwood equation for the region where 2300<Re<10000 and the mechanisms in this region are unclear (Gekas & Hallstrom,1987).

2.4.4 Gel-polarization model

Since fouling usually occurs during macromolecule filtration, the osmotic-pressure-controlled model is not suitable in most cases. Therefore, a model combining the theory of CP and fouling, called Gel-polarization model, and occurred, and is nowadays widely accepted in practice. Based on the filtration model, the theory can be formed as given in equation 2.10.

$$\mathrm{J} = \frac{\Delta P - \Delta\pi}{\mu(R_m + R_f)} \tag{2.10}$$

This model is most frequently used in explaining the experimental data and predicting the flux decline. However, as already reported by Porter (1972), the biggest problem of this model is that the concentration of the gel layer (gel type layer) is different in different experimental conditions, which makes it hard to predict the filtration behaviour in one specific condition.

2.5. Combined new model

With the enhanced comprehension of CP and fouling, many other, different methods and new models occurred to describe the flux decline.

The new method created by Zaidi et al. (2004) combined the Gel-polarization model and the differential equation with respect to time. The core point in their research is to calculate the actual filtration resistance by analysing post steady state transient filtration data which is obtained by opening a crack and decreasing the driving pressure as a function of time. Gel-controlled or osmotic-pressure-controlled filtration is then possible to be defined by analysing the data. However, the method did not consider the influencing factors of osmotic pressure, for example, cross-flow velocity should keep the same during the decreasing pressure process. In addition, the results showed several negative data with a high concentration of PEGs which is unconvincing in demonstrating the controlling factors.

As the development of the CP layer is much quicker compared to the development of a cake layer (Gel-type layer), several cake growth models with respect to time usually neglect the cp development (Song,1998). Therefore, the time-dependent flux is able to be modelled by

combining one type of the cake growth models and the fractions of the unblocked surface part at a specific time. Also, a combination of cake growth model and Gel-polarization model is possible to be used for the non-steady state (Vela et al.,2006). However, the results simulated by the model do not agree with all the experimental data which makes that the flux prediction by the model should be questioned. Moreover, the model is only suitable for the finite situation since the cake growth can lead to zero flux at an infinite time which is not realistic in a cross-flow module.

In addition to these models, other models are also popular in practice, especially in RO systems: combined diffusion-solution models with film theory, combined Spiegler-Kedem with film theory, velocity variation method with film theory, etc. These models are more suitable in investigating the CP effect of salt solutions, like saline water, and less suitable for macromolecules. A summarising diagram for the flux decline theory is given in Figure 2.6.

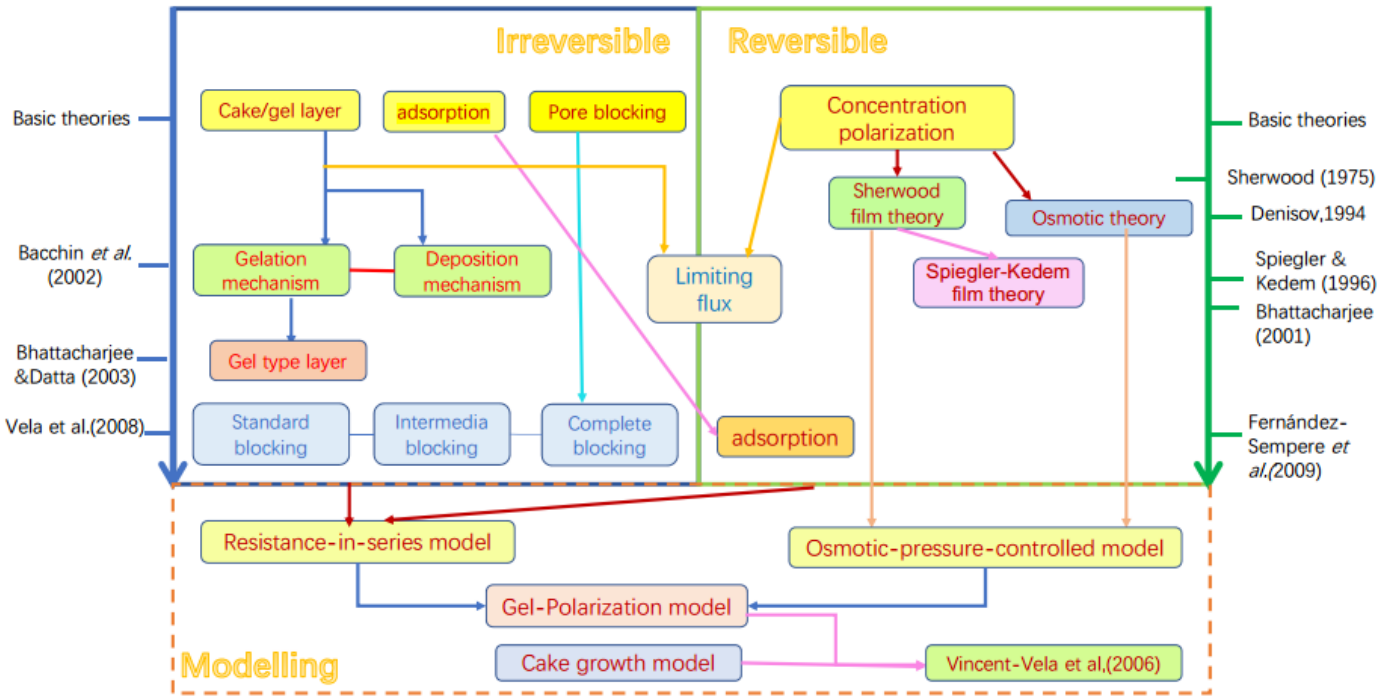

Figure 2.6 *Diagram for the flux decline theory*

3 Literature review on P filtration & CECP

3.1. Retention mechanisms for phosphate

The fundamental membrane retention mechanisms for ions or organics can be distinguished by steric hindrance (determined by pore size), electrostatic repulsion (determined by charge) and CECP (Heijman et al., 2007; Nghiem et al., 2010). As for phosphate, a detailed discussion is given below.

3.1.1 Steric hindrance

Steric hindrance is determined by the relative size of the membrane pore and the solute. MWCO is a property of the membrane to show the pore size by relating it to the solute weight. It refers to the lowest molecular weight that can be rejected for 90% by the membrane (Heijman et al., 2007).

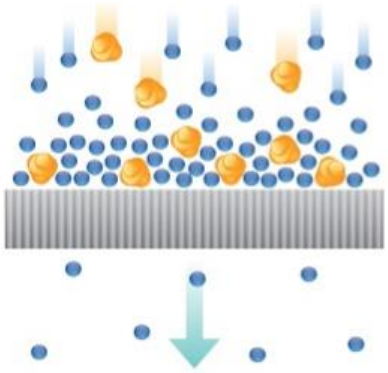

Figure 3. 1 *Steric hinderance mechanism (Synderfiltration,2019)*

It is reported by Shang et al. (2013) that phosphate cannot be rejected by ultrafiltration membranes by only steric hindrance. For clean 1kDa tight ceramic UF membrane, the membrane pore size (1.77nm) compared to the hydrated size of $H_2PO_4^-$ (0.102nm) or HPO_4^{2-}(0.129nm) is much larger. From the experiment carried out by Shang et al.(2014), compared to the virgin membrane, the retention rate of the phosphate increased with the presence of effluent organic matter (EfOM), while the rejection rate decreased with the presence of EfOM and Ca^{2+}.If the retention rate was determined by the steric hindrance alone, the organic fouling would lead to pore blocking and the retention rate should increase. However, the decreasing phosphate retention rate with the presence of EfOM and Ca^{2+} means that steric hindrance was not the dominant mechanism.

3.1.2 Electrostatic repulsion

Electrostatic repulsion is therefore considered as playing an important role in phosphate retention by ultrafiltration membranes. Ceramic membranes are negatively charged (pH=7, -31.1+-1.3 mV) due to the dissociation of functional groups both on the membrane surface and inside the membrane pores (Heijman et al, 2007; Shang et al.,2014). According to Donnan equilibration

theory (Donnan,1995), when the solute passing through the membrane, the negatively charged membrane tends to attract cations on the membrane surface and reject the anions. Therefore, the concentration of anions decreases on the membrane surface which reduces the chances of passing through the membrane. In Figure 3.2 (a) a schematic representation of electrostatic repulsion is given. In Figure 3.2 (b) the decrease of potential of the wall is shown as the distance from membrane increases (electrical double layer structure).

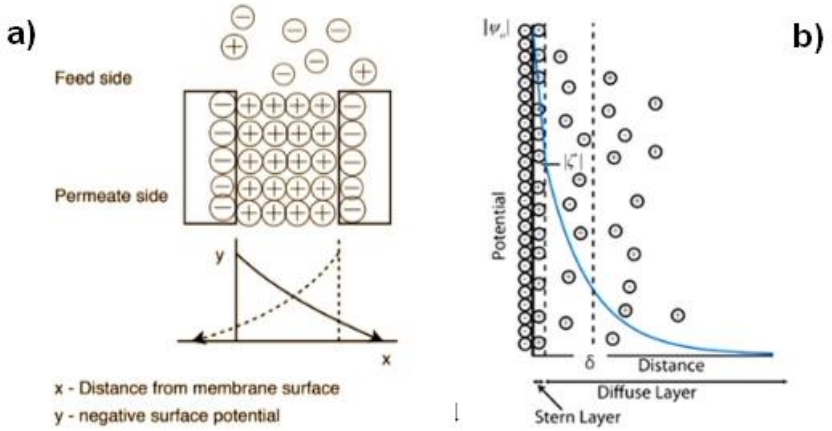

Figure 3. 2 *a) electrostatic repulsion for a negatively charged membrane b) potential of the wall decreases as the distance from membrane increases (Web.mit.edu, 2018)*

3.1.3 Concentration polarization

For molecules smaller than the membrane pore size, like phosphate, as long as the membrane has a certain retention function to the solute, solute accumulation can occur near the membrane which leads to CP. The concentration difference between the membrane surface and the permeate can create an extra driving force which pushes more solute through the membrane and decreases the retention of the solute. As it is reported by Sherwood (1975), for ions, CP could also be a reason for the flux decline. Therefore, the parameters which can represent or evaluate the influence of CP could be both flux decline and the change of solute retention rate.

Since the resistance model has several limitations, the combination of film theory and the osmotic pressure became an alternative method. The film theory (equation 2.5) can be rearranged to equation 3.1:

$$\Delta\pi = f_{os}\left(c_m - c_p\right) = f_{os} c_b R_o \exp\left(\frac{J}{K}\right) \tag{3.1}$$

where f_{os} is an osmotic coefficient that converts salt concentration to osmotic pressure, $R_o (= 1 - \frac{c_p}{c_b})$ is the retention rate. Rearrangement of equation 2.5 again, an estimation of CP modulus can be provided based on rejection rate,

$$\frac{c_m}{c_b} = (1 - R_o) + R_o \exp\left(\frac{J}{K}\right) \tag{3.2}$$

The mass transfer correlation K can be calculated based on the Sherwood relationships. f_{os} can be determined by van't Hoff equation if low-to-moderate salt concentrations are used(Hoek et al., 2002). For 1:1 electrolyte like sodium chloride, f_{os} is 2RT (R is the universal gas constant and T

is the absolute temperature). However, $\frac{c_m}{c_b}$ cannot fully represent the CP coefficient β if the concentration in the permeate is not negligible. Another limitation is that for multi-valent ions or mixed solutions, the expressions of f_{os} are difficult to determine and extra measurements are needed.

3.2. Influencing factors for phosphate retention

Since the mechanisms of phosphate retention are complicated, there are several factors that can influence phosphate retention, such as fouling, concentration of the solute, pH, ion strength, CECP, etc.

The charge of the membrane is represented by zeta potential which varies with different pH. The membrane material is TiO_2 and the following reaction takes place with a pH higher than the iso-electric point (Shang et al., 2014),

$$\equiv \mathrm{Ti} - \mathrm{OH} + \mathrm{OH}^- \rightarrow \equiv \mathrm{Ti} - \mathrm{O}^- + \mathrm{H_2O} \qquad (3.1)$$

When the pH is higher, the concentration of OH^- in the solution increases and the reaction tends to right which will lead to a more negatively charged zeta potential. When the pH is lower than the iso-electric point, a positively charged membrane can be obtained. It is also worth noting that often the Lewis acid site will play a role for the charge of the ceramic membrane. A more negatively charged membrane can be achieved through interaction with neighboring hydroxyl groups, which makes these hydroxyl groups more acidic (Shanefield, 1995). It is reported by Shang et al. (2014) that the effect of pH on phosphate retention results from the changing surface charge. At a higher pH, a more negatively charged membrane attracts more positively charged ions accumulated on the pore surface. At the same time, the negatively charged ions are partly excluded from the surface. In addition, the valent of phosphate changes from monovalent to divalent as pH increases. Divalent phosphate will lead to a stronger electrostatic repulsion and a higher phosphate retention.

The presence of divalent ions and ion strength in the feed could also influence the phosphate retention. When the ion strength is high, the double layer on the membrane surface is compressed which leads to less phosphate retention (Shang et al.,2014). As for the presence of divalent anions, such as $\mathrm{SO_4^{2-}}$, co-ion competition could happen. Since the retention of ions is governed by the convection and diffusion, the ions with high diffusion coefficient have more chances to diffuse back to the bulk solution, while the ions with low diffusion coefficient are dragged into the permeate due to the electroneutrality effect. Therefore, a low retention for phosphate occurs. If the solution is full of divalent cations, like calcium, the cations can accumulate on the membrane surface which influence the charge of the membrane and decrease the electrostatic repulsion.

When there are some macromolecules or organic matters exist in the feed, several possible mechanisms occur which could influence the phosphate retention. Organic matters usually have larger molecules than the pore size of the nanofiltration membrane. Due to pore blocking, adsorption and cake layer formation, the effective pore size of the membrane is decreasing, which can decrease the flux and increase the effect of steric repulsion. Moreover, molecules with

positive or negative charges can influence the membrane surface charge and then make the electrostatic repulsion become weaker or stronger. Also, as it is reported by Mahlangu (2014), the presence of the cake layer or fouling could enhance the CP effect which will decrease the phosphate retention rate dramatically.

3.3. Cake-enhanced concentration polarization

Numerous studies have been reported that the fouling on the membrane can cause the decline of permeate flux and the decline of retention rate of ions or organics (Shang et al.,2014; Vogel et al.,2010; Mahlangu et al.,2014). Bellona et al. (2010) and Vogel et al. (2010) linked the phenomena to the mechanism of cake-enhanced concentration polarization (CECP) in addition to the hydraulic resistance (pore blocking). CECP is a phenomenon that the organic fouling on the membrane hinders the back-diffusion of solute from the membrane surface to the feed stream which leads to the increasing concentration on the membrane surface. The existence of organic fouling can increase the effect of CP greatly and lead to a lower retention of solutes (Figure 3.3).

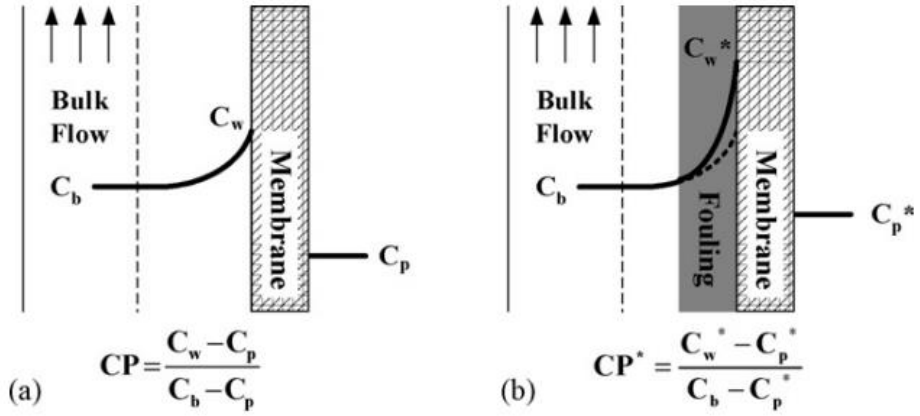

Figure 3. 3 *CP in a reverse osmosis membrane system. (a)before membrane is fouled and (b) after membrane is fouled. (Chong et al.,2007)*

Since CECP can influence the permeability of membrane, it is possible to investigate CECP by studying the change of permeability on the fouling membrane with and without ions in the feed. Results from Kramer (2019) showed that a clear permeability drop after injected phosphate to the feed. The most possible explanation for the drop is CECP. However, accelerated pore blocking process and the increased fouling resistance could also be an explanation. Therefore, more experiments need to be carried out to exclude the influence of pore blocking. Based on the fact that CECP is a reversible process, while pore blocking is not, a recovery of permeability can be expected after changing the feed from the phosphate solution to demineralized water.

Plenty of previous studies focused on the natural organic matter (NOM) fouling instead of EfOM (Heijman et al.,2007; Mahlangu et al.,2014; Bellona et al.,2010). The main difference between these two foulants is that the NOM mainly consists of humic substances while EfOM contains soluble microbial products and polymeric substances. The composition difference can produce more complicated effects. The bridging effect between the biopolymer and the present

multivalent-cations can lead to phosphate adsorption by polymers (Eberhardt & Min, 2008). This process can decrease the phosphate concentration in the feed and increase the retention in the end. To model the EfOM fouling, sodium alginate could be used.

Sodium alginate, known as a hydrophilic polysaccharide, is a kind of extracellular polymeric substances (EPS) produced by microorganisms (Katsoufidou et al., 2007). It is usually used to model the EPS fouling on the membrane filtration system on the lab scale (Frank & Belfort, 2003; Ye et al., 2005). As it is reported, EPS (also called macromolecular compounds) is responsible for membrane fouling in the wastewater treatment system (Laspidou& Rittmann, 2002.; Hao et al.,2013). Therefore, using sodium alginate to simulate the EfOM fouling is possible. However, the fouling performance of sodium alginate alone is not stable. The presence of multivalent cations, such as calcium, has a huge influence on the fouling structure (Hashino et al.,2011). Hashino et al. (2011) found that the flux decreased significantly with an addition of calcium chloride into the sodium alginate solution due to the thicker fouling layer. To achieve a stable fouling layer, calcium should be added in the sodium alginate solution. In addition, the cake layer caused by EPS showed an irreversible characteristic under long-term subcritical flux operation, according to Ye et al. (2005). It makes it possible to investigate the CECP effect based on its reversible property.

4 Modification of Gel-polarization model & CECP modelling

4.1. Modification of Gel-polarization model for PEGs and silica

Since it is hard to separate CP and fouling factors in the Gel-polarization model, a method based on the reversibility of CP and fouling was derived. In this method, the filtration process is divided into three stages and a modified Gel-polarization model is obtained.

First stage:

In the first stage, the demi water is filtrated by the clean membrane, and we can use the formula below.

$$\mathrm{J}_w = \frac{\Delta P}{\mu_w R_m} \tag{4.1}$$

Where ΔP is the transmembrane pressure, J_w is the permeate flux of demi water, μ_w is the dynamic viscosity of demi water and R_m is the hydraulic membrane resistance. The permeability of the membrane (P_w) can be defined as the inverse of hydraulic membrane resistance with demi water.

$$\mathrm{P}_w = \frac{1}{\mu_w R_m} = \frac{\mathrm{J}_w}{\Delta P} \tag{4.2}$$

Second stage:

In the second stage, the target solution/suspension (PEGs /silica) is filtrated by the membrane, an extra osmotic pressure difference and the resistance of fouling occur.

$$\mathrm{J}_t = \frac{\Delta P - \Delta\pi}{\mu_t (R_m + R_f)} \tag{4.3}$$

$$\mathrm{P}_t = \frac{1 - \frac{\Delta\pi}{\Delta P}}{\mu_t (R_m + R_f)} = \frac{\mathrm{J}_t}{\Delta P} \tag{4.4}$$

In this stage, the transmembrane pressure is the same as stage one and the R_m in the first stage is used. R_f is the resistance caused by the irreversible fouling. J_t, P_t, and μ_t are permeate flux, permeability from experiment and dynamic viscosity of target solution, respectively. The two unknown parameters are R_f and $\Delta\pi$

Third stage:

In the third stage, the same transmembrane pressure is used. The feed solution is changed from

target solution to demi water. During this process, the concentration gradient on the membrane surface is eliminated which means that there is no osmotic pressure difference, but irreversible fouling still exists. Flux recovers (subscript r) in a certain degree.

$$J_r = \frac{\Delta P}{\mu_w (R_m + R_f)} \tag{4.5}$$

$$R_f = \frac{\Delta P}{J_r \mu_w} - R_m \tag{4.6}$$

$$P_r = \frac{1}{\mu_w (R_m + R_f)} = \frac{J_r}{\Delta P} \tag{4.7}$$

In the third stage, the fouling resistance can be calculated and then, the $\Delta\pi$ in stage two can be calculated.

The final combined equation could be derived.

$$\Delta\pi = \Delta P - J_t\, \mu_t (R_m + R_f) = \Delta P - J_t\, \mu_t \frac{\Delta P}{J_r \mu_w} = \Delta P (1 - \frac{J_t\, \mu_t}{J_r \mu_w}) \tag{4.8}$$

If the difference of dynamic viscosity between the target solution and demi water can be neglected, equation 4.8 can be simplified as equation 4.9.

$$\Delta\pi = \Delta P \left(1 - \frac{P_t}{P_r}\right) \tag{4.9}$$

According to the definition of CP and Formula 2.1, the CP factor (β) can be calculated by equation 4.10.

$$\beta = \frac{\pi_m}{\pi_f} = \frac{\Delta\pi - \pi_p}{\pi_f} \tag{4.10}$$

This method is suitable for calculating the CP factor of a solution with a known osmotic pressure in the feed, or there is a specific relation between the solute concentration and osmotic pressure. Moreover, this method is only suitable for the situation that the flux decline is caused by the reversible CP and irreversible fouling. If there is an extra reversible fouling, like reversible adsorption, the modified Gel-polarization model is not suitable anymore.

4.2. CECP modelling for phosphate

The model built for CECP for phosphate is mainly based on the theory of Sherwood, resistance model, and cake layer theory. Relative theoretical analysis for the model was presented in chapter 7.1. Due to the limitation of the experiment, the model built in chapter 4.2 was not used to explain the experiment.

4.2.1 Sherwood film theory

As it is discussed in chapter 2.4.3, Sherwood film theory is suitable for osmotic-pressure-controlled filtration process. As for phosphate, since the diameter of ion is much smaller than the membrane pore size, there is no obvious fouling like pore blocking or cake layer formation during the filtration. Therefore, Sherwood is suitable for describing CP for phosphate. One of the main problems in using Sherwood is that, the empirical formula may not be suitable for specific situation.

In practice, an extra constants calibration should be done before the experiment. Here, the empirical formula is used as an example to show the model building process. There is an empirical relationship available for tubular membrane based on eddy diffusion models (Notter & Sleicher, 1971; Gekas & Hallstrom,1987).

$$\mathrm{Sh} = 0.0149\ \mathrm{Re}^{0.88} Sc^{0.33} \qquad (Sc > 100) \tag{4.11}$$

Combine equation 2.5-2.9, the model for the clean membrane is shown below

$$\beta = \exp\left(\frac{J}{K}\right) = \exp\left(\frac{J\ d_h}{0.0149\ \mathrm{Re}^{0.88} Sc^{0.33}\ D}\right) = \exp\left(\frac{J \cdot {d_h}^{0.12} \cdot v^{0.55}}{0.0149\ u^{0.88} \cdot D^{0.67}}\right) \tag{4.12}$$

$$d_h = \frac{4A}{P_w} = \frac{4\pi r^2}{2\pi r} \quad = 2r \tag{4.13}$$

where d_h is the (tubular) hydraulic diameter of the membrane channel, A is the membrane cross-section area, P_w is wetted perimeter and r is the radius of the channel. From the equation 4.12, we can see that CP factor is only influenced by the cross-flow velocity, permeate flux for a tubular membrane and the temperature (influenced v).

$$v = \frac{\mu}{\rho} \tag{4.14}$$

$$\mu = \frac{497 \times 10^{-3}}{(t + 42.5)^{1.5}} \qquad (Roorda, 2004) \tag{4.15}$$

where ρ is the density of the feed solution and t is the feed water temperature (°C). This model is suitable for describing the CP on a clean membrane. On the fouled membrane, the value of D and d_h(r) are changed. More parameters need to be assumed based on the fouling condition.

4.2.2 Resistance model theory

For the fouling membrane in the resistance model, the total resistance can be described by the sum of membrane resistance (R_m) and the cake layer resistance (or irreversible deposit of solute) R_f. The resistance of fouling layer according to the filtration theory can be written as equation 4.17

$$\mathrm{J} = \frac{\Delta P - \Delta\pi^*}{\mu(R_m + R_f)} \tag{4.16}$$

$$R_f = \alpha \frac{M_d}{A_m} \tag{4.17}$$

where $\Delta\pi^*$ is the osmotic pressure difference under fouling condition, α is the specific resistance of the deposit layer, M_d is the mass of deposit layer and A_m is membrane area. The value of α related to the spherical particles can be estimated by the Carman-Kozeny relationship (Carman,1938).

$$\alpha = \frac{180(1 - \varepsilon)}{\rho_p d_p^2 \varepsilon^3} \tag{4.18}$$

where ε is the porosity of the deposit layer, ρ_p is the density of the particle and $d_p$is the mean diameter of the particle. The deposit layer thickness δ_c is related to the deposited mass by equation 4.19.

$$\delta_c = \frac{M_d}{A_m \rho_p (1-\varepsilon)} \tag{4.19}$$

Combine equation 4.16-4.20, the transmembrane osmotic pressure on the fouling membrane can be written as equation 4.20.

$$\Delta\pi^* = \Delta P - J\mu R_m - J\mu \frac{180(1-\varepsilon)}{\rho_p d_p^2 \varepsilon^3} \cdot \frac{M_d}{A_m} \tag{4.20}$$

For a cycled system, the mass of fouling agent is decreasing in the feed tank results from the solute accumulaed on the membrane. Therefore, M_d can be obtained by a decreased mass in a certain period in the feed tank (Ng, H., & Elimelech, M., 2004; Hoek et al.,2002). The limitations of this method mainly exist in two aspects. On the one hand, the porosity of the deposit layer is unknown, or the deposit layer thickness is hard to measure. On the other hand, the model is only suitable for the known diameter of the deposit particle. For the sodium alginate, with the presence of calcium, it is quite hard to define the particle diameter.

4.2.3 CECP Model building

According to all these theories, a combination of Sherwood film theory and the resistance model is used to build this model. A diffusion coefficient (D^*) and mass transfer coefficient (K^*)in the fouling layer were used (Figure 4.1).

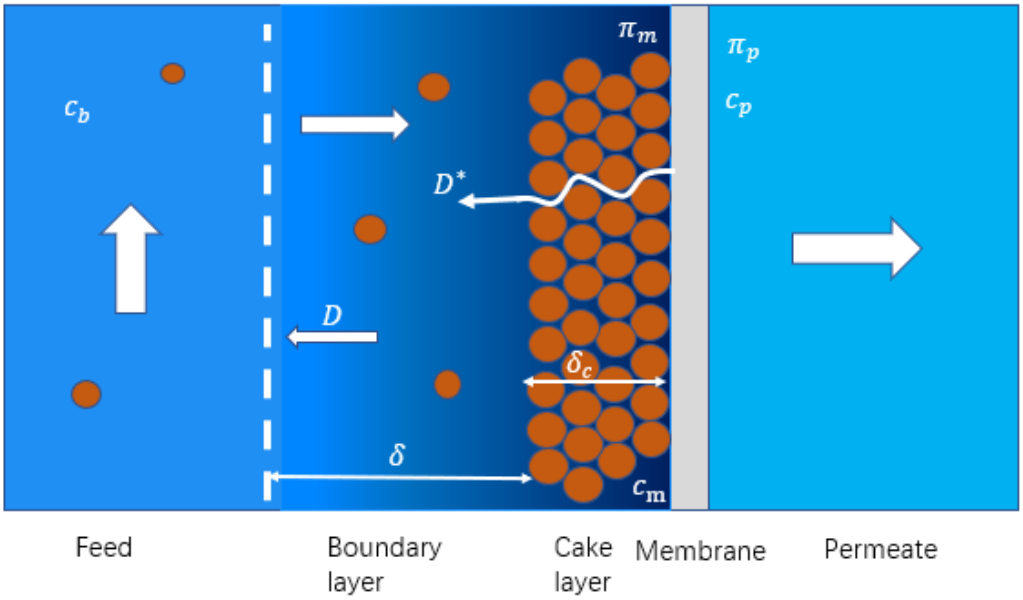

Figure 4. 1 *Fouling membrane filtration profile with CECP parameters*

The effective mass transfer coefficient K_{eff} can be seen as two parts, one describes the mass transfer through fouling layer by using K^*, the other describes the mass transfer from the fouling layer interface to the bulk solution K_s (Chong et al.,2008)

$$\frac{1}{K_{eff}} = \frac{1}{K_s} + \frac{1}{K^*} \tag{4.21}$$

$$K^* = \frac{D^*}{\delta_c} \tag{4.22}$$

$$D^* = \mathrm{D}\left(\frac{\varepsilon}{1 - ln\varepsilon^2}\right) \tag{4.23}$$

K_s can be calculated based on the Sherwood relationships or experiments of the clean membrane. δ_c is the fouling layer thickness. K^* can be recalculated from equation 4.21-4.23,

$$K^* = \frac{D^*}{\delta_c} = \frac{\mathrm{D}\left(\frac{\varepsilon}{1 - ln\varepsilon^2}\right)}{\frac{M_d}{A_m \rho_p (1-\varepsilon)}} = \frac{D A_m \rho_p (1-\varepsilon)\varepsilon}{M_d (1 - ln\varepsilon^2)} \tag{4.24}$$

Therefore, the CECP coefficient β_c can be calculated based on this equation.

$$\beta_c = \exp\left(\frac{J}{K_{eff}}\right) = \exp\left(J\left(\frac{{d_h^*}^{0.12} \cdot v^{0.55}}{0.0149\, u^{0.88} \cdot D^{0.67}} + \frac{M_d(1 - ln\varepsilon^2)}{D A_m \rho_p (1-\varepsilon)\varepsilon}\right)\right) \tag{4.25}$$

where d_h^* is the hydraulic diameter of the membrane under fouling condition. If the thickness of the fouling layer can be neglected compared to the membrane channel, the d_h^* is equal to 2r. If the influence of the fouling layer is significant, the d_h^* is 2r-2δ_c (δ_c from equation 4.19). However, the porosity of the cake layer is not able to be measured. For a fouled membrane, if the filtration is conducted under a constant pressure, cross-flow velocity, and no extra source of fouling agent, the porosity of the fouling layer should be constant. The porosity of a fouling layer can be assumed at first in the model to investigate the relation between parameters and β_c.

5 Research approach, Materials and methods

In this study, flux decline and CP during ceramic nanofiltration for PEGs, silica, and phosphate retention were investigated. A cross-flow filtration setup with ceramic nanofiltration membrane was used to carry out experiments. In order to make sure that PEGs and silica are well rejected by the membrane, MWCO was measured before executing further experiments. Membrane permeability measurement and membrane cleaning were carried out before and after solute filtration to make sure that the membrane is at the same condition before each experiment.

As for the PEGs and silica, filtration experiments were carried out based on the method discussed in chapter 4.1, simplified as ‘demi water - target solution - demi water’ filtration. The combination of the data obtained from experiments, the modified Gel-polarization model, and the Sherwood model can be used to investigate the control factor in flux decline and calibrate the constants in Sherwood. As for the phosphate, the same filtration method as PEGs and silica was used to investigate CP with a clean membrane. A ‘demi water - foulant - transitional solution – phosphate – demi water’ filtration method was used to investigate CECP in phosphate retention. An experiment with injecting calcium during phosphate retention with the clean membrane was used to see the effect of calcium on phosphate retention and CP.

5.1. Filtration Setup

The filtration setup was designed for cross-flow membrane filtration. The lab-viewed operational interface is shown in Figure 5.1. The feed solution for the membrane was from tank 1 or tank 2 with 2 L in volume. The setup was able to realize switching the feed tank without shutting down the pump. The transmembrane pressure and the cross-flow velocity were controlled by pump frequency (maximum 2790 rmp) and the concentrate valve. The concentrate from the membrane configuration recycled back to the feed tank, while the small amount of permeate from the membrane was collected and weighted as a function of time. The actual permeate flux was calculated based on the weighted data collected by the software Kern Balance Connection. The weighing balance with the precision of 0.01g is from Kern.

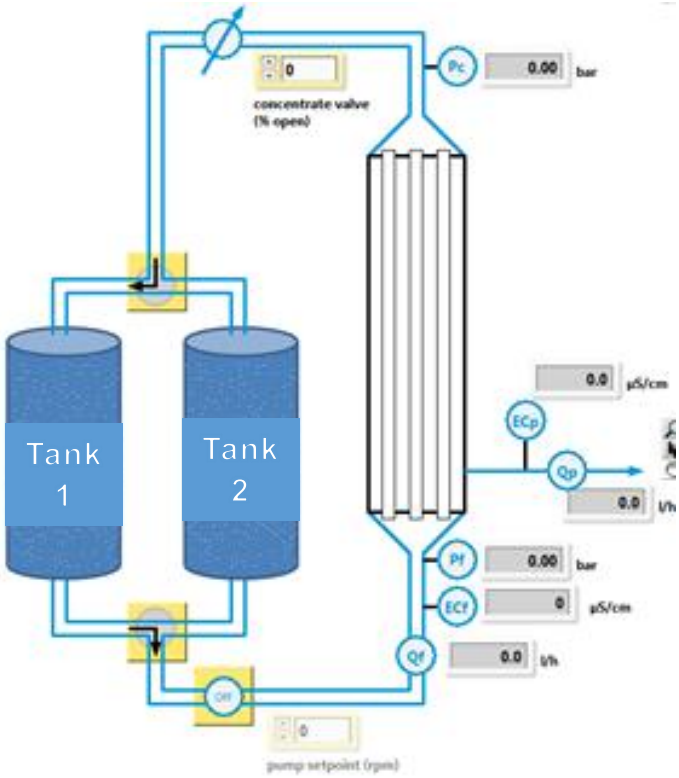

Figure 5. 1 *Cross-flow filtration setup*

5.2. Ceramic nanofiltration membrane

A commercial TiO_2 nanofiltration membrane provided by Inopor (Inopor GmbH, Germany) with an indicated MWCO of 450 Da and tubular single-channel configuration was employed in the experiment. The membrane has a mean pore size of 0.9 nm, 1 channel of 7 mm diameter and 100 mm in length, an open porosity of 30-40%, and an effective filtration area of $0.163 dm^2$ (Inopor, ceramic nanofiltration membranes). The membranes used in PEGs tests, silica tests, and phosphate tests were in different batches. Both ends of the membrane were sealed with silica which can decrease the chances of defect. The filtration was using inside-out mode with the module of PVC material (Figure 5.2).

Figure 5. 2 *a) ceramic nanofiltration membranes b) membrane house*

5.2.1 Membrane cleaning

Membrane chemical cleaning was carried out with a 0.2wt% (weight percent) sodium hypochlorite (NaClO) solution (2 hours) for the fouling produced by sodium alginate and MWCO measurement. NaClO solutions with 0.2wt% for 20min and 0.4wt% for 30min were used for the membrane after phosphate filtration and PEG filtration, respectively. NaOH with 0.3wt% at 60-80℃ for 30min was used for colloidal silica cleaning. Then the membrane was cleaned by ultrapure water 2 times with 30min of each to remove the residual chemical. System flushing was carried out with a 0.2wt% NaClO solution (0.3wt% NaOH for silica) for 1 hour (recycled) and demi water 10L (not recycled).

5.2.2 Membrane permeability

The permeability of membrane was determined by demineralised water (demi water) at room temperature (18-22℃) for 20 minutes. The cross-flow velocity was set at 0.5 $\pm$ 0.05 m/s and the transmembrane pressure was set at 3 $\pm$ 0.1 bar. The permeate flux was recorded by the Kern balance software continuously with 3 minutes one point, and relative parameters (temperature, pressure) were recorded manually with each point. The permeability became constant within 10 minutes and the average was calculated. However, the temperature was increasing from around 18℃ to 27℃ due to the extra energy obtained by the pump. An extra formula was used to calibrate the permeability(Mulder & Kragl,1997).

$$L_{20℃} = \frac{J \cdot e^{-0.0239 \cdot (T-20)}}{\Delta P} \tag{5.1}$$

where, $L_{20℃}$ is the temperature-corrected permeability at 20 ℃$(L/(m^2 \cdot \mathrm{h} \cdot \mathrm{bar})$, T is the temperature of water (℃), J is the permeate flux $(L/(m^2 \cdot \mathrm{h})$ and ΔP is transmembrane pressure(bar). To make it simplified, the following permeate flux J was corrected by formula 5.1. The permeability measurement was carried out before each solute experiment to guarantee the same initial membrane condition. If the permeability is lower than the original value, an extra cleaning should be carried out.

5.2.3 Membrane MWCO measurement

PEGs were chosen to be the trace materials for the MWCO measurement. Several research studies (Blanc et al., 1998; Sarrade et al.,1994) showed that PEGs are reliable materials with no ion charged. Therefore, the rejection mechanism for the PEG is only steric repulsion which prevents the influence of electrostatic repulsion. A solution containing mixed solute with the MW of PEG fractions of 200,300,400, 600, 800,1000 and 1500 Da with 0.6g/L was used. The TMP of the experiment was controlled at 3 $\pm$ 0.1 bar and the cross-flow velocity was controlled at 1.3 m/s to produce a turbulent flow which can decrease the influence of CP. The MWCO measuring period was 3h for each experiment with 3 sampling points at 90min, 120min and 150min from both feed and permeate. High-performance liquid chromatography system (HPLC) was used to measure the concentration of PEGs.

The concentrations of PEGs in the feed and permeate were measured to generate a molecular weight distribution curve. The retention rates for PEGs with different molecular weight were calculated based on the following equation.

$$R_i(\%) = \frac{c_f - c_p}{c_f} \tag{5.2}$$

where, c_f is the PEG concentration in the feed stream, c_p is the PEG concentration in the permeate. The rejection curve from the experiment can be described by the model below (Van der Bruggen & Vandecasteele, 2002).

$$\sigma(\mathrm{MW}_s) = \int_0^{\mathrm{MW}_s} \frac{1}{S_{MW}\sqrt{2\pi}} \frac{1}{MW} \exp\left[-\frac{(\ln(MW) - \ln(MWCO) + 0.56S_{MW})^2}{2S_{MW}^2}\right] dMW \tag{5.3}$$

where $\sigma(\mathrm{MW}_s)$ is the reflection coefficient for different molecular weight (MW_s)of PEGs, S_{MW} is a standard deviation of molecular weight. The molecular size of PEG (dp in nm) is able to be calculated with its molecular weight (MW in Da) by formula 5.4.

$$d_p = 0.065(MW)^{0.438} \tag{5.4}$$

5.3. Filtration experiments for PEGs and silica

5.3.1 Chemicals for PEGs and silica

The feed for PEG tests were prepared by dissolving the solid PEGs in demineralised water with continuous string. The bioultra PEG solutes were purchased from SIGMA-ALDRICH. The solution of PEG-6000 was clear and colorless with the solubility of 50g/L ($\mathrm{H_2O}$) at 20℃ and pH of 5.5-7.0 at 25 ℃. PEGs with the MW of 4000,6000,8000,10000 Da were used in experiments, while PEG-6000 was the main objective.

Two different kinds of commercial silica were used in the experiments: powder fumed nanoparticle silica with an average diameter of 7nm and LUDOX SM colloidal silica with 30wt% suspension in H_2O purchased from SIGMA-ALDRICH. The concentrations of the silica were set at 0.5g/L, 3g/L and 6g/L with the pressure of 1.6, 2.2, 3, 4 and 4.6 bar. Powder fumed silica was dispersed by ultrasonic disperser at 50% efficiency for 10min at pH12. The solution became more transparent after treating by the disperser, shown in Figure 5.3.

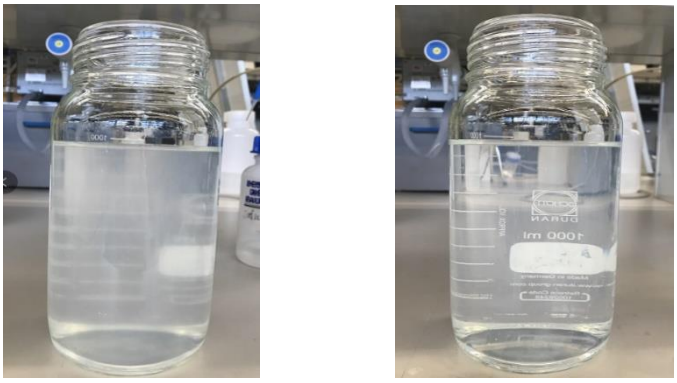

Figure 5.3 *0.5g/L powder silica. Original(left), After dispersion(right)*

5.3.2 Filtration process

In order to investigate the control factor in flux decline for PEGs and silica, the method discussed in chapter 4.1 was used. The initial permeability tests for all experiments were set at the same condition, that is, 3 bar, cross-flow 70 L/h with demineralised water for 18 minutes. Then the operational parameters were changed to the required condition with the same demi water. After the flux became stable, usually 9 minutes, the feed was changed from demi water to the target solution (PEGs and silica). To investigate the flux decline, the filtration of PEG and silica lasted 45 min. At the end of PEG/silica filtration, the feed was switched to demi water under the same operational condition. The demi water used before and after silica filtration was adjusted to the same pH as silica solution to avoid the extra influence caused by pH. The initial temperature of PEG solution was controlled at 20.6℃ by heating with a heater or cooling in a water bath.

The changing variables were the MW of PEGs, operational pressure, cross-flow, and the concentration of the solutes. The concentrations of PEGs were set to 3 values, 1g/L, 5g/L and 10g/L, while the concentrations of silica were set to 3g/L and 6g/L. Due to the restrictions of the setup, the pressure was changing from 1.5 bar to 5.5 bar with 4 to 6 points for each concentration. The cross-flow was changing from 40-150 L/h with 3 or 4 points at the pressure 3 or 4 bar. The results of flux decline under these changing conditions provide the data for further Sherwood constants calibration. The summary of changing parameters is shown in Table 5.1.

Table 5. 1 *Experimental conditions*

C (g/L)	Pressure [bar]	Cross-Flow [L/h]	PEG/silica
1	1.65, 3, 4, 5	70, 120,145 (4 bar)	6000
5	1.65, 2.1, 3, 4, 4.8, 4.9	40,70,100,130 (3 bar)	4000,6000,8000,10000
10	1.65, 2.16, 3, 4, 5		6000
0.5	3	80	Powder/colloidal silica
3	1.5, 2.3, 3, 4, 4.6	80,90,120,145(3 bar)	Colloidal silica
6	1.6, 2.15, 3.2, 4.1	80	Colloidal silica

5.4. Filtration experiments for phosphate

5.4.1 Chemicals

Sodium phosphate dibasic (Na_2HPO_4) was used as the main component of salt solution to perform phosphate retention tests. The salt solution consists of 10 mM NaCl as background and different Na_2HPO_4 concentrations with 0.3mM, 0.6mM. Sodium alginate was used as the EfOM foulant. The fouling feed solution consists of 0.8g/L sodium alginate (Sigma-Aldrich), 10 mM NaCl (Sigma-Aldrich) as background salt concentration, 1 mM $NaHCO_3$ (Sigma-Aldrich) as a buffer, and 3 mM $CaCl_2$ (Sigma-Aldrich). The original pH of the fouling solution was 8, additional NaOH or HCl solution was used to keep the same pH in all experiments. A transitional solution which contains 1 mM $NaHCO_3$ (Sigma-Aldrich) and 10 mM NaCl (Sigma-Aldrich) was used after fouling layer formed to maintain the layer thickness and reduce the influence of the changing composition on membrane permeability.

5.4.2 Filtration process

To investigate CP and flux decline in phosphate retention, filtration experiments were carried out with the cross-flow velocity of 1m/s and pressure of 3.5 bar. The permeability of the membrane was measured with a duration of 20 min. Then the feed solution changed from demi water to salt solution by switching the feed tank. The permeate flux was calculated by the data from a weighing scale with a 3 min interval automatically. During the salt filtration tests, the permeate and feed samples were taken at 60min, 65min and 70min after the running began. After 80 min, the feed solution was changed from salt solution to demi water again. The aim of this step is to see if the permeability can recover to a certain degree and the CP is reversible. Another group of experiments was carried out with injecting 3 mM $CaCl_2$ and 10mM NaCl in the feed, then changed to phosphate solution with extra 3 mM $CaCl_2$, the last stage changed to 3 mM $CaCl_2$ and 10mM NaCl again to see the influence of the calcium on phosphate retention and CP.

In order to investigate CECP in phosphate retention, a fouling layer was formed by filtrating fouling solution for 40min. After the fouling layer formed, the feed was changed from fouling agents to the transitional solution and filtrated for 30 min to keep the fouling layer stable. Then the salt solution was used and the samples for phosphate retention rate measurement (both feed and permeate) were taken after 15 min, 55 min and 95 min. After 100min, demi water was used to be the feed to see if the permeability of the membrane is recoverable.

A feed tank with 5Lwas used to measure the mass of deposit layer. The mechanical stirring was used to make sure that the feed is homogeneous during the fouling tests. The deposit mass measurement was carried out for 4 hours. The samples with 5ml were taken every 15 minutes from the feed tank and the volume of the feed tank was recorded at each time point. The permeate flux was measured along the fouling test with a weighing scale.

5.5. Analytical method

The ProfIC15-AnCat ion chromatography(IC) was used to measure the concentration of phosphate in the feed and permeate. The detect range of the IC is 0.1-100 ppm. The samples need to be filtered through 0.45 μm filters before the IC analysis. Concentrations of the fouling agent were measured by TOC analyser after filtration of samples through 0.45 μm filters. Particle Size Distribution(PSD) was used to measure the particle size of colloidal silica through light scattering technology. The measure range of the PSD is from 10.7 nm up to 2000 μm.

6 Results and discussions for flux decline and CP during PEGs and silica retention

6.1. Membrane characteristics

6.1.1 MWCO

Using the method discussed in chapter 5.2.3, the MWCO graph is shown in Figure 6.1. The measured curve is not matching the model curve obtained from equation 5.3 completely which could be caused by the non-uniform structure of the membrane, thus, lead to an inaccurate MWCO. Since the highest MW of PEGs used in the experiment was 1500 Da, the results of the part 1500-2000 Da could be inaccurate. The MWCO of the membrane was 1623 Da and the corresponded pore diameter is 1.66nm calculated from equation 5.4. The diameter of the PEG 6000 molecule is 2.94 nm (PEG 4000 is 2.46nm) which is much larger than the diameter of membrane pores, thus, all the PEG molecules can be rejected by the membrane through the steric repulsion effect.

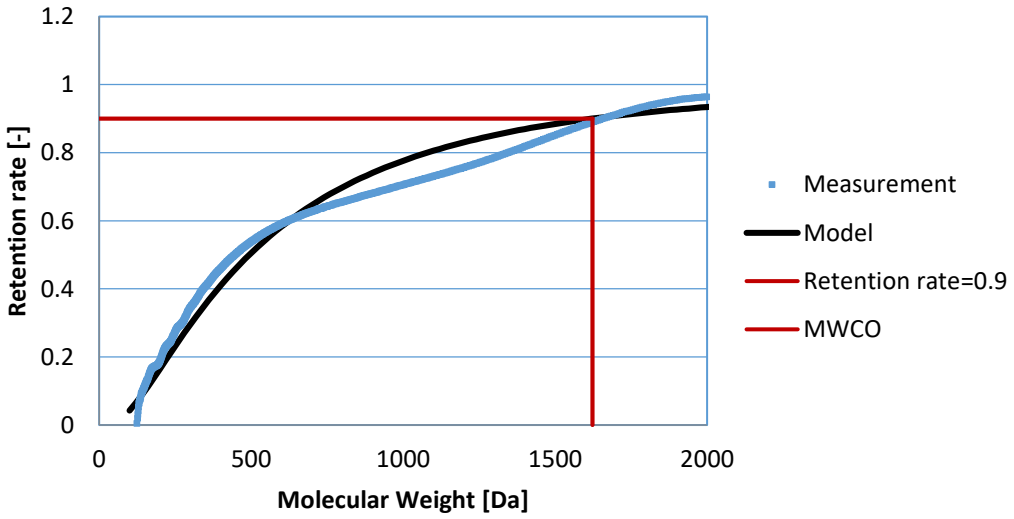

Figure 6. 1 *MWCO of the ceramic nanofiltration membrane used for PEG tests*

6.1.2 Influence of pressure on membrane permeability

Membrane permeability change with different pressures is presented in Figure 6.2. It is interesting to find that the membrane permeability decreased a little bit as the pressure increased, which goes against the previous knowledge, that is, permeability is an inherent quality of the membrane which should stay the same regardless of measuring conditions. However, in practical experiments, several factors can influence the measured permeability, for example, the

temperature, which is discussed and corrected by formula 5.1. As it is reported by Huisman et al. (1997), the water permeability can be affected by the electroviscous effect, temperature effect, membrane compressibility, and feed viscosity. They attributed the permeability decreased with the increasing pressure to the membrane compressibility. At the high pressure, the membrane resistance becomes larger, especially for the polymeric membrane which is sensitive to the pressure. Unfortunately, in the paper of Huisman et al. (1997), they did not discover the compressibility changes with the pressure of the ceramic MF membrane. The changes of the permeate flux, the Debye ratio, and the fluid rheological character caused by the changing pressure can influence the electroviscous effect (Tang, et. al,2010) which could be responsible for the results of Figure 6.2. However, the exact explanation for Figure 6.2 needs more explorations.

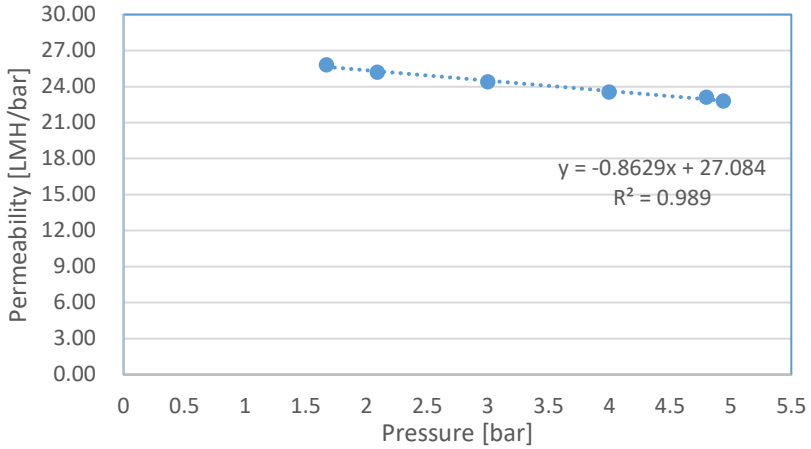

Figure 6. 2 *Membrane permeability as a function of pressure with Demi water at the cross-flow velocity of 0.5m/s.*

6.2. Flux decline by PEGs

6.2.1 Flux decline and recovery with time

Due to the fact that the permeability changes with pressure, the initial measurement of permeability or flux was conducted at the same pressure as 3 bar (first 18min in Figure 6.3) to make sure the permeability recovered completely after the cleaning. From the 20min, the pressure was conducted at 4 bar with the demi water and the clean membrane. At the 26min, the feed was changed from demi water to the PEG solution. During the first several minutes, permeate flux started to decline dramatically with all concentrations. In particular, the higher the concentration was, the faster the flux declined, for example, it took 9 and 3 minutes (started from the 26min in Figure 6.3) to achieve a relatively stable flux for 1g/L and 10g/L PEG filtration, respectively. After the dramatical decline, the permeate flux started to decline slowly. The feed was changed to demi water again at 45mins after PEG filtration. A considerable and quick flux recovery was shown in 10 minutes and then the flux stayed the same.

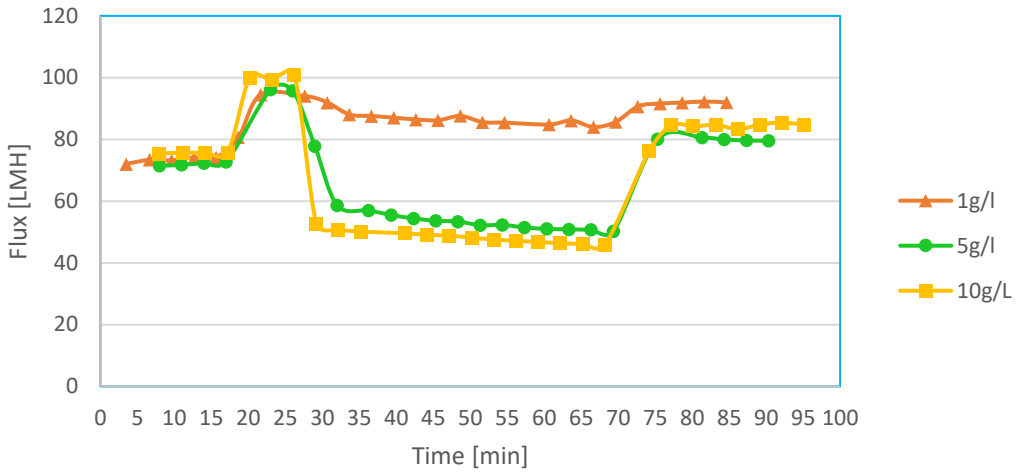

Figure 6. 3 *Flux decline with time during demi water – PEG6000 - demi water filtration process of 1g/L, 5g/L and 10g/L PEG 6000 at 4 bar (first 18 min is 3 bar), crossflow velocity 0.5m/s.*

Since CP is reversible while fouling is not, the recovered part of the flux can be seen as the degree of CP. The concentration of PEG had a huge influence on CP, especially at a lower concentration, compared with the flux decline of 1g/L to 5g/L PEG and 5g/L to 10g/L PEG. The level of flux decline caused by the fouling layer also became larger with the increased concentration, especially from1g/L to 5g/L. Due to the initial permeability of the membrane became larger for the experiment of 10g/L than 5g/L PEG (cleaning effect), a higher recovered flux of 10g/L showed in the last 20 min can be explained by a cleaning effect of the high concentration PEG. By analyzing the flux decline curve, we can not only demonstrate that CP and fouling are the reasons for flux decline of PEG, but also provide a new perspective to analyse the control factor without calculation by the model.

6.2.2 Fouling formation

In order to investigate the formation time of fouling layer, an experiment was performed with the feed changed from PEG to demi water immediately. From the curve special 5g/L PEG in Figure 6.4, we can observe that the flux recovered after 12min was the same as the flux recovered after 45min PEG filtration. It can be concluded that the formation of the fouling layer is happening within the first few minutes, while in the slow flux decline process, there is almost no fouling build up on the membrane. The possible explanation for the slow flux decline curve is that the permeate was not recycled to the feed tank which led to the water loss and the increased PEG concentration, thus, enhanced CP during the process. The feed tank used in the experiment was 2L and the total water loss during PEG filtration was 89 ml which means the concentration of PEG was increased from 5g/L to 5.23 g/L. Therefore, the slow flux decline is not significant. Compared the special 5g/L PEG with the normal 5g/L PEG, we observe the same amount of the recovered flux in the last stage, even though, the normal 5g/L had a lower permeate flux during PEG filtration. The fouling layer was not growing with time which means that there was no gel layer formation, and the most probable fouling mechanisms are pore blocking and adsorption.

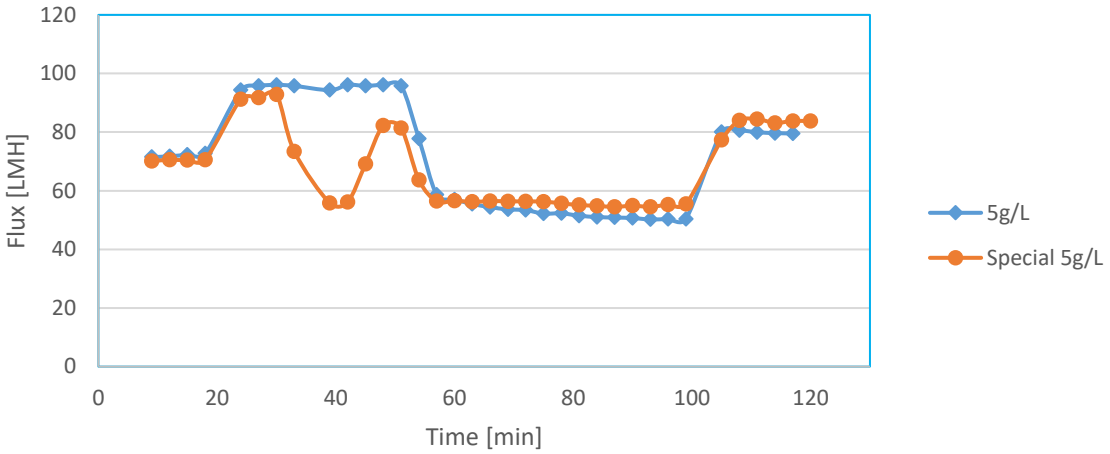

Figure 6. 4 *Flux decline with time of 5g/L PEG 6000 at 4 bar, 0.5m/s. (Special 5g/L was filtrated with demi water in the beginning. Then the feed was changed from demi water to PEG solution, after 12min, changed to demi water, after 9min, changed to PEG again, 45min later changed to demi water.)*

6.2.3 Flux decline with different pressures and concentrations

It can be concluded that the degree of flux decline depends on the pressure and the feed concentration by comparing different PEG curves with the standard demi water curve. At a higher concentration and a higher pressure, the level of flux decline increased. It is worth noticing that for the 10g/L PEG at high pressure (4-5 bar), the flux is independent on pressure which can be seen as the limiting flux discussed in chapter 2.3.

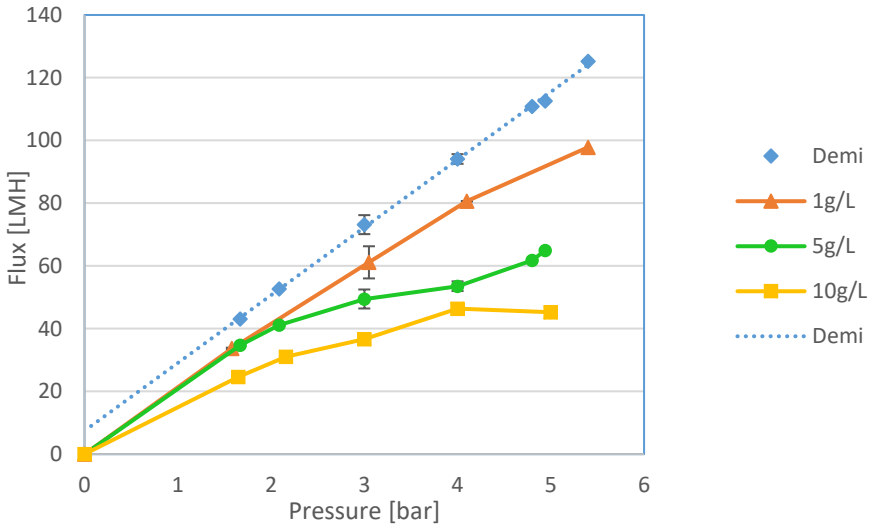

Figure 6. 5 *Flux of 45min after PEG filtration with different PEG concentrations as a function of pressure.*

It is worth noting that the trend line of demi water (dash blue in Figure 6.5) did not across the zero point. The ratio between the flux and the pressure is the permeability of the membrane. It means that the measured permeability of the membrane with different pressures are not the same which is consist with chapter 6.1.2.

6.2.4 Influence of CP and fouling on flux decline

Figure 6.6 presents the flux at different pressures of different stages (demi water-PEG-demi water). The flux curve of the PEG showed the flux decline due to both CP and fouling effects, while the curve of the demi water after PEG filtration was only affected by the fouling. Therefore, it is possible to study the influence of the pressure on CP based on the difference between the PEG curve and the demi after PEG curve. From Figure 6.6, it is clear to see that the flux decline caused by the CP effect became larger with the increased pressure. As for the fouling, there is almost no irreversible flux decline (fouling) at the pressure below 2 bar and the fouling effect became larger as the pressure increased.

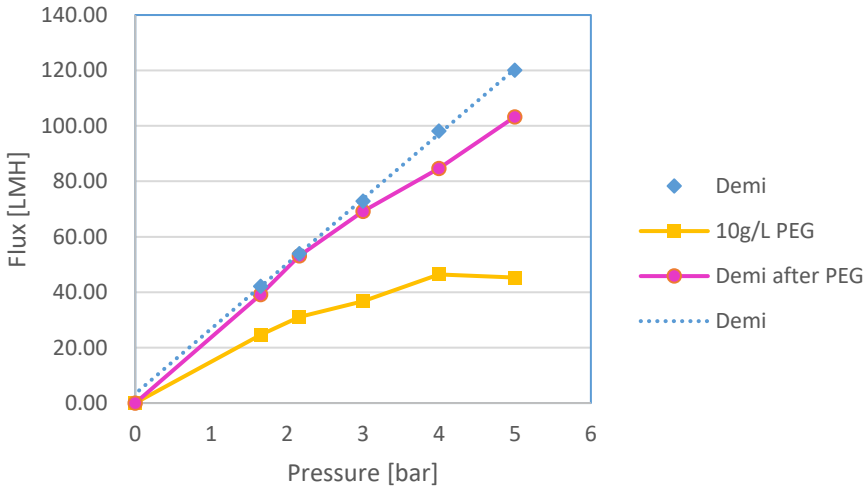

Figure 6. 6 *Flux at different pressures for initial demi water with clean membrane, PEG 6000 10g/L 45min and demi water after PEG filtration.*

6.2.5 Fouling resistance change with pressure and concentration

The resistance of the fouling layer is calculated by the Gel-polarization model described in chapter 4.1. From Figure 6.7, we can see that the resistance of the fouling layer is much smaller compared to the averaged resistance of the clean membrane $1.48 \times 10^{13}\ m^{-1}$. At the low pressure, the influence of the fouling layer can be neglected, thus the flux decline can be attributed to the CP phenomenon. As the pressure increased, the influence of the fouling layer became significant. For 1g/L PEG, fouling resistance increased to $1.88 \times 10^{12}\ m^{-1}$ at 5.4bar. However, for the concentration of 5g/L, membrane resistance obtained a peak value at 4 bar and decreased after that. As for 10g/L, the fouling resistance increased from 3 to 4 bar but had a lower increasing rate from 4 to 5 bar. In our expectation, the resistance of the fouling layer should increase with the increasing pressure due to the more compact or thicker fouling layer. This behaviour could be explained by the increasing temperature caused by pump running under the high frequency at high pressure. In experiments, only the initial temperature was controlled to the same value. The temperature during the experiment was not controlled due to the limit of equipment. The temperature for 5g/L was increasing from 20.6 to 25.8℃ at 4 bar and from 20.6 to 26.8 ℃ at 5 bar. Even though the permeability or the flux was calibrated to the same temperature 20℃, the diffusion coefficient was changing with the temperature. At a high temperature, the molecules of PEGs were more active, and their movement were accelerated in the solution which led to a

relatively thin or less compact fouling layer.

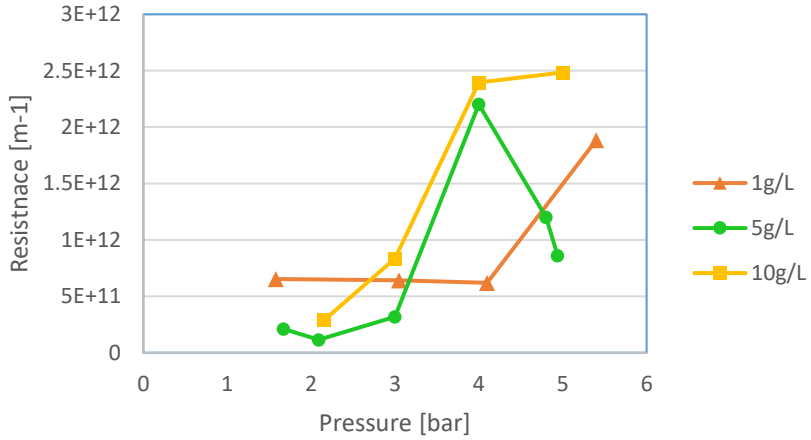

Figure 6. 7 *Fouling resistance changes with pressure and concentration for PEG 6000.*

6.2.6 Influence of cross-flow velocity on flux decline

Experiments with different crossflow velocities were conducted with 1g/L and 5g/L PEG 6000 solution. When the crossflow velocity achieves an infinite value (Re→ ∞), the flow is turbulent flow without any stagnant layer, thus, no CP. At the same time, high crossflow velocity can flush the wall of the membrane which makes it hard to form a fouling layer. Therefore, when the velocity→ ∞,$\mathrm{Re} \to \infty$, $1/\mathrm{Re} \to 0$, both CP effect and fouling effect can be neglected. Due to the low osmotic pressure in the feed PEG solution, the permeate flux can be seen the same as the flux by using the demi water (Nikolova & Islam,1998). In order to contain the information of the infinite velocity, $1/\mathrm{Re}$ was used as the abscissa.

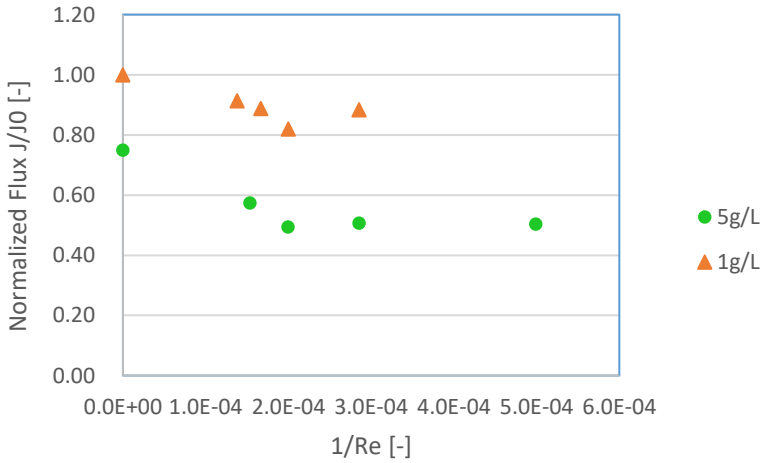

Figure 6. 8 *Normalized flux as a function of 1/Re for PEG 6000 with 1g/L at 4 bar and 5g/L at 3 bar*

Due to the sensibility of the initial permeability for clean membrane, normalized flux (permeate flux of PEG 6000 divided by the permeate flux of demi water) was used as the ordinates. Since the pressures used for 1g/L and 5g/L were different, to make the comparison more straightforward, the normalized flux at 4bar, $1/\mathrm{Re} = 0$ was defined as 1, and the normalized flux at 3bar needs to

multiply a correct factor 3/4. Except the point at $1/\mathrm{Re} = 0$, the flux decline with different $1/\mathrm{Re}$ was caused by both CP and fouling mechanisms. From Figure 6.8, we can see that for both concentrations, the curves have two slopes. At the high crossflow velocity ($1/Re \to 0$), the curves have more negative slopes, indicating that changing the crossflow velocity at turbulent flow can have a huge influence on permeate flux. At the low velocity, which corresponded with the laminar flow, we can see the curves are kind of stable. From the experiments of Nikolova & Islam(1998), they obtained the same curve at high velocities, but a slowly decreasing curve at low velocities. The difference of the slope may be caused by the error from experiments. Due to the dimension of the membrane (short), it is hard to guarantee there was actual laminar flow at the low cross-flow velocity. By analysing the flux decline with different Re, the boundary Re which can separate laminar flow and turbulent flow can be roughly estimated, which is around 5000 in our experiment.

6.2.7 Influence of MW on flux decline

Permeate flux of 5g/L PEG with different MW, permeate flux of demi water before and after PEG filtration are shown in Figure 6.9. The flux of clean membrane and the flux decline caused by the fouling layer were almost the same with different PEG molecules. However, the contribution of CP to the flux decline is increasing with the increased MW. It could be explained by the different diffusion coefficients of the PEG molecule based on the MW. The PEG molecules with a higher MW has a relatively larger diameter which leads to a lower diffusion coefficient. A lower diffusion coefficient will increase the concentration gradient and result in a higher concentration near the membrane wall, therefore, a higher CP.

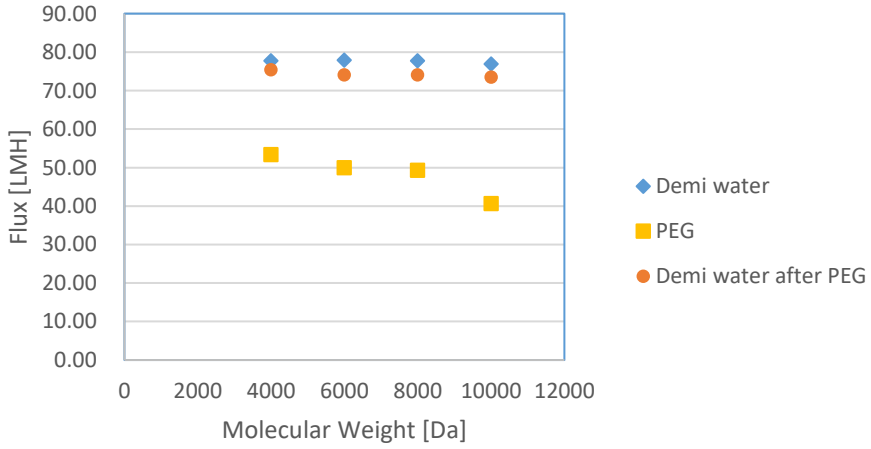

Figure 6. 9 *Flux of PEG of different MW at 3 bar, 5g/L*

6.2.8 Conclusions of flux decline by PEGs

By analysing the flux decline curve based on the method discussed in chapter 4.1, the control factor in flux decline for PEGs, that is CP, can be figured out without calculation by the models. With the flexible change of the experiments, like in chapter 6.22, the existence of cake layer can be investigated (no cake layer formation for PEGs). Flux decline under different operational conditions, such as the pressure and cross-flow velocity, can give us more information of the influencing factors for CP and fouling. The flux change with different cross-flow velocities could also provide a method to estimate the boundary Re for laminar flow and turbulent flow.

6.3. CP factor of PEGs and Sherwood model calibration

6.3.1 Comparison of empirical Sherwood formulas

There are several different empirical Sherwood formulas based on different theories exist to describe the behaviour of the flow. However, the difference between the formulas can produce a huge deviation of the calculated CP. Three existing formulas were used as examples.

Formula 1: $\mathrm{Sh} = 0.0149\,\mathrm{Re}^{0.88}Sc^{0.33}$ $(Sc > 100)$ from equation 4.11

Formula 2: $\mathrm{Sh} = 0.020\,\mathrm{Re}^{0.91}Sc^{0.25}$ $(2600 < Re < 10000)$ (Sutzkover et al.,2000) (6.1)

Formula 3: $\mathrm{Sh} = 0.102\,\mathrm{Re}^{0.9}Sc^{0.33}$ $(Sc > 1000)$ (Pinczewski & Sideman, 1974) (6.2)

Experiments were performed at the cross-flow of 70 L/h (0.5 m/s) with the membrane diameter of 0.007m, the kinematic viscosity of the PEG 6000 solution was calculated by equation 4.14 and 4.15 (correlated density was obtained from Ninni et al. (2003)) which is 1.0092E-06 m^2/s of 5g/L with equation $\rho = \mathrm{a} + \mathrm{bw}$. (a, b are coefficients and w is mass fraction). The calculated kinematic viscosities are shown below.

.

Table 6. 1 *Kinematic viscosity of different PEG MWs and concentrations at 20*℃

MW	a	b	w [g/kg]	Density [kg/m^3]	Dynamic viscosity [kg/(m· s)]	Kinematic viscosity [m^2/s]
6000	0.99575	0.18059	0.001	0.995931	1.0059E-03	1.0100E-06
6000	0.99575	0.18059	0.005	0.996653	1.0059E-03	1.0092E-06
6000	0.99575	0.18059	0.01	0.997556	1.0059E-03	1.0083E-06
4000	0.99601	0.17836	0.005	0.996902	1.0059E-03	1.0090E-06
8000	0.99667	0.17701	0.005	0.997555	1.0059E-03	1.0083E-06
10000	0.99542	0.18295	0.005	0.996335	1.0059E-03	1.0096E-06

The diffusion coefficient of the PEG can be obtained by the following 2 methods:

Formula 1 *From formula provided by Sherwood (1975) and Bhattacharjee & Datta (2001)*

$$\mathrm{D} = 2.74 \times 10^{-9}\, M^{-\frac{1}{3}}\left(1 - \frac{c}{\rho}\right)^{6.5} \tag{6.3}$$

where M is the molecular weight of PEG, c and ρ are the concentration and the density of the PEG with the same unit.

Formula 2 *From Einstein-Stokes' equation (Wang & Song,1999)*

$$\mathrm{D} = \frac{kT}{6\pi\mu a_p} \tag{6.4}$$

where k is Boltzmann constant ($1.38 \times 10^{-23}\,J/K$), T is the absolute temperature in K, and μ is

the dynamic viscosity kg/(m•s), a_p is particle radius in m (calculated with formula 4.11).

Table 6. 2 *Diffusion coefficient calculated from different formulas at 20 ℃*

MW	C [g/L]	a_p [m]	D [m²/s] from method 1	D[m²/s] from method 2	D [m²/s] Average
6000	1	1.478E-09	1.506E-10	1.445E-10	1.476E-10
6000	5	1.478E-09	1.500E-10	1.445E-10	1.473E-10
6000	10	1.478E-09	1.493E-10	1.445E-10	1.469E-10
4000	5	1.237E-09	1.717E-10	1.726E-10	1.722E-10
8000	5	1.677E-09	1.363E-10	1.273E-10	1.318E-10
10000	5	1.850E-09	1.265E-10	1.155E-10	1.210E-10

From the results of table 6.2, it can be seen that the differences in diffusion coefficient calculated by these two methods are small which make it acceptable to use the average value in this case.

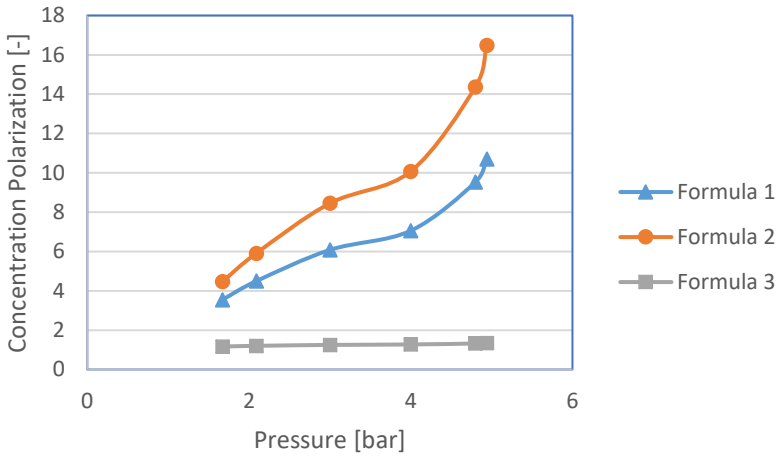

Figure 6. 10 *CP calculated with different Sherwood empirical formulas of PEG 6000 5g/L at 1.65-5 bar, velocity of 0.5m/s*

Figure 6.10 presents the CP factor calculated by different Sherwood empirical formulas. From the results we can see that the differences between these three formulas are huge, even though, the variation is smaller at the low pressure compared with the high pressure. In practice, it can be not appropriate to choose an empirical formula randomly. Therefore, it is essential to calibrate the constants in the Sherwood empirical formula before it can be used for calculating CP in a specific system (membrane, molecules, solvent etc.).

6.3.2 Osmotic pressure on the membrane

Gel-polarization model and the experimental data were used to calculate the osmotic pressure on the membrane. Figure 6.11 shows that the relations between the osmotic pressure on the membrane and the pressure are almost linear. The slopes of the curves are increasing with the increased concentrations, especially for the PEGs at the low concentrations. Figure 6.12 depicts the osmotic pressure on the membrane as a function of PEG concentration with different

pressures at 0.5m/s. At the low pressure of 1.65 bar, the relation between the PEG concentration and the osmotic pressure on the membrane is linear. As the operational pressure increased, slopes of 1g/L to 5g/L became larger, after 5g/L, slopes became smaller. It means that changing the PEG concentration in the low concentration range has a larger influence on the osmotic pressure on the membrane than that in the high concentration range.

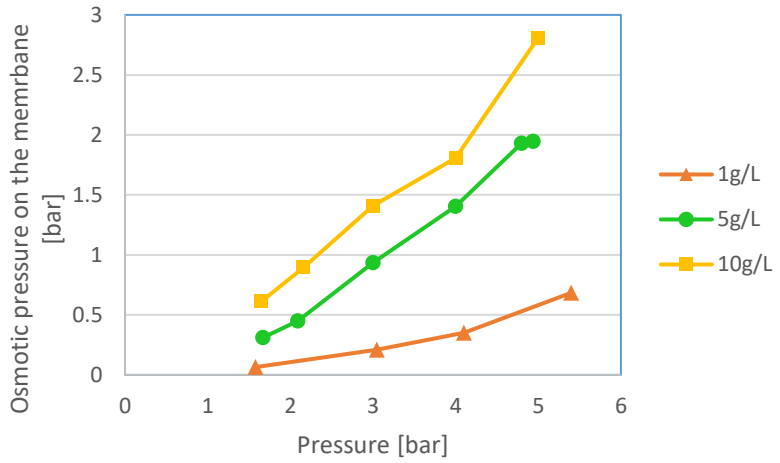

Figure 6. 11 *Osmotic pressure on the membrane as a function of pressure with different concentrations of PEG6000 at 0.5m/s.*

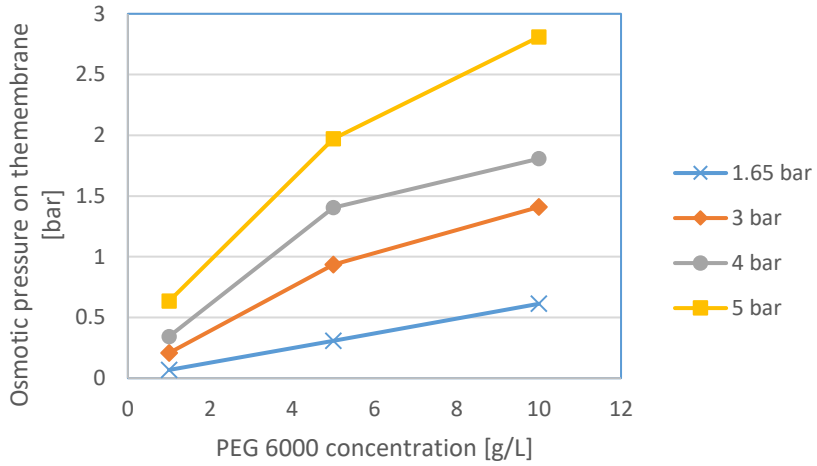

Figure 6. 12 *Osmotic pressure on the membrane as a function of PEG concentration with different pressure at 0.5m/s.*

6.3.3 Gel-Polarization model vs osmotic-pressure-controlled model

In order to investigate the influence of fouling layer on the calculated osmotic pressure on the membrane, osmotic – pressure - controlled (OPC) model discussed in chapter 2.4.2, which assumes the flux decline was caused by CP alone, was used to make a comparison in Figure 6.13. At the low pressures (below 3 bar) for all PEG concentrations, the influence of fouling layer can be neglected in calculating π_m. As the pressure increased, the influence of the fouling layer cannot be neglected and lead to a higher calculated π_m. Therefore, for PEG 6000 filtration under

the pressure below 3 bar, OPC model can be used as a simplified alternative method to estimate the osmotic pressure on the membrane without the experiment of demi water filtration after PEG filtration.

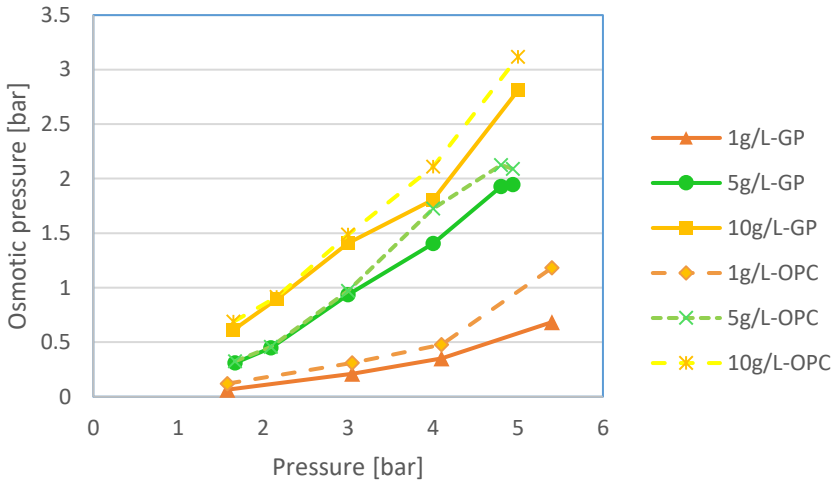

Figure 6. 13 *Osmotic pressure on the membrane calculated based on Gel-polarization model and osmotic-pressure-controlled model at 0.5m/s.*

6.3.4 Osmotic pressure in the feed for PEGs

In order to compare the Gel-polarization model with the Sherwood model, it is quite essential to calculate CP factor which contains the osmotic pressure in the feed solution (equation 4.10). However, in practice, there is no known accurate osmotic pressure for PEG solution at low concentrations. Therefore, several different models for osmotic pressure are shown below.

Method 1 *Formula from Nikolova & Islam (1998)*

$$\pi = A_1 c + A_2 c^2 + A_3 c^3 \tag{6.5}$$

$$A_1 = \frac{RT}{M} \tag{6.6}$$

where c is the solute concentration (kg/m^3), M is the average MW of the polymer (g/mol), R is the universal gas constant L·bar/(mol·K) and T is the absolute temperature K. It is reported by Nikolova & Islam(1998), if the concentration below 10 wt% (100 kg/m3), the influences of the second and third virial coefficient can be negligible. The highest concentration in the experiments is 10g/L (1wt%), thus, the osmotic pressure depended only on the first virial coefficient. Method 1 is a theoretical formula which has a huge deviation against the measured one. The calculated osmotic pressure shown in table 6.3.

Method 2 *Osmotic potential from Michel & Kaufmann (1973)*

$$\varphi_s = -(1.18 \times 10^{-2})C - (1.18 \times 10^{-4})C^2 + (2.67 \times 10^{-4})CT + (8.39 \times 10^{-7})C^2T \tag{6.7}$$

where φ_s is the osmotic potential for PEG 6000 in bar which is a negative value and the opposite number of osmotic pressure, C is the concentration in g/kg H_2O, T is the temperature in degree C. Method 2 obtained by measuring the osmotic pressure and finding the equation which fitted in the data. The equation is widely used in the study of plant growth with the concentration higher

than 100g/L.

Method 3 *Measured data and equation by Rand (2019)*

$$\log(\mathrm{P}) = 5.12 + 0.28 \times (\mathrm{wt\%})^{0.59} \tag{6.8}$$

where P is the osmotic pressure in dynes/cm^2, $\mathrm{wt\%}$ is the weight percent of PEG 6000. From the website, osmotic pressure of different MW of PEGs can be obtained. However, the formula is only accurate for the measured pressure which means that it is only suitable for the concentration between 10% to 35%, not accurate enough for the low concentrations. For the dilute solution, osmotic pressure should have a linear relation with the concentration (van't Hoff relation) (pass through zero point). From table 6.3 we can see that it does not match the principle. Therefore, method 3 cannot be used.

Table 6. 3 *Osmotic Pressure calculated with different method*

Mw	C	Osmotic Pressure [bar]		
[g/mol]	[g/L]	Method 1	Method 2	Method 3
6000	1	0.004	0.007	0.156
6000	5	0.020	0.035	0.202
6000	10	0.041	0.075	0.251

6.3.5 Sherwood constants calibration

Since the uncertainty of the osmotic pressure in the PEG feed solution, three existing Sherwood formulas the relation between osmotic pressure and the PEG concentration were used to find the suitable osmotic pressure which can match Sherwood formulas. In the matching process, not all of three concentrations can match perfectly. The main objectives are 5g/L and 10g/L, and at the same time, 1g/L can be used to see the deviation of the fitting degree.

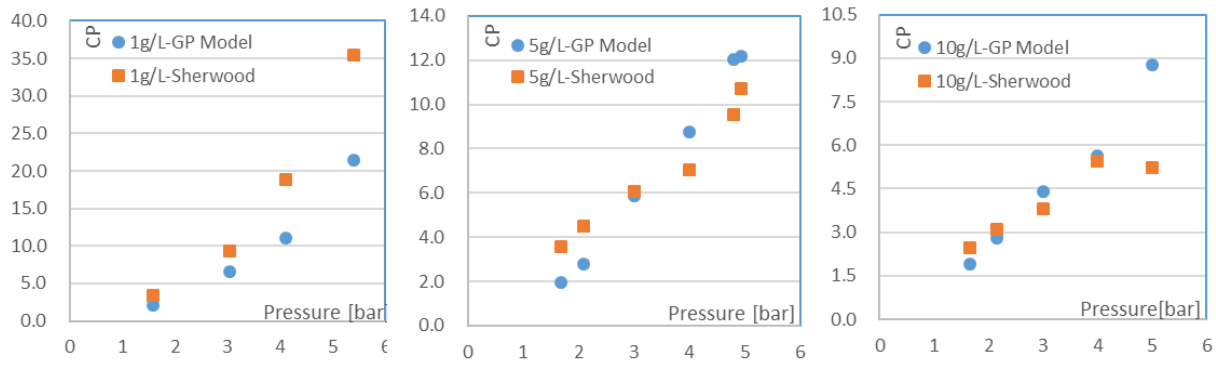

Figure 6. 14 *CP factor calculated by Sherwood formula 1 and GP Model with osmotic pressure in the feed solution of 0.032, 0.16 and 0.32 bar for 1g/L, 5g/L and 10g/L respectively.*

Figure 6.14 showed the matching degree of the empirical Sherwood formula 1 and the GP Model with the osmotic pressure in the feed solution of 0.032, 0.16 and 0.32 bar for 1g/L, 5g/L and 10g/L

respectively. It can be seen that the chosen osmotic pressures for 5g/L and 10g/L are similar to the values from method 3 discussed in the previous chapter. For the concentration of 10g/L, the CP factors match well under the pressure below 4 bar. The CP factor of 5 bar could be caused by an error due to the experiment or the fouling layer enhanced the CP which cannot be calculated by Sherwood formula. As for the concentration of 5g/L, at the pressure below 3bar, CP factors calculated by Sherwood formula have larger values, while CP factors calculated by GP Model have larger values at the pressure higher than 3 bar. As it is discussed before, the temperature in the experiment cannot be controlled to the same value. At the high pressure, the temperature increased by the pump leads to a high diffusion coefficient of PEG molecules. However, in the Sherwood formula, one diffusion coefficient was used in all calculations which can cause a lower calculated value at high temperature and a higher calculated value at low temperature. This could be one possible reason for the deviation of these two curves. For 1g/L, the curves from two models have the same shape, however, the CP factor at 5.4 bar calculated by Sherwood formula is much larger than calculated by GP model.

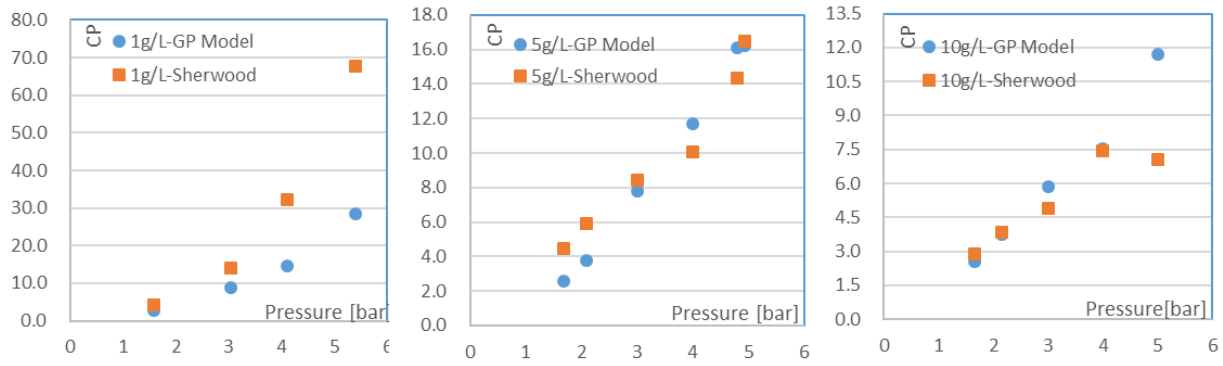

Figure 6. 15 *CP factor calculated by Sherwood formula 2 and GP Model with osmotic pressure in the feed solution of 0.024, 0.12 and 0.24 bar for 1g/L, 5g/L and 10g/L respectively.*

Figure 6.15 depicts the fitting curve of Sherwood formula 2 and GP Model with osmotic pressure in the feed solution of 0.024, 0.12 and 0.24 bar for 1g/L, 5g/L and 10g/L respectively. For the concentration of 5g/L and 10g/L, the curves have almost the same characteristics as Figure 6.14, except the relatively larger CP values. However, the deviation of 1g/L can achieve 40 at pressure 5.4 which is much larger than the deviation calculated by formula 2. Therefore, formula 1 is better than formula 2 considering all the concentrations. The CP factor calculated by Sherwood formula 3 is not possible to match the GP model no matter which osmotic pressure is chosen. Based on the results of these two matchings, the best match can be obtained by changing both osmotic pressure and the constants in Sherwood formula. After tried several times, there could be only one possible group of osmotic pressures for different concentrations and one Sherwood formula (based on $\mathrm{Sh} = \mathrm{a}\,\mathrm{Re}^{0.88}Sc^{0.33}$) which can match each other perfectly, shown in Figure 6.16.

The constant-adjusted Sherwood formula $\mathrm{Sh} = 018\,\mathrm{Re}^{0.88}Sc^{0.33}$ is able to match the GP model perfectly even at the concentration of 1g/L. All the curve fitting processes are based on the principle of the proportional relation of the osmotic pressures under different concentrations. It should be noticed that if the relationship is not correct, the final calibrated Sherwood formula is not suitable as well. If a more accurate Sherwood formula is needed, osmotic pressure obtained by extra measuring equipment should be used.

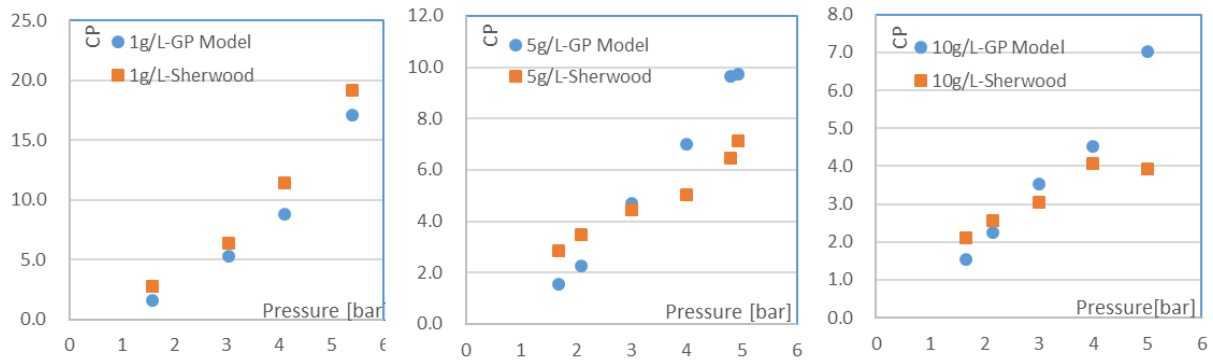

Figure 6. 16 *CP factor calculated by Sherwood formula* $\mathrm{Sh} = 0.018\ \mathrm{Re}^{0.88} Sc^{0.33}$ *and GP Model with osmotic pressure in the feed solution of 0.04, 0. 2 and 0.4 bar for 1g/L, 5g/L and 10g/L respectively*

6.3.6 Application range of calibrated Sherwood formula

After finding the suitable Sherwood formula in chapter 6.3.5, determining the range of application is essential. As it is known to all, the empirical Sherwood formulas are different with different flow conditions which can be represented by the Reynolds number. Reynolds numbers were changing by the cross-flow velocity in the experiments. Figure 6.17 showed the CP factor as a function of cross-flow velocity at 4bar for 1g/L and 3 bar for 5g/L with Sherwood formula obtained in chapter 6.3.5.

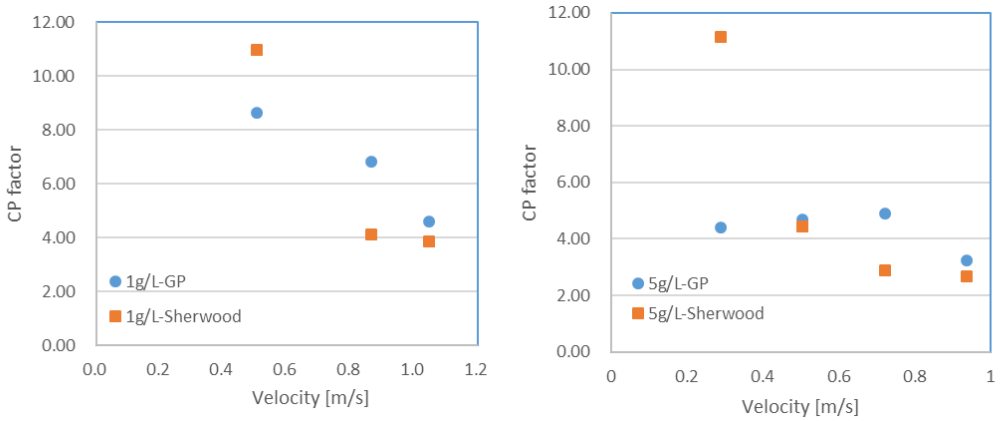

Figure 6. 17 *CP factor as a function of cross-flow velocity at 4bar for 1g/L and 3 bar for 5g/L with Sherwood formula* $\mathrm{Sh} = 0.018\ \mathrm{Re}^{0.88} Sc^{0.33}$

From Figure 6.17, we can see a decreasing trend of cp factor with the increasing cross-flow velocity by Sherwood formula. Due to the short size of the membrane, it is not possible to simulate the laminar flow completely or keep the low velocity during the experiments all the time, experiment errors could occur and make a low matching degree. Even though the matching curve is not perfect, the same decreasing trend can give some positive feedback on the Sherwood model. As for 5g/L, when the cross-flow velocity changed to 0.3m/s, there is a huge deviation between the two different models. It would be better to say that the Sherwood formula is not suitable for the velocity smaller than 0.5m/s (Reynolds number 3500) than a complete experiment error. Therefore, the possible application range of the Sherwood model could be 3500<Re<7300.

6.3.7 Conclusions of CP factor of PEGs and model calibration

The huge deviations of CP factors calculated by different empirical Sherwood formulas make it essential for Sherwood constants calibration. The unknown osmotic pressure in the feed caused difficulties in constants calibration. Based on the principle that the osmotic pressure of solute is proportional to the concentration in dilute solution, a group of osmotic pressures for different concentrations can be found for constants calibration by matching GP model and Sherwood model. The application range of Sherwood model can be figured out by comparing GP model with Sherwood model under different cross-flow velocities. The calibrated Sherwood model and the possible application range are $\mathrm{Sh} = 0.018\,\mathrm{Re}^{0.88}Sc^{0.33}$ and 3500<Re<7300.

6.4. Flux decline by silica and CP calculation

6.4.1 Flux decline by powder silica & colloidal silica

Two different kinds of silica were used in the experiment. Colloidal silica with different concentrations were diluted from colloidal silica suspension with 30wt% in H_2O. Due to the preparation technics, colloidal silica was already dispersed uniformly, and the dilution process will not lead to any agglomerates. However, the suspension of powder silica was made by ourselves and the dispersion quality cannot be guaranteed. To achieve a more homogeneous suspension of powder silica, the pH was set at 12 and ultrasonic disperser was used. Since the permeate flux of the membrane can be influenced by the pH due to the electroviscous effect (discussed in chapter 7.2.1), the pH of demi water was adjusted to the same pH as the colloidal silica (around 10)/ powder silica (12). Therefore, the original permeate flux was different between different kinds of silica, shown in Figure 6.18.

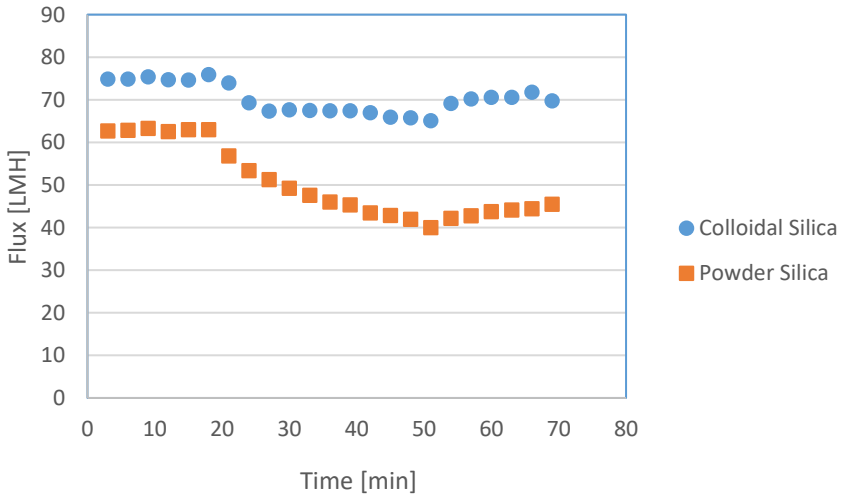

Figure 6. 18 Flux decline of 0.5g/L colloidal silica and powder silica at 3 bar,0.5m/s

After changing the feed from demi water to the colloidal silica, there was a quick flux decline in the first 10 min and followed by a slowly flux decline. The colloidal silica had the same flux decline and recovery trend as PEG solution. As for the powder silica, the flux was declining with a fixed

rate and the permeability did not recover back to the initial state with demi water. Compared with the colloidal silica, the flux decline by powder silica is more like particle deposit fouling. The possible explanation for no CP could be that, the dispersion of nanoparticle silica was not exactly homogeneous which can lose the stable state under the changing external conditions. Therefore, it is better to choose the colloidal silica to investigate the concentration polarisation in the ceramic membrane.

6.4.2 Membrane cleaning

If the powder silica is not dispersed by the ultrasonic disperser, the permeability of membrane cannot be easily recovered to the initial state. If the membrane was scaled by silica, the scale is almost impossible to remove (Weng,1996). From Figure 6.19, it is able to see that no matter which kinds of chemical were used in the membrane cleaning process, the permeability of the membrane was not recovered back. Therefore, a new membrane was used in the following experiments with colloidal silica. As for the membrane filtrated by the dispersed powder silica, the permeability was able to achieve the initial value under 30 min 0.1% NaOH 35℃ soaking. This is also applicable to colloidal silica. However, as the concentration of colloidal silica increased in the experiments, the fouling layer became thick and hard to clean. The cleaning condition became 30min 0.3% NaOH at 60-80℃. Unfortunately, the high temperature and the strong base can damage the membrane, thus, the membrane permeability became higher after 4- or 5- times cleaning, for example, from 27 to 29 $\mathrm{L}/(m^3 \cdot h \cdot bar)$.

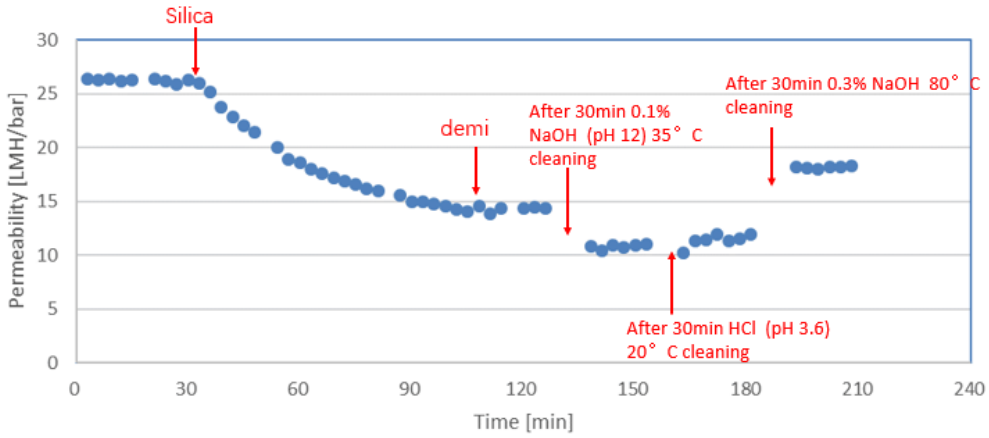

Figure 6. 19 *Permeability of no disperser pre-treatment 1g/L powder silica filtration and membrane cleaning*

6.4.3 Flux decline with different pressures

Colloidal silica was used for the remaining experiments to investigate the CP and the flux decline. Figure 6.20 (left) depicts the permeate flux under 3g/L silica increased as a function of pressure. As for 6g/L, the permeate flux increased as a function of pressure below 3 bar, and the limiting flux occurred with the further increasing pressure. Unlike PEGs which have little fouling potential, colloidal silica is more likely to produce a gel layer or 'gel type' layer. From the left diagram of Figure 6.20, even though the influence of CP on flux decline is increased with the operational pressure, the influence of the fouling layer on flux decline is obvious as well. For 6g/L silica, the

limiting flux could be caused by the formation of cake (gel layer) which discussed in chapter 2.3. In addition, the existence of gel layer can increase the portion of flux decline caused by CP which can be seen from the huge increasing difference between the flux of silica and 'demi water after silica' in Figure 6.20 (right).

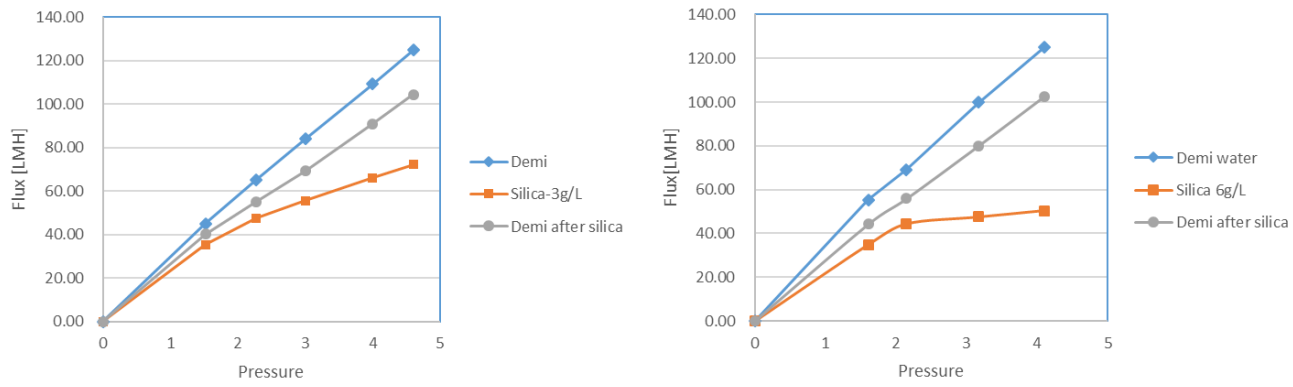

Figure 6. 20 *Flux at different pressures for initial demi water with clean membrane, colloidal silica 3g/L (left) 6g/L(right) 45min and demi water after silica filtration.*

6.4.4 Fouling formation

Figure 6.21 depicts the flux decline curves with original and special 6g/L at 3bar with the crossflow velocity of 0.5m/s which is similar to Figure 6.4. From Figure 6.21, we can see that the fouling layer was mainly formed in the first a few minutes which was similar to the PEG solution. However, the final demi water permeate flux is lower than the medium demi water permeate flux which means that the irreversible fouling layer was growing in the 45 min silica filtration and the slow flux decline was more probably caused by the fouling layer. The probable fouling mechanisms are pore blocking, adsorption and cake/gel layer formation.

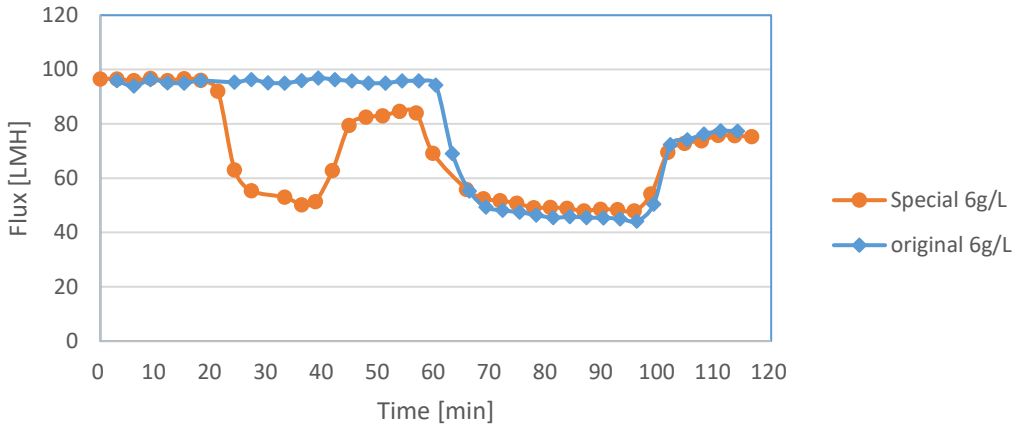

Figure 6. 21 *Flux decline with the time of 6g/L silica at 3 bar, 0.5m/s.(Special 6g/L was filtrated with demi water in the beginning. Then the feed was changed from demi water to silica suspension, after 30min, changed to demi water, after 15min, changed to silica again, 45min later changed to demi water.)*

Figure 6.22 presents the fouling resistance in the silica filtration with different pressures and concentrations. For 3g/L, the fouling resistance increased from 1.5 to 3 bar and then kept almost constant at the high pressure. As the pressure increased from 3 to 5 bar, fouling resistance had a little bit decrease which can be explained by the increased temperature. Compared with the PEG, the declining trend is much smaller for silica. This is because of the much larger molecule diameter of silica (10 nm) than PEG 6000 (2.94nm), which leads to a smaller diffusion coefficient (see equation 6.4) and is less sensitive to the temperature.

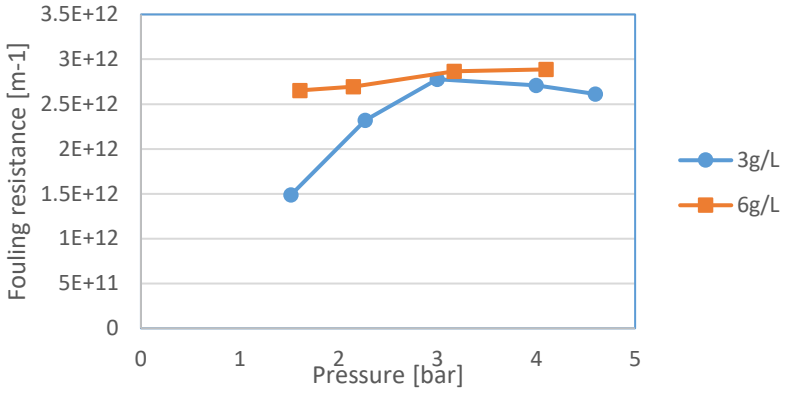

Figure 6. 22 *Fouling resistance changing with pressure and concentrations*

6.4.5 Osmotic pressure on the membrane

Osmotic pressure on the membrane calculated by the modified Gel-polarization model is shown in Figure 6.23. For 3g/L, the shape of the curve is smoother and more like exponential function which is similar to the PEG curve. For 6g/L, osmotic pressure on the membrane was increasing with a smaller rate at the low pressure but increased dramatically as the pressure increased. This unusual shape of curve can be explained by the formation of cake layer which increased the concentration of silica on the membrane surface.

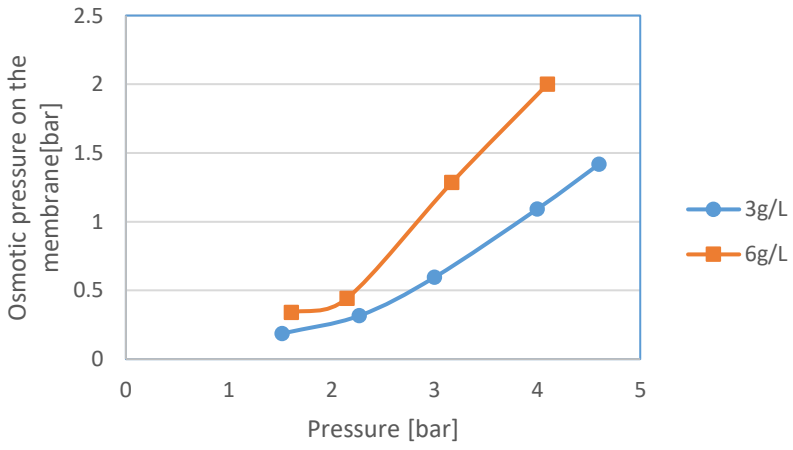

Figure 6. 23 *Osmotic pressure on the membrane as a function of pressure with different concentrations of silica at 0.5m/s.*

6.4.6 Sherwood parameters & CP factor

The particle diameter of the colloidal silica was measured by the particle size distribution(PSD) equipment which is 11.8nm. Since the result is close to the lower limit of the application range of PSD (10.7nm), it is better to use the information from Rose et al. (2014). Therefore, 10nm was used as the diameter of the colloidal silica to calculate the diffusion coefficient based on formula 6.4. The data used in the Sherwood formula is shown in Table 6.4.

Table 6. 4 *Parameters used in Sherwood calculation for silica*

Concentration [g/l]	Kinematic viscosity [m2/s]	Particle radius [nm]	Diffusion coefficient [m2/s]
3	1.00405E-06	5	4.2714E-11
6	1.00224E-06	5	4.2714E-11

Using Gel-polarization model to calculate CP factors has the same problem for silica, that is, the osmotic pressure in the feed suspension is difficult to find out. Sherwood formula calibrated from PEGs was used to find a suitable osmotic pressure to fit in the GP model. The osmotic pressure also followed the relation with concentrations, for 3g/L is 0.02 bar and for 6g/L is 0.04 bar. The calculated CP factor is shown in Figure 6.24.

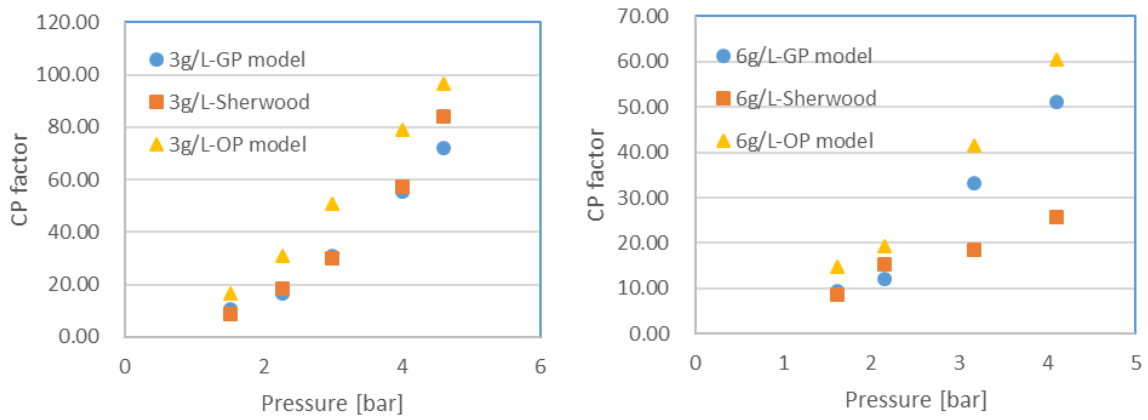

Figure 6. 24 *CP factor calculated by Sherwood formula* $Sh = 0.018\, Re^{0.88} Sc^{0.33}$*, GP Model, and OPC model with osmotic pressure in the feed of 0.02 and 0.04 bar for 3g/L and 6g/L respectively.*

From Figure 6.24, as for 3g/L colloidal silica, osmotic pressure calculated by the Sherwood formula perfectly matches the CP factor calculated by the GP model with an assumed osmotic pressure in the feed suspension. The fitting degree of silica is much better than the PEG solution. It could be that the PEG experiments had much larger experimental errors since the diffusion coefficient is much easier influenced by the temperature due to the small particle size. Compared to 3g/L, 6g/L silica has a worse fitting degree at high pressure. The possible explanation is that the extra CP caused by the gel layer (discussed in chapter 6.4.3) cannot be taken into consideration by the Sherwood formula. It means that Sherwood formula is not suitable when the silica on the membrane forms a gel layer which hinder the back diffusion of the molecules. Limiting flux could also be a sign for the formation of cake layer. For both concentrations, it is not suitable

to estimate CP factor by the OPC model since the influence of fouling cannot be neglected. A much larger CP factor can be obtained by the OPC model.

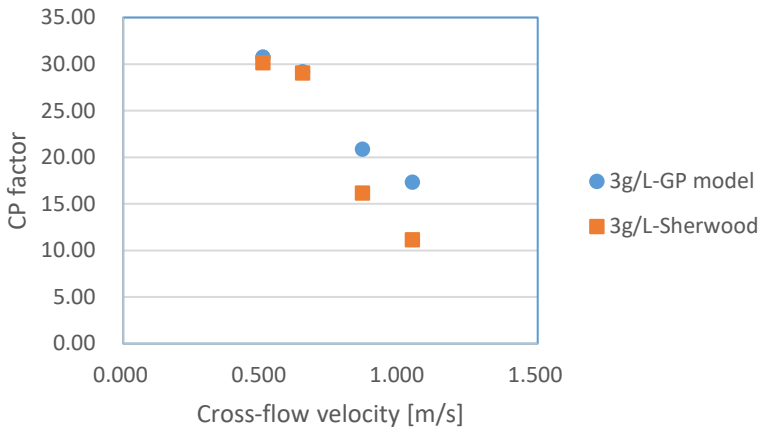

Figure 6. 25 *CP factor as a function of cross-flow velocity at 3bar for 3g/L at 3 bar with Sherwood formula* $\mathrm{Sh} = 0.018\ \mathrm{Re}^{0.88} Sc^{0.33}$

As the cross-flow velocity increased, the calculated CP factor decreased with both models. At the low crossflow velocity, two models fit each other well, however, Sherwood model has a lower CP factor compared to the GP model at high velocity. That could also be caused by the higher actual diffusion coefficient at a higher temperature.

6.4.7 Conclusions of flux decline by silica and CP calculation

Colloidal silica was used to investigate CP and flux decline during silica filtration since it has a better dispersion than powder silica. Both CP and fouling are control factors in flux decline for silica. The gel layer and limiting flux occurred with 6g/L colloidal silica and Sherwood formula is not suitable with the presence of the gel layer.

7 Results and discussions for flux decline and CP &CECP during P retention

7.1. Theoretical analysis of the CECP model

The theoretical analysis of CECP is based on the model discussed in chapter 4.2, which separates the effective mass transfer coefficient into two parts: one part is from original Sherwood correlation, another part is calculated from the fouling characteristics. In the model analysis, the calibrated Sherwood correlation which discussed in chapter 6 was used.

7.1.1 Parameter determination

$$\beta_c = \exp\left(\frac{J}{K_{eff}}\right) = \exp\left(J\left(\frac{{d_h^*}^{0.12} \cdot v^{0.55}}{0.018\, u^{0.88} \cdot D^{0.67}} + \frac{M_d(1 - ln\varepsilon^2)}{DA_m\rho_p(1-\varepsilon)\varepsilon}\right)\right) \quad (7.1)$$

The calibrated formula is shown in equation 7.1. The parameter J [m/s] is the permeate flux which varies from $3 \times 10^{-6}\, m/s$ to $1.0\times 10^{-5}\, m/s$ during the nanofiltration with salt or under fouling conditions. Therefore, a medium value $8 \times 10^{-6}\, m/s$ was chosen. Kinematic viscosity is calculated by the formula 4.14 and 4.15, which is $1.01437\times 10^{-6}\, m^2/s$ at 20°C. In the experiment, the cross-flow velocity (u) was set at 1m/s (initial number), where the Reynolds number is larger than 7000 (turbulent flow). A_m is the effective membrane area which is $0.00163\mathrm{m}^2$. The density of pure alginic acid gel is $1.6\times 10^3 kg/m^3$,which is a reasonable assumption to represent the density of the fouling layer.

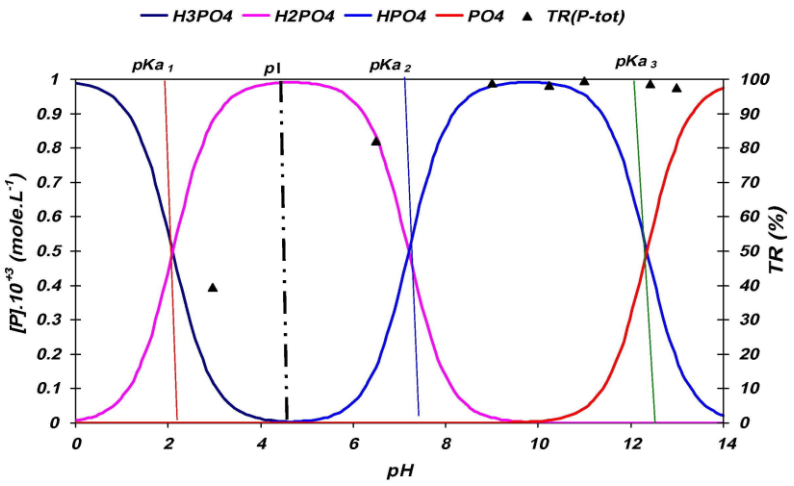

Figure 7. 1 *Effect of pH on the evolution of the phosphate retention rate on the diagram of species prevalence (Abdi et al, 2016)*

At the operational pH 8, both hydrogen phosphate ion ($\mathrm{HP}O_4^{2-}$) and the dihydrogen phosphate ion ($\mathrm{H_2P}O_4^-$) which have different diffusion coefficients exist. The diffusion coefficient used in this

model is a combination of these two components according to their proportion in the solution. At pH 8, according to the Figure above, there are around 4/5 of HPO_4^{2-} with a diffusion coefficient of $7.34 \times 10^{-10}\, m^2/s$, 1/5 of $H_2PO_4^-$ with a diffusion coefficient of $8.46 \times 10^{-10}\, m^2/s$. Therefore, the diffusion coefficient used in the model is $7.564 \times 10^{-10}\, m^2/s$.

The mass of sodium alginate accumulated on the membrane, M_d, is difficult to predict before experiments. Results from (Hoek et al., 2003) showed that the thickness of fouling layer of silica colloid on the cross-flow nanofiltration membrane with the channel height of 0.864mm was in the level of micrometre. According to the different operational conditions, the thickness of the layers varies from 0 to 25 um with an assumed porosity of 0.4. As it is reported from Hoek et al. (2002), the variation of different models is significant. They suggested the porosity of the silica during their experiments should be higher than 0.5 and the relative thickness of the silica layer should be higher than 100um. Compared the possible thickness of the fouling layer with the diameter of the membrane channel, the thickness of the fouling is able to be neglected. Therefore, the value of d_h^* can be seen the same as d_h.

The diameter of sodium alginate, as it is reported by Contreras et al. (2009), should be 5.12 ± 2.2 nm. While the diameter of the colloidal silica used in Hoek's experiment is 100nm. Since the existence of the calcium, the effective diameter of the sodium alginate could be changed and become larger. In some extent, the results from silica fouling have some reference value. Therefore, considering the compact gel of the alginate with the presence of calcium, the porosity of 0.38 and the fouling layer thickness of 35um were used in the model. The calculated mass is 0.05g. Compared the concentration in the feed solution 0.8g/L, the assumed values make some sense.

According to the change of the operational conditions, the possible variables in the phosphate filtration experiments are cross-flow velocity, mass accumulated per membrane area, permeate flux and porosity. Therefore, the analysis is focused on the influence of these four parameters on CP and CECP.

7.1.2 CECP theoretical analysis for cross-flow velocity

From Figure 7.2, it can be seen that the curve trend as a function of cross-flow velocity for both CP and CECP are the same: at the low cross-flow velocity, from 0.2-0.4m/s, the changing rate of CP and CECP decreases as the velocity increased. After around 0.6 m/s, the decreasing rate stays the same which creates a linearly decreasing curve for both CP and CECP. Even though the influence of the velocity is not that significant on both factors, the influence of the fouling layer on phosphate concentration near the membrane is significant. With the fouling layer, the concentration on the membrane surface can be 2.6- 3 times higher than the situation without fouling. The changing rate of the curve with the increasing velocity is consistent with the theory of the laminar flow and the turbulent flow, see table 7.1.

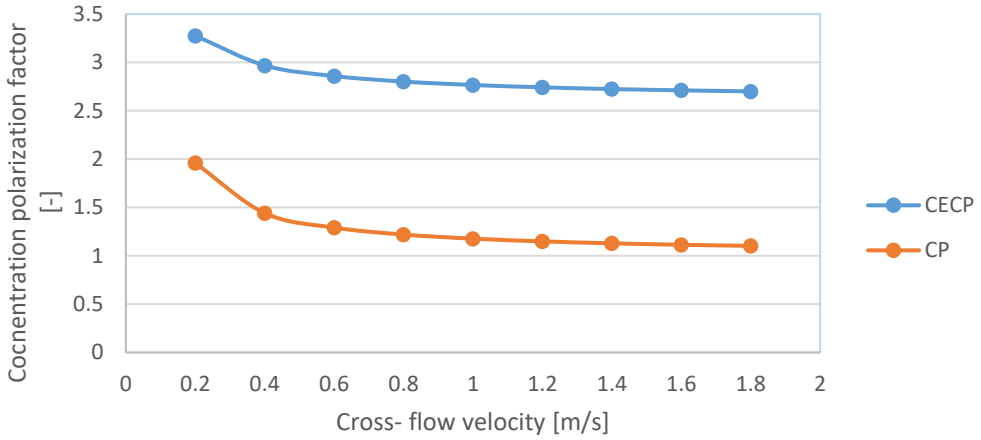

Figure 7. 2 *CP and CECP factor at different cross-flow velocity for phosphate filtration under clean and fouling membrane condition at pH 8, 20°C, ε=0.38, M_d =0.05g and J=8E-10 m/s*

Table 7. 1 *Reynolds number under different Cross-flow velocities*

Velocity [m/s]	0.2	0.4	0.6	0.8	1	1.2	1.4	1.6	1.8
Re	1380.2	2760.3	4140.5	5520.7	6900.9	8281.0	9661.2	11041.4	12421.6

As it is discussed in chapter 4.1.3, the common division for flow regime based on Reynolds number is turbulent flow (Re>4000), laminar flow (Re<2300) and the transition flow (2300<Re<4000). The Reynolds number calculated in Figure 7.1 showed that the flow with a cross-flow velocity between 0.2 to 0.4 m/s is almost laminar flow. At this region, a stagnant layer is formed due to the motion of molecules moving in straight lines parallel to the membrane surface. Therefore, the CP effect is higher at a low velocity. As the velocity increases, the state of the flow transfers from laminar flow to turbulent flow and the thickness of the stagnant layer decreases at the same time. After a certain value, 0.6 m/s, it is completely turbulent flow where pressure and velocity have chaotic changes. Thus, after the flow regime changed to the turbulent flow, the effect of the velocity change on CP is not obvious anymore. To reduce the effect of CP or CECP, control the operational condition to create a turbulent flow is a feasible approach.

7.1.3 CECP theoretical analysis for permeate flux

The range of permeate flux varies from $3 \times 10^{-6}\, m/s$ to $1\times 10^{-5}\, m/s$ according to the results of nanofiltration experiments. From the results of Figure 7.3, the CP factor increases from 1.02 to 1.23 as the permeate flux increases. Compared with the CP factor, CECP increases significantly which achieves 3.5 at $1\times 10^{-5}\, m/s$. When it achieves a larger permeate flux, the driving force is larger with the same membrane, which pushes more solute accumulate on the membrane surface and increase the concentration. At the same time, the torturous structure inside the cake layer can hinder the back diffusion of solute and has a greater influence than the clean membrane. It is worth noticing that if the permeate flux is smaller than $3 \times 10^{-6}\, m/s$, the value of CECP will below 1 (following the trend). The unrealistic value can be explained by the model itself. If the parameter J which can represent the forward convection is smaller than the parameter K_{eff}

which can represent the solute back diffusion, the CECP factor is smaller than 1. However, in practice, it is less likely to make the P concentration on the membrane smaller than that in the bulk solution. Therefore, the model has a limitation in the application range of flux.

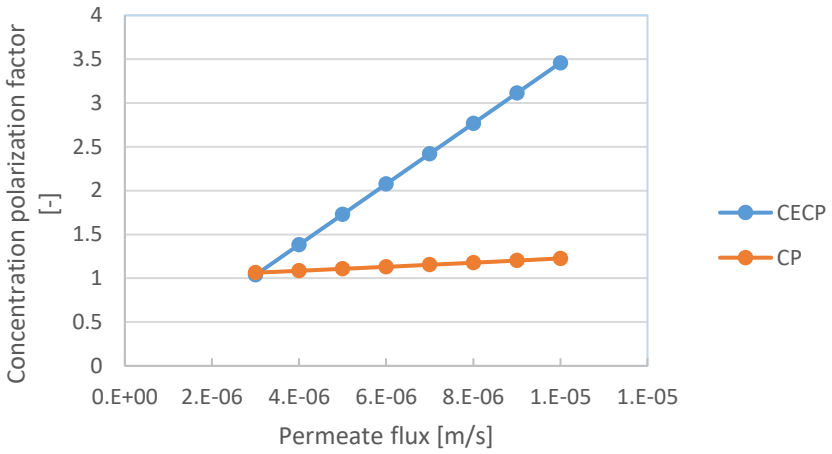

Figure 7. 3 *CP and CECP factor at different permeate flux for phosphate filtration under clean and fouling membrane condition at pH 8, 20°C, ε=0.38, M_d =0.05g and u=1.0 m/s*

7.1.4 CECP theoretical analysis for mass

The plot of Figure 7.4 showed the same linear trend as Figure 7.3. The amount of fouling mass has no influence on CP factor. Therefore, the value of CP stays the same. As the mass increases, the thickness of the fouling layer increases, which enlarges the path in the cake layer during the solute back diffusion and leads to the dramatically increasing CECP factor. However, the same 'factor smaller than 1' problem can occur. The limitation for the range of the fouling mass needs to be noticed.

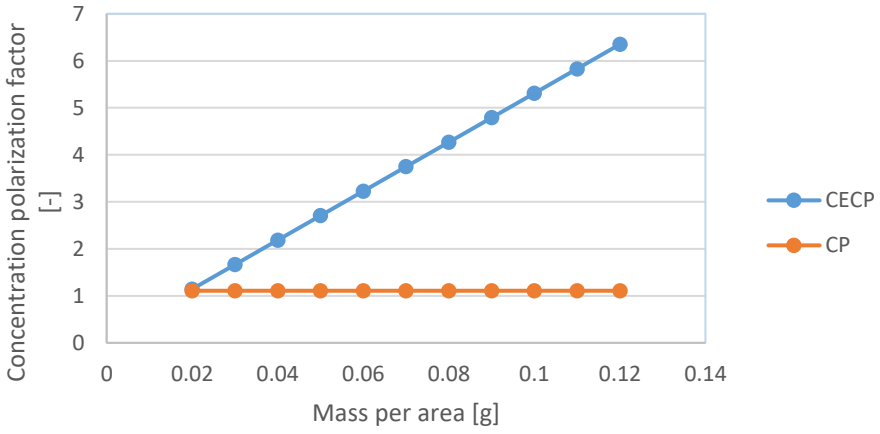

Figure 7. 4 *CP and CECP factor at mass per area for phosphate filtration under clean and fouling membrane condition at pH 8, 20°C, ε=0.38, J=8E-6 m/s and u=1.0 m/s*

7.1.5 CECP theoretical analysis for porosity

The actual porosity of fouling layer is not able to be measured directly. One possible method is using electroscope to catch the image of cross-section of the membrane with the fouling layer. Then, the fouling layer thickness and the mass per unit area are used to calculate the porosity of the membrane. However, the dehydration of the fouling layer makes the process very difficult and the accuracy cannot be guaranteed. The possible range of the porosity for silica, as described in chapter 7.1.1, could be lower than 50. During the real experiment, the porosity change could be small. To make the trend clearer, the range of the porosity here is 0.22-0.5.

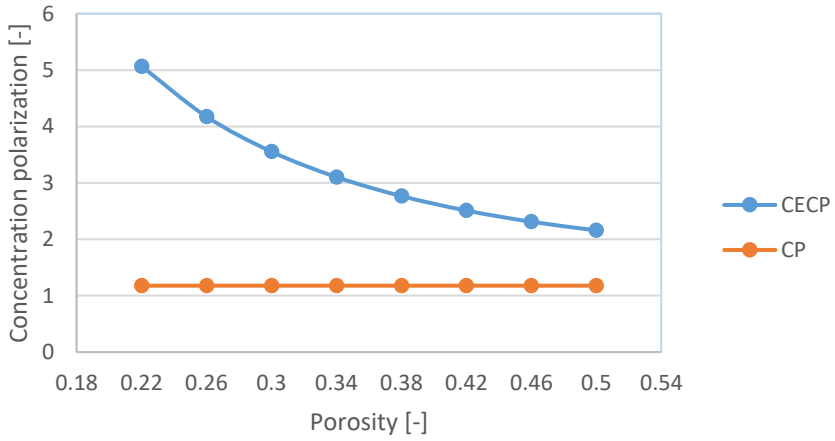

Figure 7. 5 *CP and CECP factor at different porosity for phosphate filtration under clean and fouling membrane condition at pH 8, 20°C, M_d =0.05g, J=8E-6 m/s and u=1.0 m/s*

From Figure 7.5, it is able to see that the CECP is decreasing as the porosity increases, and the curve seems like a quadratic function type. When the fouling layer has a high porosity, the solutes have more motion space and stress less hindered force from the alginate. On the contrary, the compact fouling layer has a more significant influence on narrowing the transport passage, which influences back diffusion of the solute from the membrane surface. Therefore, at a low porosity, the CECP effect is more obvious which is corresponded with the transport theory.

7.1.6 CECP theoretical analysis for combined factors

Four changing parameters are analysed in the previous chapters. However, in a real filtration condition, all these factors are changing at the same time. Therefore, simulating a situation that a combined solution of both phosphate and alginate is filtrated under an increasing operational pressure can make the analysis more real. Due to the increasing pressure, the permeate flux will increase (assume changing homogeneously from $3 \times 10^{-6} m/s$ to $1\times 10^{-5} m/s$), the mass will accumulate (assume changing homogeneously from 0.03-0.11g, the porosity will decrease (assume changing homogeneously from 0.5-0.29). The cross-flow velocity is not changed since it is a variable can be controlled easily. The final CECP factor change is shown below.

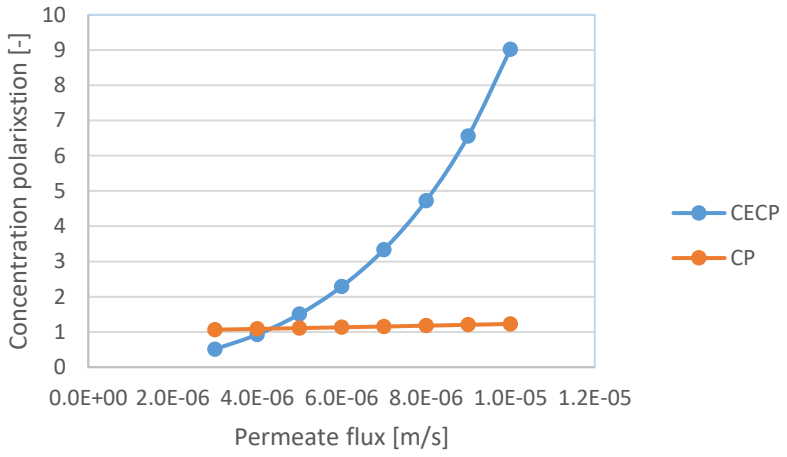

Figure 7. 6 *CP and CECP factor at different combined factors (showed as permeate flux) for phosphate filtration under clean and fouling membrane condition at pH 8, 20°C,* $M_d = 0.03 - 0.11$*g, J=3E-6—1.0E-5 m/s,* ε*=0.5-0.29 and u=1.0 m/s*

Results from the combined factors show a quadratic function type curve of CECP which dramatically increases as the permeate flux increases. It can be seen that the CECP factor from Figure 7.6 is almost 3 times higher than the single variable of permeate flux at*1.0E-5 m/s* and the increasing rate becomes larger as the flux increases. Even though all the variables will not create a CECP factor smaller than 1 individually, the combination will influence the results at the low flux. Therefore, the CECP effect in the real case could be more complicated than the model and it is essential to consider the application range before putting it into practice.

7.2. Permeability change during phosphate retention

7.2.1 Phosphate retention on clean membrane

The permeability decline during ceramic nanofiltration of the salt solution with 10 mM NaCl and the 0.3 mM, 0.6 mM phosphate by the clean membrane under 3.5 bar, cross-flow velocity of 1m/s are shown in Figure 7.7. The results showed the influence of the phosphate concentration on the permeability was not obvious and the curves trend were almost the same for different concentrations. Demi water was filtrated by the membrane at the first 18min (stage 1), and then the feed solution changed from demi water to salt solution. A significant permeability decrease occurred immediately. During the 80 min phosphate retention process (stage 2), the permeability decreased a little bit as the time increased. After the feed changed to demi water again, the permeability increased immediately (stage 3). However, the permeability did not recover to the initial state.

As it is discussed in chapter 3, CP is a reversible phenomenon which leads to an expectation that the permeability in stage 3 should achieve the same permeability as in stage 1. The results did not correspond with the prediction. It means that besides the reversible CP, there could be other

irreversible phenomenon or a fact which can influence the demi water permeability occurred at the same time.

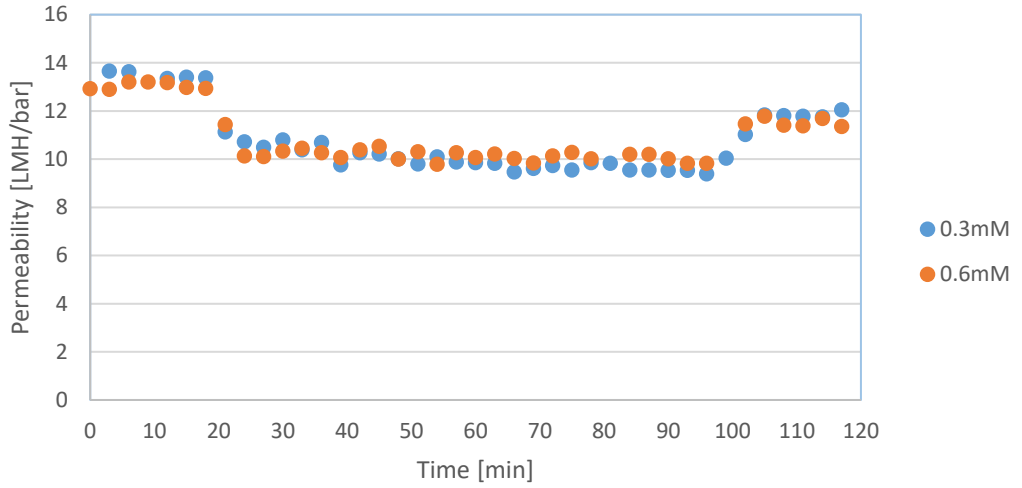

Figure 7. 7 *Permeability change as a function of time during the filtration of the solution with 0.3- or 0.6-mM phosphate and 10 mM sodium chloride under 3.5 bar and cross-flow velocity of 1m/s.*

The presence of phosphate can influence the zeta potential of the membrane. It is reported by Shang et al. (2014), the zeta potential of the membrane increased from -20 mv to -30 mv with the presence of the phosphate 1mg/L. The adsorption effect can occur during the salt filtration with phosphate and the zeta potential can increase (more negatively) (Randon et al.,1995). One possible explanation could be that the adsorbed phosphate decreased the effective size of the membrane pore. Compared the diameter of the phosphate ion (0.102 nm) with the membrane pore (1.66nm), the smaller permeability in stage 3 could be caused by the phosphate adsorption.

Due to the phosphate adsorption in phase 2, the zeta potential of the membrane increased (more negatively) in the demi water filtration stage 3. As it is reported by Farsi et al. (2014), the permeation of the solvent through the membrane could be influenced by the membrane surface charge. Another possible explanation for the not fully recovered permeability is the electroviscous effect. A streaming potential is established when an electrolyte flows through charged pores under a pressure gradient. “This potential produces a backflow of liquid by the electro-osmotic effect, and the net effect is a diminished flow in the forward direction. The liquid appears to exhibit an enhanced viscosity (usually called apparent viscosity) if its flow rate is compared with the flow in absence of double-layer effects.” (Sbaï et al.,2003).

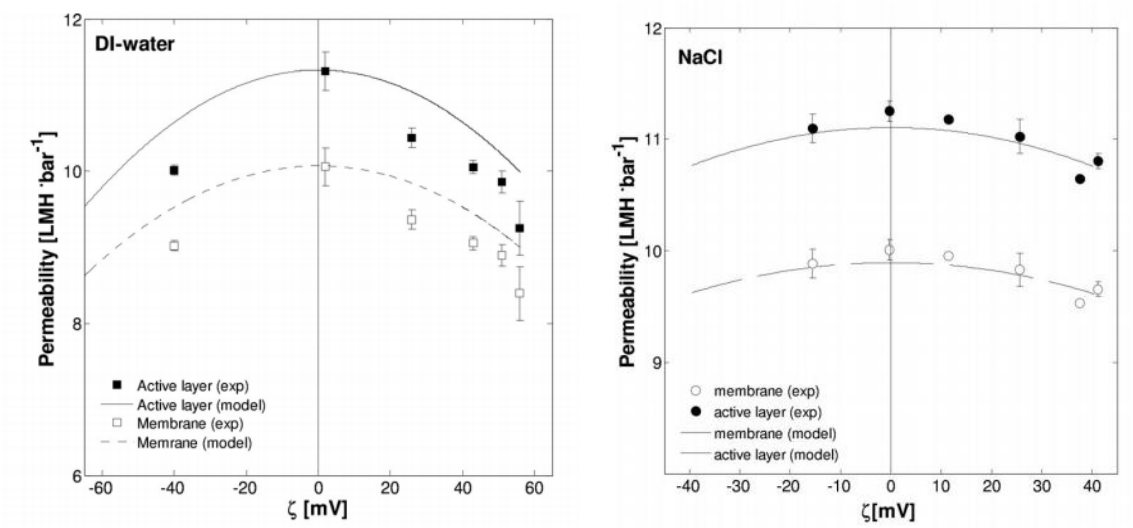

Figure 7. 8 *Membrane/active layer permeability versus z-potential for demineralized water (DI-water) and NaCl (0.01mM) by Farsi et al. (2015)*

The electroviscous effect is determined by the membrane pore size, surface zeta potential and the electrolyte concentration. Farsi et al. (2015) reported that electroviscous effect is significant for NF membranes with an average pore radius r<3 nm, ζ - potential < -20 mV and dilute electrolytes (ionic strength <0.05 m). By changing the pH of demi water and measuring the permeability of the membrane, the relationship between the membrane permeability and the zeta potential concluded by Farsi et al. (2015) are shown in Figure 7.8 (left). From Figure 7.8, we can see that for both the active layer and the membrane, the permeability is decreasing as the zeta potential increased from the isoelectric point in both negative and positive directions.

It is worth noting that the electroviscous effect also occurred in the salt filtration, stage 2, which can lead to a permeability decrease. It means that the method for CP calculation which using the permeability is not suitable since the permeability decrease was caused by both CP and electroviscous effect. As it is reported by Huisman et al. (1997), the membrane permeability during NaCl filtration is increasing with the increased NaCl concentration within a certain range. The electroviscous effect decreases with the increasing ion strength. Figure 7.8 (right) showed the same conclusion. With the same increasing zeta potential, the variation of the permeability for the solution with 0.01M NaCl is much smaller than the DI water. Even though the degree of the electroviscous effect of salt filtration in stage 2 is not fully clear, the degree in stage 2 is much smaller than that in stage 3.

7.2.2 Phosphate retention on fouling membrane

The experiment of phosphate filtration on fouling membrane was carried out next to the clean membrane phosphate filtration experiment. Thus, the initial membrane permeability of the demi water was the same as the end situation of Figure 7.7. After the 25 min demi water's filtration, sodium alginate solution was used to create a fouling layer (30min). A transitional solution containing 10mM NaCl and 1 mM $NaHCO_3$ was used to keep the fouling layer stable for 1h. Then the phosphate solution was used as the feed. The permeate and feed samples were taken to

measure the retention rate of the phosphate. From Figure 7.9, it is able to see that the permeability was decreasing dramatically in the first 6 minutes of sodium alginate filtration and then the curve dropped slowly later on which was corresponded with the filtration behaviour of organic matter. The permeability increased a little bit when the feed changed to the transitional solution and kept stable for an hour. The increase of the permeability can be caused by the unstable fouling layer. Due to the lack of sodium alginate in the transitional solution, the unstable fouling layer had a tendency to be dissolved in the transitional solution and decreased the mass of the fouling layer. After the unstable particles flushed away or dissolved in the solution, a relatively stable fouling layer left which produced a constant permeability.

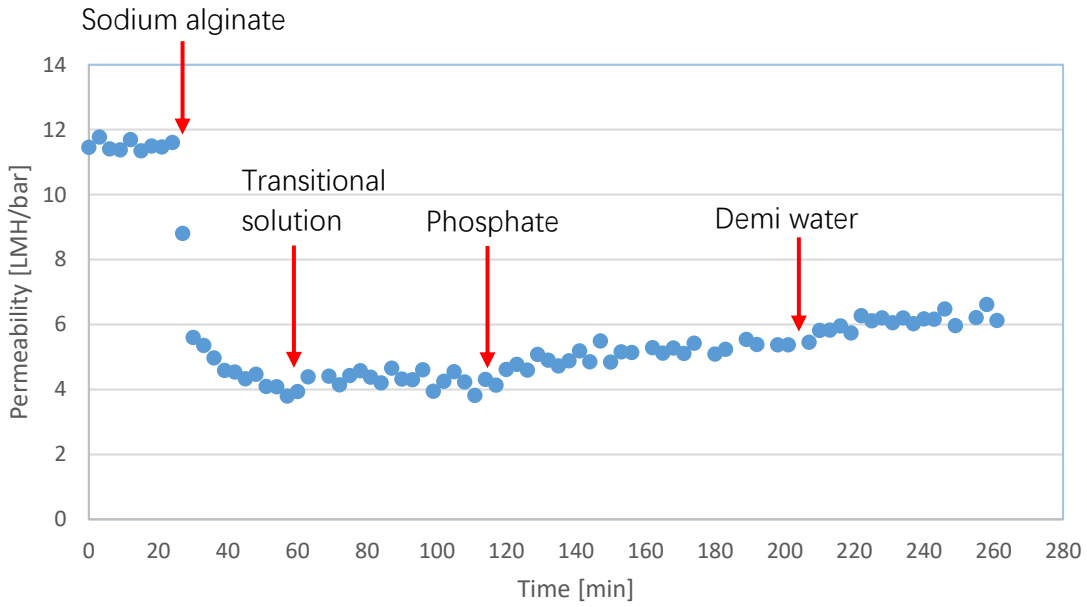

Figure 7. 9 *Permeability vs time during demi water, sodium alginate(0.8g/L sodium alginate, 10 mM NaCl, 1 mM* $NaHCO_3$ *and 3 mM* $CaCl_2$*), transitional solution (10mM NaCl, 1 mM* $NaHCO_3$*), phosphate (0.6mM P and 10mM NaCl), demi water filtration process under 3.5 bar with cross-flow velocity of 1m/s*

When the phosphate was used as the feed, an obvious drop did not occur as expected. On the contrary, the permeability was increasing from 4.2 to 5.8 LMH/bar. The difference of the composition between the transitional solution and the phosphate is 0.6mM P and 1 mM $NaHCO_3$ which had little influence on the total ion strength. If there is no CP effect, the permeability should keep stable for the phosphate filtration. Therefore, there could be other factors which can influence the permeability during the phosphate filtration. At pH 8, hydroxyapatite can form with the presence of calcium and phosphate (chapter 7.4). A possible explanation for the increased permeability is that the phosphate in the solution extracted the calcium in the compact fouling layer to form the hydroxyapatite and made the structure of the fouling layer loose. A relatively loose fouling layer caused an increasing permeability which can cover the permeability decrease caused by the CP. In addition, the permeability of fouling membrane with the transitional solution was much smaller than the clean membrane with demi water, the permeability decrease could be smaller and hard to discover. Therefore, the CECP effect is not able to be discovered by the changing permeability directly. The phosphate retention rate could give more valuable information.

In addition, the loss of fouling mass made it not possible to obtain an accurate mass value that made the CECP model hard to be used into practice.

7.3. Influence of CECP on phosphate retention

Figure 7.10 presents the phosphate retention rate for clean and fouled membrane at 3.5 bar. For the clean membrane, higher phosphate concentration led to higher phosphate retention rate. The possible explanation is that the adsorption of 0.6mM P to the membrane surface was stronger than the 0.3mM which made the membrane surface charge more negative and led to a higher electrostatic repulsion. The phosphate retention rate for the fouling membrane was smaller than the clean membrane. This could be caused by two factors. One is the CECP, the other is the low permeate flux which led to a smaller driving force for P filtration of the fouling membrane.

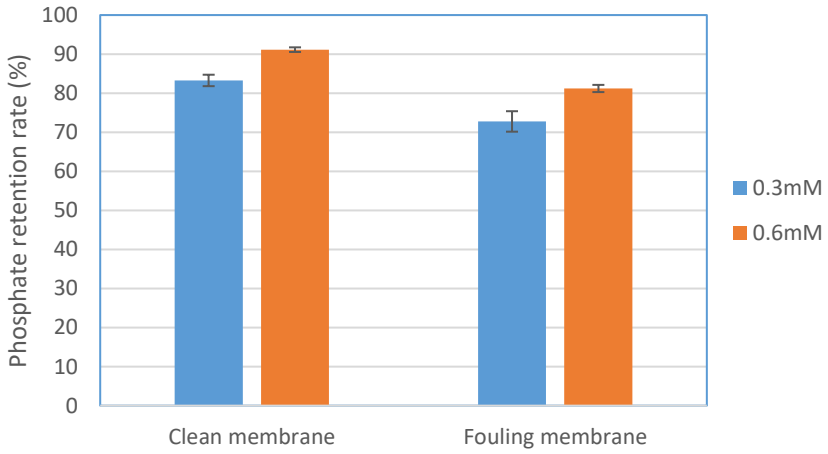

Figure 7. 10 *Phosphate retention rate for clean and fouling membrane at 3.5 bar*

Table 7.2 presents the CP factor calculated by the two models. Due to the electroviscous effect, the CP factor was calculated with two groups of data, the permeability of initial demi water(left) and P filtration, the permeability of final demi water (right) and P filtration. Results from these two groups can be seen as the two bounds and the calculated averaged value is shown in Table 7.2. The CP calculated from permeability is much higher than that from the Sherwood model. It is hard to say which method is better, but the CP factor calculated from permeability showed a smaller value at the higher concentration which is corresponded with the higher phosphate retention rate for 0.6mM. The same CP value was obtained by the Sherwood formula. From this perspective, the CP results from permeability are more convincing than the Sherwood model.

Table 7. 2 *CP factor calculated from model and experiments*

	P in the feed/permeate (mg/L)	π in the feed/permeate (bar)	Δπ left/ right (bar)	CP from left/right	Average CP	CP from model
0.3 mM	22.6/3.8	0.499/0.482	0.568/0.901	2.10/2.77	2.44	1.07
0.6 mM	60.6/5.3	0.533/0.483	0.568/0.901	1.97/2.60	2.29	1.07

7.4. Influence of calcium on phosphate retention

7.4.1 pH effect for Hydroxyapatite precipitation

In order to keep the fouling layer compacted, calcium chloride was added to the alginate solution. However, the calcium in the fouling layer can lead to hydroxyapatite ($Ca_5(PO_4)_3(OH)$) precipitation, with the presence of phosphate at a certain condition. In order to investigate the formation condition of the hydroxyapatite, PhreeqC was used. In the simulated conditions, the concentration of calcium was set the same as the fouling condition. The concentration of the phosphate and sodium chloride were set as 0.6mM and 10mM. By changing the pH of the feed solution, the Saturation index (SI) of the hydroxyapatite can be obtained.

Table 7. 3 *Saturation index of the hydroxyapatite with different pH*

pH	5.5	6	6.052	6.5	7	8	9
SI	-3.72	-0.34	0.00	2.84	5.65	10.14	13.46

It is able to see that the SI is increasing from the negative to positive value when pH increases. At pH 6.052, the SI value is zero which means the water and the mineral are at chemical equilibrium. When the pH is higher than 6, SI is higher than 0, the solution will tend to precipitate a particle. In order to investigate the influence of the calcium in phosphate filtration and avoid the hydroxyapatite precipitation, the pH should be controlled lower than 6.

7.4.2 Effect of Calcium on phosphate retention

When the feed changed from demi water to the calcium and NaCl at pH6, there was a slow permeability decrease (Figure 7.11) which could be caused by calcium adsorption or the electroviscous effect. At the negatively charged membrane surface, ions with positive charge, especially for the divalent ions, are more easily adsorbed on the membrane. When the feed was changed to the P, Ca and NaCl, there was a quick permeability decrease and was not recovered when changed the feed to the Ca and NaCl solution. The permeability did not recover means that there was no CP occurred. The 0.3% phosphate retention rate also verified there was no CP and almost all the phosphate passed through the membrane. The possible explanation for the permeability decreased after phosphate filtration could be that the positively charged calcium was adsorbed by the membrane surface which increased its concentration near the membrane surface. Higher concentration of calcium made it easier to create precipitation with phosphate and deposit on the membrane, thus, causing an irreversible fouling. The less negatively charged membrane surface caused by the low pH, adsorbed calcium, and the possible deposition should be responsible for the low phosphate retention rate.

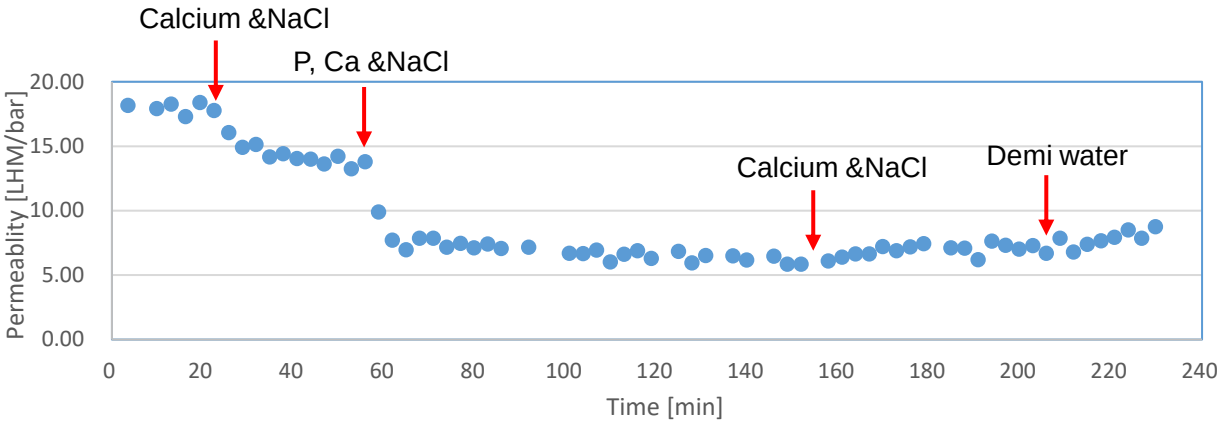

Figure 7. 11 *Permeability change with calcium, phosphate, demi water filtration*

7.5 Conclusions of CP&CECP during phosphate retention

The influencing factors for CECP during phosphate retention are cross-flow velocity, mass accumulated per membrane area, permeate flux, and porosity of the cake layer. The change of cross-flow velocity and permeate flux can influence CECP by changing the hydrodynamic conditions, while the change of mass accumulated per membrane area and porosity of the cake layer can influence CECP by changing the characteristics of the cake layer. The application range of the CECP model should be determined based on specific influencing factors.

The change of permeability in phosphate retention can be used to calculate CP factors, however, the adsorption and electroviscous effect had influence on the accuracy of the results. CECP factor is not able to be discovered by the change of permeability since the unstable fouling layer can influence the discovery of permeability decrease. The concentration of phosphate in the feed can influence the phosphate retention rate by influencing the electrostatic repulsion due to the phosphate adsorption. The presence of calcium has a serious negative impact on phosphate retention probably due to the lower electrostatic repulsion of phosphate.

8 Conclusions and recommendations

8.1. Conclusions

The conclusions of flux decline and CP during ceramic nanofiltration for PEGs and silica retention are drawn based on the research questions:

- *What is the control factor (CP or fouling) in flux decline under different operational conditions?*

By analysing the flux decline curve for PEGs and silica, the control factor in flux decline can be figured out without calculation by the models. The control factor in flux decline for PEG 6000 under the pressure below 5 bar is CP. It is possible to use osmotic-pressure-controlled model to estimate CP factors under the condition that the operational pressure is below 3 bar and the concentration of PEG is lower than 10g/L. For colloidal silica, both CP and fouling have significant impact on flux decline which makes it not suitable to use osmotic-pressure-controlled model. Under the condition of the high pressure and the high concentration, limiting flux occurs.

- *How to modify the Gel-polarization model to make it suitable for investigating CP and fouling with measured data? And what are the advantages and disadvantages of the modified Gel-polarization model?*

Based on the reversibility of CP and fouling, the Gel-polarization model together with the ‘demi water(stage 1) - target solution(stage 2) - demi water(stage 3)’ filtration method generated the modified Gel-polarization model, $\Delta\pi = \Delta P\left(1 - \frac{P_t}{P_r}\right)$. The modified Gel-polarization model is suitable for calculating the fouling resistance and the osmotic pressure on the membrane. It is difficult to estimate the CP factor due to the fact that the osmotic pressure of the solutes/colloids in the feed is not known. It can be estimated based on literature, but it might be better to measure it by the equipment.

- *How to calibrate the constants in the Sherwood model and what is the calibrated equation? And what are the advantages and disadvantages of the Sherwood model?*

The method by using the data obtained from the modified Gel-polarization model to calibrate Sherwood constants is difficult without exact osmotic pressures in the feed. Based on the principle that the osmotic pressure of solute is proportional to the concentration in dilute solution, several groups of osmotic pressures for different concentrations can be found for constants calibration. By matching the CP factor curves of the two models, modified Gel-polarization model with different groups of osmotic pressures and Sherwood model with different constants, a group of osmotic pressures and a group of constants can be found to

make the CP curves perfectly matched with each other. The calibrated Sherwood formula is $\mathrm{Sh} = 0.018\,\mathrm{Re}^{0.88}Sc^{0.33}$, and the possible application range could be 3500<Re<7300. Sherwood formula is appropriate for calculating CP factor while the empirical formula could not be suitable in practical application and extra complicated constant calibration work should be done. When the limiting flux occurs, Sherwood formula is not suitable anymore.

The conclusions of flux decline and CP&CECP during ceramic nanofiltration for phosphate retention are drawn based on the research questions:

- *What are the influencing factors for CECP in phosphate retention by building a CECP model and making theoretical analysis?*

CECP model based on Sherwood relation can be used to investigate the influence of fouling layer on CP. The influencing factors for CECP in phosphate retention are cross-flow velocity, mass accumulated per membrane area, permeate flux, and porosity of the cake layer. The change of cross-flow velocity and permeate flux can influence CECP by changing the hydrodynamic conditions, while the change of mass accumulated per membrane area and porosity of the cake layer can influence CECP by changing the characteristics of the cake layer. Based on the CECP model analysis, lower crossflow velocity and cake layer porosity, larger permeate flux and fouling mass can produce a higher CECP factor.

- *Can the CP&CECP factor be calculated by the change of permeability/flux and is it the same with the theoretical model?*

The change of permeability in phosphate retention can be used to calculate CP factors, however, the adsorption and electroviscous effect had influence on the accuracy of the results. CECP factor is not able to be measured by the permeability method since the unstable fouling layer can influence the discovery of permeability decrease. The deviations of CP factors calculated by the Sherwood model and the change of permeability are large.

8.2. Recommendations

Based on the results from the experiments and models, the following recommendations are made:

- To obtain a more accurate Sherwood formula, the osmotic pressure in the feed solution should be measured by the equipment instead of using uncertain assumptions.

- Equipment which can control the temperature in the experiment is needed to diminish the deviation between the GP model and the Sherwood model, especially for the solute with small molecular weight.

- To control the flux decline in PEGs and silica retention, a relatively high cross-flow velocity which can achieve a turbulent flow can be used to decrease CP. The concentration of

solute/colloids and the operational pressure should be determined with care to avoid the cake layer formation and the liming flux.

- In order to achieve a high phosphate retention rate, a high phosphate concentration within a certain range and the crossflow velocity which can achieve a turbulent flow should be used. It is also important to find a balance between the operational pressure which influences the characteristics of fouling layer (porosity and accumulated mass) and the satisfying permeate flux. The pH and the composition of the solution, especially the presence of the divalent cations, should be taken into considerations.

Reference

Abidi,A., Gherraf,N., Ladjel,S., Rabiller-Baudry, M., Bouchami,T.,(2016). Effect of operating parameters on the selectivity of nanofiltration phosphates transfer through a Nanomax-50 membrane. *Arabian Journal of Chemistry, 9,* S334-S341.

Bacchin, P., Si-Hassen, D., Starov, V., Clifton, M.J. & Aimar, P. (2002). A unifying model for concentration polarization, gel-layer formation and particle deposition in crossflow membrane filtration of colloidal suspensions. *Chem. Eng. Sci., 57,* 77–91.

Bader, M.S.H. & Veenstra, J.N. (1996). Analysis of concentration polarization phenomenon in ultrafiltration under turbulent flow conditions. *Journal of Membrane Science, 114,* 139-148.

Bernstein, R., Belfer, S.& Freger, V. (2011). Toward improved boron removal in RO by membrane modification: Feasibility and challenges. *Environ. Sci. Technol., 45*, 3613–3620.

Bellona, C., Marts, M.& Drewes, J.E. (2010). The effect of organic membrane fouling on the properties and retention characteristics of nanofiltration membranes. *Sep. Purif. Technol.74*, 44–54

Belfort, G., & Nagata, N. (1985). Fluid mechanics and cross-flow filtration: Some thoughts. *Desalination, 53,* 57-59.

Bhattacharjee, C.& Datta, S. (2003). Analysis of polarized layer resistance during ultrafiltration of PEG-6000: an approach based on filtration theory. *Separation and Purification Technology, 33 ,*115-126.

Bhattacharjee, C.& Datta, S. (2001). A numerical simulation for the prediction of flux and rejection during ultrafiltration in unstirred batch cell using variable diffusivity concept. *Separation/Purification Technology, 24,* 13–22.

Bhattachajee, C.& Bhattacharya, P.K. (1993). Flux decline analysis in ultrafiltration of kraft black Liquor. *Journal of Membrane Scie*nce, 82,1-14.

Blanc, P., Larbot, A., Palmeri, J., Lopez, M. & Cot, L. (1998). Hafnia ceramic nanofiltration membranes. Part I: Preparation and characterisation. *J. Membr. Sci., 149,* 151–161.

Brikov, A.V., Markin, A.N., Sukhoverkhov, S.V. et al. (2016). Rheological properties of poly (ethylene glycol) solutions and gels. *Dokl Phys Chem* 469, 121.

Carman, P.C. (1938). *Fundamental principles of industrial filtration.* Trans. Inst. Chem. Eng., 16, 168-188

Cherkasov, A.N., Tsareva, S.V. & Polotsky, A.E. (1995). Selective properties of ultrafiltration membranes from the standpoint of concentration polarization and adsorption phenomena, *Journal of Membrane Science, 104*, 157-164.

Choe, T. B., Masse., P. & Verdier., A. (1986). Flux decline in ultrafiltration: Concentration polarization and cake formation. *Journal of Membrane Science, 26,* l- 15.

Chong, T., Wong, F., & Fane, A. (2007). Enhanced concentration polarization by unstirred fouling

layers in reverse osmosis: Detection by sodium chloride tracer response technique. *Journal of Membrane Science, 287(2),* 198-210.

Chong, T., Wong, F., & Fane, A. (2008). Implications of critical flux and cake enhanced osmotic pressure (ceop) on colloidal fouling in reverse osmosis: Experimental observations. Journal of Membrane Science, 314(1-2), 101-111. doi:10.1016/j.memsci.2008.01.030

Contreras, A., Kim, A., & Li, Q. (2009). Combined fouling of nanofiltration membranes: Mechanisms and effect of organic matter. *Journal of Membrane Science, 327*(1), 87-95. doi:10.1016/j.memsci.2008.11.030

Craig D.Q.M. (1995). A review of thermal methods used for the analysis of the crystal form, Solution thermodynamics and glass transition behaviour of polyethylene glycols. *Thermochim Acta 248,* 189–203.

Churaev, N.V., Holdich, R.G., Prokopovich, P.P., Starov, V.M. & Vasin, S.I. (2005). Reversible adsorption insid.e pores of ultrafiltration membranes. *Journal of Colloid and Interface Science, 288,* 205–212.

COSMOL. (2019). Access available at https://www.comsol.com/multiphysics/diffusion-coefficient

Davis, R.H. (1992). Modeling of fouling of crossflow microfiltration membranes. *Separation and Purification Methods, 21(2)*, 75-126.

Déon, S., Dutournié, P., Limousy, L.& Bourseau, P. (2009). Transport of salt mixtures through nanofiltration membranes: Numerical identification of electric and dielectric contributions. *Separation and Purification Technology, 69(3)*, 225-233.

Denisov, G.A. (1994). Theory of concentration polarization in cross-flow ultrafiltration: gel-layer model and osmotic-pressure model. *Journal of Membrane Science, 91,* 173-187.

Donnan, F. G. (1995). Theory of membrane equilibria and membrane potentials in the presence of nondialysing electrolytes. A contribution to physical-chemical physiology. *Journal of Membrane Science, 100(1),* 45-55.

Eberhardt, T., & Min, S. (2008). Biosorbents prepared from wood particles treated with anionic polymer and iron salt: Effect of particle size on phosphate adsorption. *Bioresource Technology, 99*(3), 626-630. doi: 10.1016/j.biortech.2006.12.037

Farsi, A., Boffa, V., & Christensen, M. (2015). Electroviscous effects in ceramic nanofiltration membranes. *Chemphyschem, 16*(16), 3397-3407. doi:10.1002/cphc.201500600

Farsi, A., Boffa, V., Qureshi, H., Nijmeijer, A., Winnubst, A., & Lykkegaard Christensen, M. (2014). Modeling water flux and salt rejection of mesoporous γ-alumina and microporous organosilica membranes. *Journal of Membrane Science, 470*, 307-315.

Fernández-Sempere, J., Ruiz-Beviá, F., García-Algado, P. & Salcedo-Díaz, R. (2009). Visualization and modelling of the polarization layer and a reversible adsorption process in PEG-10000 dead-end ultrafiltration. *Journal of Membrane Science, 342*, 279–290.

Filtration. (2019). *Membrane technology,* Retrieved September 3, 2019 from Synder filtration. Access available at: http://synderfiltration.com/products/membrane-technology/

Flörke, O. W., Graetsch, H. A., Brunk, F., Benda, L., Paschen, S., Bergna, H. E., ... & Kerner, D. (2000). Silica. *Ullmann's Encyclopedia of Industrial Chemistry*.

Frank, B., & Belfort, G. (2003). Polysaccharides and sticky membrane surfaces: Critical ionic effects. *Journal of Membrane Science, 212*(1), 205-212. doi:10.1016/S0376-7388(02)00502-1

Ganguly, S., & Bhattacharya, P. (1994). Development of concentration profile and prediction of flux for ultrafiltration in a radial cross-flow cell. *Journal of Membrane Science, 97(Com),* 185-185.

Garrett, P.R. (1992). *Defoaming. Theory and Industrial applications*. USA: CRC Press. pp. 239–240.

Gauthier, G., Lazarus, V., & Pauchard, L. (2007). Alternating crack propagation during directional drying. *Langmuir : The Acs Journal of Surfaces and Colloids, 23*(9), 4715-8.

Gekas, V. & Hallstrom, B. (1987). Mass transfer in the concentration polarization layer under turbulent crossflow. I. Critical literature review and adaptation of existing Sherwood correlations to membrane operations. *J. Membr. Sci., 30,* X3-170.

Ghose, S., Battacharjee, C. & Datta. S. (2000). Simulation of unstirred batch ultrafiltration process based on a reversible pore-plugging mode. *J. Membr. Sci., 169,* 29–38.

Hao, Y., Liang, C., Ishigami, T., Matsuyama, H., & Maruyama, T. (2013). Direct visualization of fouling inside a hollow-fiber ultrafiltration membrane caused by sodium alginate. *Industrial & Engineering Chemistry Research, 52*(46), 16375-16383. doi:10.1021/ie4026117

Hashino, M., Katagiri, T., Kubota, N., Ohmukai, Y., Maruyama, T., & Matsuyama, H. (2011). Effect of membrane surface morphology on membrane fouling with sodium alginate. *Journal of Membrane Science, 366*(1), 258-265. doi:10.1016/j.memsci.2010.10.014

Heijman, S.G.J., Verliefde, A.R.D., Cornelissen, E.R., Amy, G. & Dijk, J.C. van. (2007). Influence of natural organic matter (NOM) fouling on the removal of pharmaceuticals by nanofiltration and activated carbon filtration. *Water Sci. Technol. Water Supply 7,* 17–23.

Hermia, J. (1982). Constant pressure blocking filtration laws: application to power-law non-newtonian fluids. *Trans. Inst. Chem. Eng. 60,* 183.

Hoek, E.M., Kim, A.S., & Elimelech, M. (2002). Influence of Crossflow Membrane Filter Geometry and Shear Rate on Colloidal Fouling in Reverse Osmosis and Nanofiltration Separations.

Hoek, E.M.V., Elimelech, M. (2003). Cake-enhanced concentration polarization: a new fouling mechanism for salt-rejecting membranes. *Environ. Sci. Technol., 37*, 5581–5588.

Huisman, I., Dutré, B., Persson, K., & Trägårdh, G. (1997). Water permeability in ultrafiltration and microfiltration: Viscous and electroviscous effects. *Desalination, 113*(1), 95-103. doi:10.1016/S0011-9164(97)00118-5

Jonsson, G. (1984). Boundary layer phenomena during ultrafiltration of dextran and whey protein solutions. *Desalination, 51*,61-77.

Karode, S.K. (2001). Unsteady state flux response: a method to determine the nature of the solute and gel layer in membrane filtration. *Journal of Membrane Science, 188,* 9–20.

Katsoufidou, K., Yiantsios, S., & Karabelas, A. (2007). Experimental study of ultrafiltration membrane fouling by sodium alginate and flux recovery by backwashing. *Journal of Membrane Science, 300*(1-2), 137-146. doi:10.1016/j.memsci.2007.05.017

Kramer, F.C., Shang, R., Heijman, S.G.J., Scherrenberg, S. M., van Lier, J. B.& Rietveld, L.C. (2015). Direct water reclamation from sewage using ceramic tight ultra- and nanofiltration. *Sep. Purif. Technol. 147,* 329–336.

Kramer, F.C. (2019). Ceramic nanofiltration for treatment of municipal sewage. TU Delft, Netherlands

Labban, O., Liu, C., Chong, T.H. & Lienhard V, J.H. (2017). Fundamentals of low-pressure nanofiltration: Membrane characterization, modeling, and understanding the multi-ionic interactions in water softening. *Journal of Membrane Science, 521,* 18–32.

Laspidou, C. S.& Rittmann, B. E. (2002). A unified theory for extracellular polymeric substance, soluble microbial product, and active and inert biomass. *Water Res., 36,* 2711.

Mahlangu, T.O., Msagati, T.A.M., Hoek, E.M.V., Verliefde, A.R.D. & Mamba, B.B. (2014). Retention of pharmaceuticals by nanofiltration (NF) membranes: Effect of fouling on retention behaviour. *Physics and Chemistry of the Earth, 76–78,* 28–34.

Majumdar, R., Alexander, K.S., & Riga, A.T. (2010). Physical characterization of polyethylene glycols by thermal analytical technique and the effect of humidity and molecular weight. *Die Pharmazie, 65 5*, 343-7 .

Makardij, A.A., Farid, F.F., & Chen, X. (2002). A Simple and Effective Model for Cross-Flow Microfiltration and Ultrafiltration. *The Canadian Journal of Chemical Engineering, 80*, 28-36.

Michel, B. E., & Kaufmann, M. R. (1973). The osmotic potential of polyethylene glycol 6000. *Plant physiology*, *51*(5), 914-916.

Mulder, M., & Kragl, U. (1997). Basic principles of membrane technology. *Angewandte Chemie, 109*(12), 1420.

Ng, H., & Elimelech, M. (2004). Influence of colloidal fouling on rejection of trace organic contaminants by reverse osmosis. Journal of Membrane Science, 244(1), 215-226. doi:10.1016/j.memsci.2004.06.054

Nghiem, L.D., Coleman, P.J.& Espendiller, C. (2010). Mechanisms underlying the effects of membrane fouling on the nanofiltration of trace organic contaminants. *Desalination, 250,* 682–687.

Nikolova, J.D. & Islam M.A. (1998). Contribution of adsorbed layer resistance to the flux-decline in an ultrafiltration process. *Journal of Membrane Science, 146,* 105–111.

Ninni, L., Burd, H., Fung, W. H., & Meirelles, A. J. (2003). Kinematic viscosities of poly (ethylene glycol) aqueous solutions. *Journal of Chemical & Engineering Data*, *48*(2), 324-329.

Noakes, C. & Sleigh, A. (2009). "Real Fluids". An Introduction to Fluid Mechanics. *University of Leeds*. Archived from the original on 21 October 2010.Metcalf, L., Eddy, H., Tchobanoglous, G. (2010). Wastewater Engineering: Treatment, Disposal, and Reuse, McGraw-Hill

Notter, R., & Sleicher, C. (1971). The eddy diffusivity in the turbulent boundary layer near a wall. *Chemical Engineering Science, 26*(1), 161-171. doi:10.1016/0009-2509(71)86088-8

Opong, W.S. & Zydney, A.L. (1991). Hydraulic permeability of protein layers deposited during ultrafiltration. *Journal of Colloid and Interface Science, 142,* 41-60.

Pinczewski, W., & Sideman, S. (1974). A model for mass (heat) transfer in turbulent tube flow. moderate and high schmidt (prandtl) numbers. *Chemical Engineering Science,29*(9), 1969-1976. doi:10.1016/0009-2509(74)85016-5

Porter, C. (1972). Concentration polarization with membrane ultrafiltration. *Ind. Eng. Chem. Prod. Res. Develop. 11,* 234-248.

Qomariyah, L., Sasmita, F., Novaldi, H., Widiyastuti, W., Winardi, S., & 7th Nanoscience and Nanotechnology Symposium NNS 2017 7 2017 10 22 - 2017 10 24. (2018). Preparation of stable colloidal silica with controlled size nano spheres from sodium silicate solution. Iop Conference Series: Materials Science and Engineering, 395(1). doi:10.1088/1757-899X/395/1/012017

Raman, L.P., Cheryan, M. & Rajagopalan, N. (1994). Consider nanofiltration for membrane separations. *Chem Eng Prog, 90(3),* 68–74.

Randon, J., Blanc, P., & Paterson, R. (1995). Modification of ceramic membrane surfaces using phosphoric acid and alkyl phosphonic acids and its effects on ultrafiltration of bsa protein. *Journal of Membrane Science, 98*(1), 119-129. doi:10.1016/0376-7388(94)00183-Y

Randon,J.(2019) Osmotic pressure. Brock University, Retrieved from https://brocku.ca/researchers/peter_rand/osmotic/osfile.html

Roorda, J. (2004). *Filtration characteristics in dead-end ultrafiltration of wwtp-effluent* (Doctoral dissertation, 2004). S.n

Rose, S., Prevoteau, A., Elzière, P., Hourdet, D., Marcellan, A., & Leibler, L. (2014). Nanoparticle solutions as adhesives for gels and biological tissues. *Nature, 505*(7483), 382-5. doi:10.1038/nature12806

Sbaï, M., Fievet, P., Szymczyk, A., Aoubiza, B., Vidonne, A., & Foissy, A. (2003). Streaming potential, electroviscous effect, pore conductivity and membrane potential for the determination of the surface potential of a ceramic ultrafiltration membrane. Journal of Membrane Science, 215(1), 1-9. doi:10.1016/S0376-7388(02)00553-7

Sablani, S.S., Goosen, M.F.A, Al-Belushi, R.& Wilf.M.(2001). Concentration polarization in ultrafiltration and reverse osmosis: a critical review. *Desalination, 141,* 269-289.

Samaei, S.M., Gato-Trinida, S.& Altaee, A. (2018). The application of pressure-driven ceramic membrane technology for the treatment of industrial wastewaters – A review. *Sep. Purif. Technol., 200,*198-220.

Sarrade, S., Rios, G.M.& Carlès, M. (1994). Dynamic characterization and transport mechanism of two inorganic membranes for nanofiltration. *J. Membr. Sci., 97,*155–166.

Schulz, G.& Ripperger, S. (1989). Concentration polarization in crossflow microfiltration. *Journal of Membrane Science, 40,* 173-187

Shanefield, D. (1995). *Organic additives and ceramic processing : With applications in powder metallurgy, ink, and paint*. Boston: Kluwer Academic.

Shang, R., Vuong, F., Hu, J.Y., Li, S., Kemperman, A.J.B., Nijmeijer, K., Cornelissen, E.R., Heijman, S.G.J.& Rietveld, L.C. (2015). Hydraulically irreversible fouling on ceramic MF/UF membranes: Comparison of fouling indices, foulant composition and irreversible pore narrowing. *Sep. Purif. Technol., 147,* 303–310.

Shang, R., Verliefde, A.R.D., Hu, J., Heijman, S.G.J.& Rietveld, L. C. (2014). The impact of EfOM, NOM and cations on phosphate retention by tight ceramic ultrafiltration. *Sep. Purif. Technol., 132,* 289-294.

Shang, R., Verliefde, A.R.D., Hu, J., Zeng, Z., Lu, J., Kemperman, A.J.B., Deng, H., Nijmeijer, K., Heijman & S.G.J., Rietveld, L.C. (2014). Tight ceramic UF membrane as RO pre-treatment: The role of electrostatic interactions on phosphate rejection. *Water. Res., 48,* 498–507.

Shang, R., Goulas, A., Tang, C., De Frias Serra, X., Rietveld, L., & Heijman, S. (2017). Atmospheric pressure atomic layer deposition for tight ceramic nanofiltration membranes: Synthesis and application in water purification. *Journal of Membrane Science*, 528, 163-170.

Sherwood, T.K., Pigford, R.L.& Wilke, C.R. (1975). *Mass Transfer,* McGraw-Hill Inc, New York.

Song, L.& Elimelech, M. (1995). Theory of concentration polarization in crossflow filtration. *J. Chem. Soc. Faraday Trans.,* 91(19), 3389-3398.

Song. L. (1998). Flux decline in crossflow microfiltration and ultrafiltration: mechanisms and modeling of membrane fouling. *Journal of Membrane Science, 139,* 183-200.

Spiegler, K.S. & Kedem, O. (1996). Thermodynamic of hyperfiltration (reverse osmosis): criteria for efficient membranes. *Desalination1,311*.

Stanley, C.B. & Strey H.H. (2003). Measuring Osmotic Pressure of Poly (ethylene glycol) Solutions by Sedimentation Equilibrium Ultracentrifugation. *Macromolecules, 36,* 6888-6893.

Sutzkover, I., Hasson, D., & Semiat, R. (2000). Simple technique for measuring the concentration polarization level in a reverse osmosis system. *Desalination, 131*(1), 117-127. doi:10.1016/S0011-9164(00)90012-2

Tang, G., Ye, P., & Tao, W. (2010). Electroviscous effect on non-newtonian fluid flow in microchannels. *Journal of Non-Newtonian Fluid Mechanics, 165*(7-8), 435-440. doi:10.1016/j.jnnfm.2010.01.026

Van der Bruggen, B., & Vandecasteele, C. (2002). Modelling of the retention of uncharged molecules with nanofiltration. *Water Research, 36*(5), 1360-1368. doi:10.1016/S0043-1354(01)00318-9

Vela, M.C.V., Blanco, S.A., Garcia, J.L.& Rodríguez, E.B. (2008). Analysis of membrane pore blocking models applied to the ultrafiltration of PEG. *Separation and Purification Technology, 62,* 489–498.

Verberk, J.Q.J.C. (2015). *Application of air in membrane filtration*, Netherlands

Vincent-Vela, M.C., Álvarez-Blanco, S., LoraGarcía, J. & Bergantiños-Rodríguez, E. (2006). Prediction of flux decline in the ultrafiltration of macromolecules. *Desalination, 192*, 323–329.

Vivero-Escoto, J. (Ed.). (2011). *Silica nanoparticles : Preparation, properties and uses*. Retrieved from https://ebookcentral-proquest-com.tudelft.idm.oclc.org

Vogel, D., Simon, A., Alturki, A. A., Bilitewski, B., Price, W.E.& Nghiem, L.D. (2010). Effects of fouling and scaling on the retention of trace organic contaminants by a nanofiltration membrane: The role of cake-enhanced concentration polarisation. *Sep. Purif. Technol. 73*, 256-263.

Wang, L., & Song, L. (1999). Flux decline in crossflow microfiltration and ultrafiltration: Experimental verification of fouling dynamics. *Journal of Membrane Science, 160*(1), 41-50. doi:10.1016/S0376-7388(99)00075-7

Web.mit.edu. (2019). *LEMI: Laboratory for Energy and Microsystems Innovation at MIT | Research: Electrokinetics*. [online] Available at: http://web.mit.edu/lemi/rsc_electrokinetics.html [Accessed 7 Mar. 2019].

Weng, P. (1996). Silica scale inhibition and colloidal silica dispersion for reverse osmosis systems. *Desalination, 103*(1-2), 59

Xu, T.(2008). *Advances in Membrane Science and Technology,* Nova Science Publishers, Incorporated.

Yang, S., Cao, Z., Arvanitis, A., Sun, X., Xu, Z.& Dong, J. (2016). DDR-type zeolite membrane synthesis, modification and gas permeation studies. *Journal of Membrane Science, 505,* 194–204.

Ye, Y., Le Clech, P., Chen, V., Fane, A., & Jefferson, B. (2005). Fouling mechanisms of alginate solutions as model extracellular polymeric substances. *Desalination, 175*(1), 7-20. doi: 10.1016/j.desal.2004.09.019

Ye, Y., Clech, P., Chen, V., & Fane, A. (2005). Evolution of fouling during crossflow filtration of model eps solutions. *Journal of Membrane Science, 264*(1), 190-199. doi: 10.1016/j.memsci.2005.04.040

Zaidi, S.K., Karode, S.K, Kirpalani, D. & Kumar, A. (2004). A new method for identifying osmotically limited and gel layer-controlled pressure independent flux in ultrafiltration. *Can. J. Chem. Eng.,* 343-348

Zaidi, S.K, & Kumar, A. (2004). Effects of ethanol concentration on flux and gel formation in dead end ultrafiltration of peg and dextran. *Journal of Membrane Science. 237(1)*, 189-197.

Appendix： Diagram of flux decline theory